UPPER ATMOSPHERE DYNAMICS IN THE AURORAL ZONE

by Georgina. D. Price, B.Sc.(Hons)

A thesis for the degree of Doctor of Philosophy

THE MAWSON INSTITUTE FOR ANTARCTIC RESEARCH

UNIVERSITY OF ADELAIDE

October 1988

awarded 9.3.89

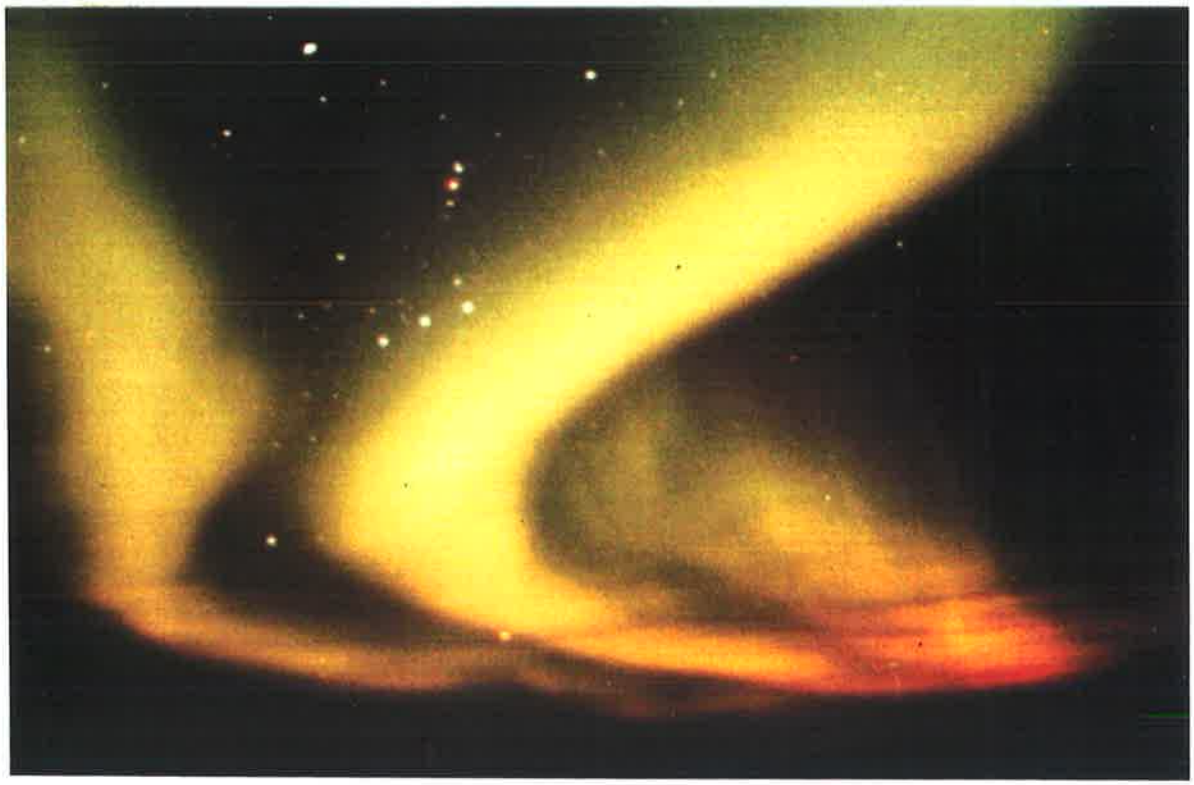

Aurora Australis: Photographed at Mawson, Antarctica by G. Price.

Contents

ABSTRACT

Coupling between ion motions in the upper thermosphere and neutral air motions in the lower thermosphere/upper mesosphere is not well understood. The dynamics of the upper thermosphere are strongly correlated with geomagnetic activity through the effects of electrodynamic forcing whereas the dynamics of the mesosphere are dominated by motions of the neutral atmosphere. The extent of the coupling is investigated through a study of the relation between geomagnetic activity and both the horizontal and vertical components of the wind.

The data presented in this thesis were collected by the author during a year spent at Mawson, Antarctica (67.6°S, 62.9°E, invariant latitude 70.1°S), as a member of the 1985 Australian National Antarctic Research Expedition. A spaced antenna partial reflection radar (SAPR radar) was run continuously throughout the year and a Fabry-Perot spectrometer (FPS) was operated on 23 nights during the spring. Additional data from the SAPR radar at Mawson, covering the following two years, have also been used.

The SAPR radar gives measurements of the horizontal wind field every 2 km, in the height range 70 to 110 km, with a time resolution of up to eight points per hour. The method is generally assumed to measure the neutral wind field up to heights near 100 km. The FPS was set to observe the λ558 nm emission of atomic oxygen from which the temperature, emission intensity and vertical component of the neutral wind are determined. The measured temperature is used to assign an approximate emission height to the observations.

Large upward winds of approximately 30 ms^{-1} appear to be a direct response of the neutral atmosphere to intense auroral events which result in a peak emission height of less than 110 km. At higher altitudes vertical winds of a similar magnitude are also measured during geomagnetically disturbed conditions, although here they do not appear to be associated with particular auroral events. The results are interpreted in terms of the relative importance of Joule and particle heating at different altitudes. The SAPR radar data have been analysed

using a randomization technique. Results show that larger winds are measured during geomagnetically active periods in both the raw wind values and in the medium and high frequency components. The raw winds tend to increase towards the geographic NW to NE quadrant during the early morning hours. The observed correlation is seen down to 86 km and shows a seasonal dependence.

This thesis contains no material which has been accepted for the award of any other degree or diploma in any University, and, to the best of the author's knowledge and belief, it contains no material previously published or written by another person, except when due reference is made in the text. I consent to this thesis being made available for photocopying and loan by the librarian of the University of Adelaide upon acceptance of the degree.

(G.D. Price)

ACKNOWLEDGEMENTS

I would like to thank Dr Fred Jacka, Director of the Mawson Institute for Antarctic Research, and Dr Bob Vincent, Atmospheric Physics Group, Department of Physics, for the sound judgement and enthusiasm shown by them in their supervision of this work. Thanks also to Don Creighton who was always ready to offer technical advice and whose efforts have ensured the overall smooth operation of the equipment. I would like to thank Dr Gary Burns, Upper Atmosphere Physics Group, Antarctic Division, who offered guidance during the time spent in Hobart and who's healthy skepticism of statistics (and background in the study of sun-weather correlations) contributed to the development of the randomization technique.

The experimental work was carried out at the Australian National Antarctic Research Expedition's station at Mawson. I would like to thank the Director, Antarctic Division, for logistic support. I was employed by the Antarctic Division for the time spent at Mawson and for over 18 months on my return. I am grateful to have had this opportunity. I extend my thanks to the staff of the Antarctic Division, particularly to John Cox for drawings, Bob Reeves for photographic work and the ADP group for computing support.

I would like to thank the Mawson, over-wintering party of 1985, who comprised four women, twenty-three men, and twenty-eight huskies. Their willingness to assist, tolerance of the interference caused by the SAPR radar during radphone skeds, and most of all good company, contributed greatly to the success of this project. Training during the first summer was ably given by the 1984 expeditioners Mark Conde, Andre Phillips and Alistair Urie.

The initial drafts of this thesis prompted constructive criticism from Dr B.H. Briggs, Prof. K.D. Cole, Ian Higginbottom, Norm Jones, Paul Wardill and Dave Heatley. I am indebted to them for their invaluable input. Dr Bruce Brown, Department of Mathematics, University of Tasmania, gave advice on statistics. The final draft was proof read by Rex Matthews and artistic design was by Barbara Matthews. Mr Tomlinson, Adelaide University, also contributed to the photographic work.

I would like to mention my fellow students and colleagues from the Mawson Institute, Atmospheric Physics group, and Upper Atmosphere Physics Section, with whom I have enjoyed working. Particular thanks must, however, go to Pene Greet, with whom I have shared an office, a house, and many valuable discussions during my 'visits' to Adelaide.

Finally I would like to thank my parents, June and Jock Price, who have provided great support by always being behind me in all my endeavors, as too have my brothers. Special thanks go to Hig.

INTRODUCTION

The term 'upper atmosphere' is used in the title of this work to describe the height range 70 to 140 km, which includes the upper mesosphere and lower thermosphere. In the auroral zones, this height range forms a region of transition; above this region electric fields drive the ionospheric plasma which in turn drives the neutral atmosphere in a process known as 'ion drag'; below this region the neutral atmosphere drives the ions. The region is penetrated by upwardly propagating tides and gravity waves and is also a major source region for thermospheric gravity waves.

During geomagnetically disturbed times the strength of the polar electric field increases and the height down to which the ion drag force is effective decreases. Particle precipitation leads to enhanced ionization which in turn leads to heating through the Joule dissipation of currents and the energy released during ionic recombination. Heating effects produce a direct response in the wind field as well as providing a principal generation mechanism for gravity waves (Hunsucker, 1982).

In this work a spaced antenna partial reflection (SAPR) radar, operating at 2 MHz, is used to measure the horizontal wind velocity over the height range 70 to 110 km. The method is generally assumed to measure the neutral wind field up to heights near 100 km, however, the effectiveness of radar techniques in measuring the neutral winds in the presence of large electric fields associated with geomagnetic disturbances has been questioned (Reid, 1983; Prikryl *et al*, 1986). A Fabry-Perot spectrometer (FPS), set to observe the oxygen λ558 nm emission, is used to measure the vertical wind and temperature in the height range 100 to 140 km. The measured emission temperature is used to assign an approximate emission height to the observations. These techniques are described in Chapters 2 and 3 respectively along with a critical discussion of the data and possible sources of error.

Vertical wind measurements are sensitive to local heating and gravity wave motions. Perturbations in the vertical wind are readily identified since the mean vertical wind is approximately

zero. There have been a number of vertical wind measurements made in the upper thermosphere (Herrero *et al.*, 1984; Rees *et al.*, 1984a and Wardill and Jacka, 1986), however, there appears to be only one set of published results of vertical winds in the auroral zone lower thermosphere (Peteherych *et al.*, 1985). The direct response of the vertical wind to auroral events is examined in Chapter 4 and the results are interpreted in terms of the heating associated with such events.

The relation between geomagnetic disturbances and neutral air motions in the upper mesosphere/lower thermosphere is not well understood. There have been several reports investigating correlations between wind observations and variations in geomagnetic activity (Balsley *et al.*, 1982; Johnson and Luhmann, 1985 a and b; Manson and Meek, 1986; Phillips and Jacka, 1987) however, the results are inconsistent. Johnson and Luhmann (1985b) have shown that anomalous correlations may be obtained if preliminary analysis is not carried out to remove the tidal components. In Chapter 5 a randomization technique is developed which allows anomalous correlations to be identified, allowing a correlation between the raw wind data and geomagnetic activity to be demonstrated.

The analysis is extended to cover three years of SAPR data from Mawson in Chapter 6. The effect of geomagnetic activity on the magnitude and direction of the raw winds and on the medium and high frequency components of the wind are also investigated. The results are discussed in relation to the physical processes which may be contributing to the observed effect, viz: ion drag, the effect of enhanced electric fields, and heating.

Chapter 1.

LITERATURE REVIEW

1.1 INTRODUCTION

Propagating atmospheric waves were first recorded as surface pressure fluctuations following the eruption of Krakatoa in 1883 and again after the Great Siberian Meteor in 1908 (Pekeris 1939, 1948). Another wave phenomenon in the lower atmosphere, lee waves, are commonly seen as banded cloud structures lying on the leeward side of mountain ranges over which a steady wind is blowing. In this case, stationary waves cause clouds to form across the path of the prevailing wind. In Figure 1.1, lee waves can be identified in the cloud formations seen in a photograph taken by the NOAA9 satellite.

The focus of the present work however, is wave phenomena in the middle and upper atmosphere. Internal propagating gravity waves, which often originate in the lower atmosphere, become amplified as they propagate upwards into the rarefied atmosphere of these upper regions. Here measurements of various atmospheric parameters including temperature, wind velocity, and ion concentration often reveal fluctuations which may be attributed to the passage of internal gravity waves. Such variations are seen in the mesospheric and lower thermospheric wind data recorded at Mawson, Antarctica, by the author. Although long period variations due to tides and planetary waves are also present this work is principally concerned with internal gravity waves and their contribution to the dynamic structure of the atmosphere.

1.2 HISTORICAL PERSPECTIVE

The importance of the dynamic structure of the atmosphere became apparent when Murgatroyd and Goody (1958) showed that the atmosphere, particularly in the high latitude regions, was not in radiative equilibrium. It is now recognised that internal gravity waves play an essential role in determining the large-scale circulation and state of the middle atmosphere through the process of momentum transfer from the wave. The mechanisms by which gravity waves interact

Figure 1.1: Cloud bands lying parallel to the south coast of New South Wales provide evidence of lee waves produced by an eastward wind blowing over the Great Dividing Range.
Photograph: NOAA9 satellite (from C. Nilsson, C.S.I.R.O. Division of Oceanography, Hobart).

with the mean flow and the importance of these processes have only been realised in the last few years. Prior to this the theory developed along two parallel paths: through the study of wave processes based on observations of gravity waves and through the development of a model to describe the structure of the middle atmosphere. A summary of the developments is given here which is based on a detailed review presented by Fritts (1984).

Quantitative studies of wave processes began with observations of travelling ionospheric disturbances (TID's) which are now recognized as ionospheric manifestations of internal gravity waves. These disturbances produce periodic variations in radio signals reflected from the ionosphere, a phenomenon which had been noticed since the first uses of radio in the 1920's. Systematic studies of TID's gave estimates of wave propagation velocities and horizontal wavelengths (Munro, 1950, 1953, 1958; Heisler, 1958). Also at this time vertical profiles of gravity wave motions were obtained from observations of meteor trails (Liller and Whipple, 1954). Variations in the wave amplitude with height are determined from measurements of the variation in the horizontal wind field which is displayed by the motion of the meteor trail. Such observations drew attention to an important characteristic of internal gravity waves, namely the tendency for wave amplitudes to increase with increasing height in the atmosphere.

The first attempt to "visualize the upper atmosphere as a whole" was made by Kellogg and Schilling (1951). Their simple model showed the summer mesopause to be typically 60 K colder than the winter mesopause, a phenomenon which could not be explained by radiative processes alone. To account for the disparity at mesospheric heights the meridional temperature gradient must reverse below this region with the important consequence that such a reversal would be accompanied by a reversal in the vertical shear of the mean zonal wind.

The next step in the development of atmospheric models was to introduce dynamic processes. Vertical motions in the polar regions were added to allow adiabatic compression/expansion to produce the required heating/cooling in the winter/summer mesosphere. A vigorous meridional flow was then required to sustain the vertical motions through continuity considerations

(Murgatroyd and Singleton, 1961). However, this increased meridional circulation resulted in large Coriolis torques and a corresponding stronger zonal circulation. Without an efficient drag mechanism the zonal winds would increase with altitude throughout the middle atmosphere, which is contrary to observations.

A drag mechanism, parametrized as a constant Rayleigh drag coefficient, was introduced by Leovy (1964) while later works featured height-varying coefficients (Schoeberl and Strobel, 1978). Although solving one problem, a Rayleigh drag of the form used by these authors is only able to decelerate the mean wind towards zero and is therefore unable to reverse the flow as required by the observations mentioned above. It was at least a decade after the first parametrization of the drag coefficient before advances were made towards identifying the source of the drag.

Gravity wave theory developed rapidly during this time following a landmark paper by Hines (1960), which was based on both TID and meteor trail observations. Hines proposed that gravity waves generated in the lower atmosphere would increase in amplitude as they propagated upwards. After suffering partial reflections and energy dissipation only certain modes would reach the ionosphere where they appear as TID's. This work formed a theoretical basis for describing internal gravity waves as large scale atmospheric waves for which the effects of gravity can no longer be ignored. Hines also realized that gravity waves must play an important role in the dynamics of the upper atmosphere through their ability to transport energy.

A number of experimental methods were developed to study gravity waves. The release of sodium clouds and gaseous aluminium compounds allowed measurements of the horizontal wind which could be resolved into mean, tidal, and gravity wave components (Kochanski, 1964; Rosenberg and Edwards, 1964). The altitude range 70 to 190 km was examined, with evidence of gravity-wave activity seen below 130 km. Rocket-based soundings in the stratosphere and mesosphere measured temperature oscillations of up to 40 K in the winter mesosphere, with a decrease in summer (Theon *et al.*, 1967). This suggested that gravity-wave activity had a seasonal

dependence. Photographs of noctilucent clouds provided visual evidence of waves around the high-latitude mesopause (Witt, 1962; Haurwitz and Fogle, 1969) and wavelike structures were later reported in the intensity of the green airglow emission (Korobeynikova and Nasirov, 1976; Tuan *et al.*, 1979).

Following the increase in experimental observations of gravity waves, two keynote ideas were developed on the theoretical side. Firstly, it was recognized by a number of authors (Hines, 1960; Orlanski and Bryan, 1969; Einaudi and Hines, 1970) that the growth of gravity waves with height must eventually break down, resulting in the deposition of wave energy through the production of turbulence. Hodges (1969) proposed that this would occur when wave-induced temperature oscillations became large enough to produce a superadiabatic condition. Secondly, Bretherton (1966) and Booker and Bretherton (1967) showed that the vertical flux of wave energy must be accompanied by the vertical flux of horizontal momentum and that in a shear flow there is momentum transfer between the mean flow and the wave. In addition, they showed that interactions between the wave and the mean flow will lead to total absorption of the wave when the horizontal phase velocity of the wave is equal to the mean wind. Waves cannot propagate beyond this point, which is known as a critical level.

The studies of gravity wave processes and the middle atmosphere circulation came together with the work of Lindzen (1981). The propagation of gravity waves into the middle atmosphere is strongly influenced by the mean flow due to the effects of critical layer absorption. A seasonal variation in the spectrum of mesospheric gravity waves is produced as changes in the tropospheric and stratospheric winds produce selective filtering of waves according to their horizontal phase velocities. Waves escaping absorption will ultimately attain a height at which instabilities in the wave field cause wave 'breaking'. At this point it is suggested that the wave will lose energy through the production of turbulence, preventing further wave growth with height. The divergence of wave momentum results in the acceleration of the mean flow towards the phase velocity of the wave. Gravity waves travelling into the mean flow are thus capable

of reducing or even reversing the flow above the height at which wave breaking commences. In this way, accelerations induced by gravity waves provide an explicit source for the 'drag' needed to reverse mesospheric winds and produce the observed meridional-temperature gradient in the middle atmosphere.

There has been a resurgence of theoretical studies of gravity waves since their importance in understanding the dynamic structure of the atmosphere has been realised. Studies of momentum deposition, wave-mean flow interactions, and gravity wave saturation and 'breaking', are aimed at quantifying these processes while observational techniques continue to determine wave and turbulence parameters.

1.3 DYNAMIC STRUCTURE OF THE UPPER MESOSPHERE/LOWER THERMOSPHERE

A summary of observations of gravity waves in the upper mesosphere/lower thermosphere is presented. Different techniques lend themselves to the measurement of different gravity wave parameters. Optical methods allow the measurement of gravity wave horizontal wavelengths and phase velocities, while single site radar-wind observations give measurements of the wave frequency, perturbation velocity, and vertical wavelength. Recently, Doppler radars with off-vertical beams have been used to provide a direct measurement of the vertical flux of horizontal momentum (Vincent and Reid, 1983; Fritts and Vincent, 1987; Reid and Vincent, 1987), and a multiple bistatic spaced antenna (SA) radar known as 'Gravnet', has allowed measurements of the horizontal wavelength and phase velocity (Meek *et al.*, 1985a, 1885b; Manson and Meek, 1988). A summary of typical values of wave parameters will now be given.

Gravity waves can interact with the environment through which they propagate as outlined in section 1.2. The processes of gravity wave saturation and critical layer absorption by which energy is exchanged between the waves and the background environment will be outlined. Observations which provide evidence of these processes are discussed.

The Brunt-Väisälä frequency is the upper boundary of the gravity wave spectrum. It is the

resonant frequency at which a parcel of air will oscillate if it is vertically displaced, by a small amount, from its equilibrium position in a stable atmosphere. As the wave frequency approaches the Brunt-Väisälä frequency the vertically acting forces of gravity and buoyancy cause the parcel to oscillate in a near vertical plane; the phase velocity propagates almost horizontally and energy propagates vertically. As the wave frequency approaches the lower frequency limit, viz. the inertial frequency, the horizontally acting Coriolis and pressure gradient forces confine the oscillations to a near horizontal plane, producing a vertical phase progression and horizontal energy propagation.

Sources of gravity waves found in the lower atmosphere include the flow of wind over topographic features, wind shear, and convection (see Figure 1.2). Waves may also be generated in the stratosphere and mesosphere by wind shear and convection and in the thermosphere by auroral processes (see section 1.5). Relatively little data exists on source distributions and spectra. Hines (1968) showed that tropospheric sources, such as fronts and jet streams, may account for wavelike deformations seen in noctilucent clouds. Krassovsky *et al.* (1977) and Vincent and Stubbs (1977) trace gravity waves back to meteorological activity and Gavrilov and Shved (1982) show that the dominant propagation direction of gravity waves in the lower thermosphere varies with the movement of cyclonic activity throughout the year.

Phase velocities of gravity waves observed in the upper mesosphere/lower thermosphere vary by two orders of magnitude. Observations of noctilucent clouds have revealed small phase velocities of 10 - 30 ms^{-1} (Haurwitz and Fogle, 1969). The wavelike structure in the 558 nm airglow has led to phase speed measurements of; 77 ms^{-1} (Armstrong, 1982), 50 - 100 ms^{-1} (Freund and Jacka, 1979) and up to 300 ms^{-1} (Gavrilov and Shved, 1982). Meek *et al.* (1985a) observed phase speed to decrease from 72 ms^{-1} at a period of 10 min to 34 ms^{-1} at 100 min.

Gravity wave characteristics, determined using a number of techniques, have been collated by Reid (1986). In the 70 to 90 km height range, measurements of the horizontal phase velocity are shown to be approximately constant with increasing period. In the 90 to 100 km range

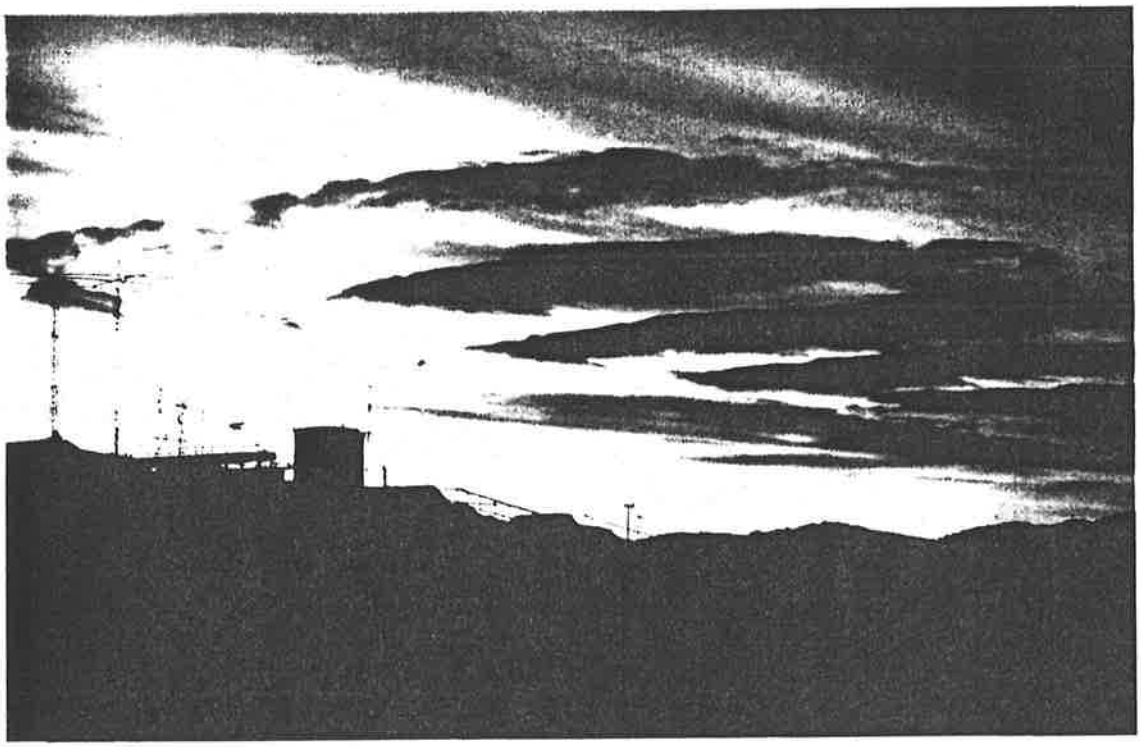

Figure 1.2: Cloud bands seen at Casey station, Antarctica, suggest the presence of gravity waves produced by wind shear at the upper boundary of the katabatic wind. Photograph by G. Wilson.

the phase velocity increases with increasing wave period. However, Reid suggests that the differences in the results for the two height ranges may not be significant as the lower phase speed waves are likely to be absent at the higher altitudes due to filtering by background winds at lower altitudes.

Horizontal wavelength measurements presented by Reid (1986) show that high frequency waves (periods < 1 h) are associated with wavelengths of the order 10 to 70 km while large period waves are associated with wavelengths of up to 6000 km. The latter were determined from airglow observations carried out by Gavrilov and Shved (1982).

Estimates of the percentage of upward propagating waves found in the middle atmosphere have been made by Vincent(1984a)and Kalchenko *et al.* (1985). Vincent uses a vector spectral decomposition of gravity wave profiles to show that at least 65 % of the vertical energy flux of longer period waves is upgoing. This method is based on the premise that the perturbation velocity vector for low frequency waves in the southern hemisphere rotates anticlockwise with increasing height due to the effects of the Coriolis force. Kalchenko *et al.* examine the phase altitude characteristics of 30 waves and suggest that energy is propagating upwards in 83 % of the waves. However, their results are based on the assumption that waves with a downward component in the phase velocity have an upward component in the group velocity and therefore transport energy upwards. Strictly, this assumption is only valid when the phase speed of the wave is at least a substantial fraction of the background wind.

Observations of the vertical wavelengths of gravity waves are limited by the height resolution on the lower side, and the height range capability of the technique on the upper side. Optical techniques used to study the airglow emission cannot observe waves with a vertical wavelength less than the thickness of the emission region. This sets a lower limit of about 10 km on the vertical wavelengths of the gravity waves which may be observed. Radar techniques cover a broader height range with a height resolution generally of 2 to 4 km. Sodium-lidar measurements have better height resolution again but are limited by the thickness of the sodium layer. The

vertical wavelengths of gravity waves measured by these three techniques lie within the range 3 - 30 km.

Wave amplitudes are limited by wave saturation and dissipation. "Gravity wave saturation refers to any process that acts to limit or reduce wave amplitudes due to instabilities or interactions arising from large amplitude motions. Dissipation processes ..., in contrast, act more or less independently of wave amplitude" (Fritts, 1984).

Saturation processes fall into two categories: linear and nonlinear. Linear saturation processes rely on instabilities within the wave field to dissipate wave energy and nonlinear saturation processes limit wave amplitudes through nonlinear interactions among the components of the wave.

Linear instabilities include both convective and dynamic instabilities. Convective overturning occurs when either -

$$\frac{\partial T}{\partial z} < -\frac{g}{c_p}, \tag{1.1}$$

where

T = temperature,

z = altitude,

g = the acceleration due to gravity, and

c_p = the specific heat at constant pressure

i.e. the temperature gradient within the wave field becomes super-adiabatic, or

$$u' > |c - \bar{u}|, \tag{1.2}$$

which implies that the particle velocity (the perturbation velocity, u', plus the mean flow velocity, $\bar{u}$) exceeds the phase speed of the wave, c.

The Richardson number, Ri, is a measure of dynamic stability and is defined as

$$Ri = \frac{N}{\frac{\partial u}{\partial z}} \tag{1.3}$$

where N is the Brunt-Väisälä frequency and u the horizontal wind velocity. Dynamic or shear instabilities occur when the Richardson number is less than 0.25.

Observations of approximately monochromatic wave motions are useful in confirming theoretical predictions of saturation processes. Only 58 such waves were observed using the Gravnet radar, in almost a year of observations (Meek *et al.*, 1985a). The Gravnet multiple bistatic SA radar facility has receivers at three sites, spaced about 40 km apart, which allow measurement of the horizontal phase velocity and horizontal wavelength. Of the 58 approximately monochromatic wave motions observed, only two satisfied the conditions for convective instability as given by Equation 1.2. Meek *et al.* suggest that this is a rather weak condition for saturation and conclude that other levels of saturation may have been operating.

Nonlinear saturation processes are not as readily defined or recognised as linear processes. Numerical simulations of nonlinear and multiple wave effects have been carried out by Fritts, (1985); he shows that a superposition of waves can lead to saturation, even though none of the waves possess saturation amplitudes independently. This has been confirmed by a study carried out by Smith *et al.* (1986), using both rocket salvos and the Poker Flat MST radar. They found that the region of strongest radar signal strength, and hence greatest turbulent mixing, was at a height where individual large scale waves had not attained the saturation amplitude. This suggests that saturation may involve a broad spectrum of waves which achieve saturation when superimposed.

Figure 1.3 shows a schematic representation of linear saturation. In the absence of dissipation the amplitude of an upwardly propagating gravity wave grows exponentially with height in order to compensate for the exponential decrease in atmospheric density, and so maintains a constant energy density flux. Eventually, "the conditions for shear or convective instability result, and the wave is assumed to lose energy through the production of turbulence", (Fritts *et al.*, 1984). The amount of turbulence produced is that required to maintain the wave amplitude at the saturation level. This produces a divergence of the vertical flux of horizontal

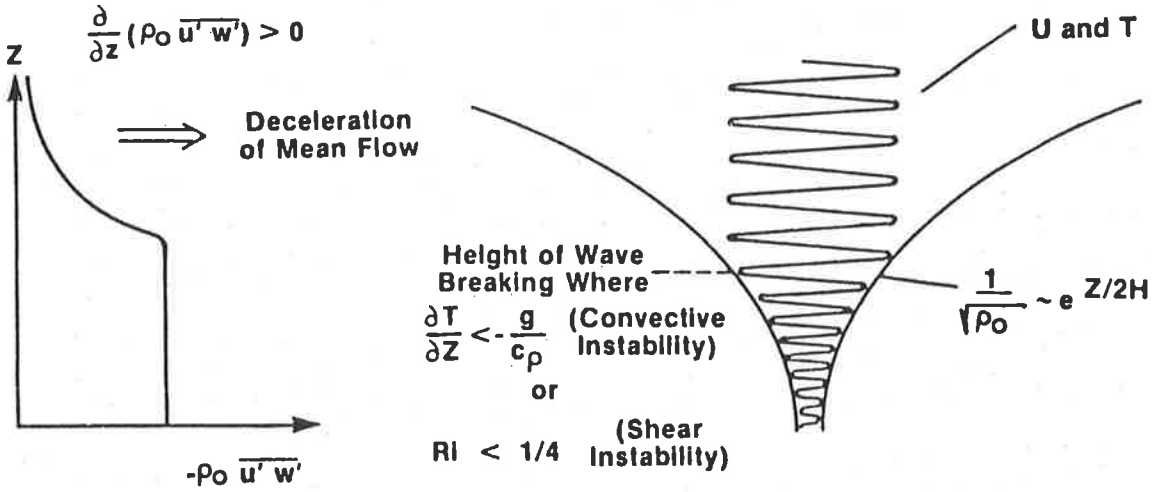

Figure 1.3: A schematic representation of the linear saturation of an upwardly propagating gravity wave (after Fritts *et al.*, 1984).

momentum which causes an acceleration of the mean flow towards the phase speed of the wave. It is in this way that the action of gravity waves is capable of reversing the mean flow.

The net acceleration of the mean flow produced by gravity wave interactions is dependent on the coherence of the gravity wave field. Vincent and Stubbs (1977) estimated that 10 % of the wave momentum was deposited in a coherent manner. This led to an estimated mean flow acceleration of 10 $ms^{-1}day^{-1}$ which is greater than the observed change of about 3 $ms^{-1}day^{-1}$. Vincent and Fritts (1987) found that at least 10 - 20 % of the wave field appeared polarised, particularly in winter. Meek *et al.* (1985a) used estimates of the zonal mean flow acceleration required to balance the Coriolis torque due to the mean meridional wind, to determine the coherence of the wave field. They deduced that approximately 30 % coherence of the wave field was required.

Vincent and Reid (1983) report direct measurements of the upward flux of horizontal momentum ($\overline{u'w'}$ and $\overline{v'w'}$) using a dual-beam Doppler radar. Measurements made over three days during autumn allowed the momentum transport by waves in the 80 - 92 km height range to be calculated. Waves of period greater than 1 h showed only a slight increase in momentum flux with height. The momentum flux due to waves of period less than one hour, on the other hand, increased from -0.4 m^2s^{-2} below 86 km to 0.15 m^2s^{-2} above, implying a convergence of westward momentum and mean flow acceleration of 10 - 20 $ms^{-1}day^{-1}$. They conclude that two-thirds of the body force over this period is caused by the absorption of dominantly shorter period waves. Fritts and Vincent (1987) and Reid and Vincent (1987), using the same technique, find that over 70 % of the zonal drag is due to gravity waves with observed periods less than one hour.

The transport of momentum to the mesosphere has been shown to be dominated by small period waves, even though most of the energy lies in the longer period waves(Vincent,1984a).The larger group velocities and steeper propagation paths of the shorter period waves (periods < 1 h) compensate for their smaller amplitudes. Meek *et al.*(1985b)suggest that at least half the zonal

mean flow acceleration due to gravity waves in the 10 min to 8 h range is produced by those waves with periods between 10 min and 1 h.

The cascading of energy from large to small scale motions accompanies saturation and produces that level of eddy diffusion required to maintain wave amplitudes at the saturation level. VHF radar observations of scattered power made during the equinoxes suggest that energy is being transferred from long period waves to short period waves and turbulence(Royrvik *et al.*, 1982). The correlation time of the scattered signal starts falling off at about 80 km indicating an increase in the number of short period waves in this region. Further evidence is provided by Kalchenko *et al.* (1985) who show that at the height at which there is a maximum in energy of the 1 - 6 h waves, there is often an increase in the energy of the high frequency waves (periods $<$ 30 min) suggesting that energy is being transferred.

Gravity waves propagating upwards in the atmosphere may be reflected or absorbed by the background flow. This is illustrated in ripple tank experiments, as shown in Figure 1.4 (Koop, 1981). Waves propagating into the background flow will be Doppler shifted up in frequency. Total reflection of the wave will occur if the Doppler shifted frequency, known as the intrinsic frequency, equals the local Brunt-Väisälä frequency. A gravity wave propagating in the direction of the background flow will be absorbed if there exists a layer for which the condition

$$\bar{u} - c = 0 \tag{1.4}$$

is met. Such a layer is known as a critical layer.

As a wave approaches a critical layer $\bar{u} - c$ approaches zero and at some stage the saturation condition, given by Equation 1.2, will be satisfied. At this level the wave is said to 'break', causing the production of turbulence and the acceleration of the mean flow. Evidence of critical layer absorption is seen in observations reported by Maekawa *et al.* (1987) who show that waves of vertical wavelength less than 10 km disappear at 85 km where the mean flow reverses.

The spectrum of waves which reach the upper atmosphere from the lower atmosphere is

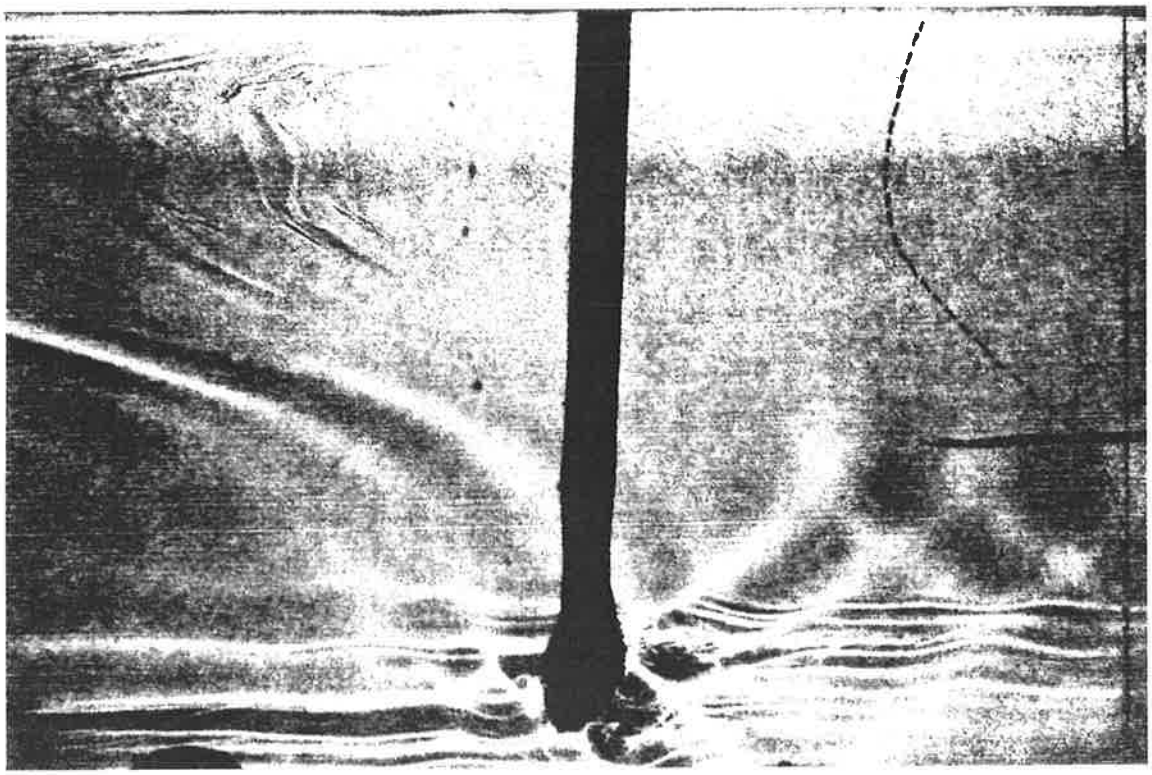

Figure 1.4: Shadowgraph images of the ray pattern generated by an oscillating cylinder in a density stratified medium containing a shear flow. The corresponding velocity profile, measured using a hydrogen-bubble wire, is shown superimposed on the photograph (after Koop, 1981).

determined by the mean wind in the intervening heights. Variations in the mean wind lead to selective filtering of the gravity wave spectrum. Waves generated by tropospheric sources during summer must penetrate a wind profile which is eastward in the troposphere and strongly westward in the stratosphere. As a result only eastward travelling waves with speeds in excess of about 20 ms^{-1} will reach the mesosphere. The mean winds are eastward up to the thermosphere during winter, so westward propagating waves and waves with speeds less than about 10 ms^{-1} eastward will reach the mesosphere (Figure 1.5). Wave activity thus tends to maximise in winter. Meek *et al.* (1985a) find an increase of 3 dB in the wave spectral density from summer to winter for waves in the 10 min to 8 h band.

Waves reaching the thermosphere are subjected to further filtering in the mesosphere. At Saskatoon (52°N), Meek *et al.* (1985a) observe predominantly eastward winds between 90 and 110 km leading to further reduction in the summer wave activity. They find that at an altitude of 106 km only 6 % of the total yearly wave activity occurs in summer compared with 46 % in winter.

A semiannual variation is observed in addition to the annual variation, producing a winter maximum, summer secondary maximum, and equinoctial minima in wave activity. The largest amplitude waves are produced during the solstices when the zonal winds in the middle atmosphere are greatest and are minimum during the equinoxes when the zonal winds are reversing. Vincent and Fritts (1987) suggest that at times of large $\bar{u}$, in the summer and winter, upward propagating waves of phase speed $c < \bar{u}$ can grow to larger amplitudes before the wave breaking condition (Equation 1.2) is attained. Semiannual variations are observed by Manson *et al.* (1981), Meek *et al.* (1985b), and Vincent and Fritts (1987).

Variations in ozone concentration and VHF echo characteristics are indicative of the level of turbulence in the atmosphere. A factor of three increase in the mesospheric ozone abundance from solstice to equinox is caused by a corresponding decrease in the level of turbulent mixing (Thomas and Barth, 1984). VHF echo intensities and return heights also show a strong seasonal

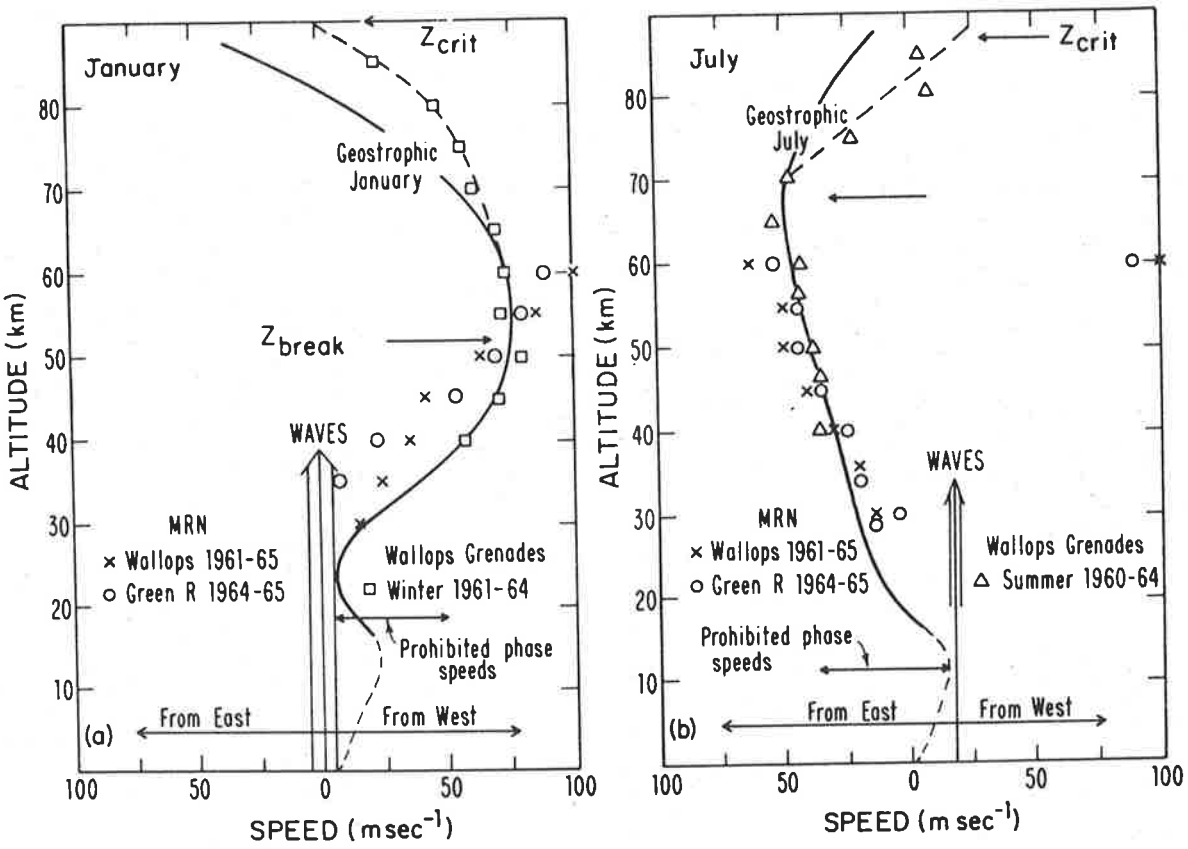

Figure 1.5: Summer and winter zonal wind profiles at Wallops Island with superposed schematic illustrating the filtering of mesospheric gravity waves of tropospheric origin (after Lindzen, 1981).

dependence at the high latitude site of Poker Flat (Balsley *et al.*, 1983). During the winter signal-to-noise (S/N) ratios vary up to 20 dB and the echoes are received from a region centred on a height of 70 km with a half-power width of 9 km. These observations are consistent with the idea that echoes are produced by turbulence generated by the breaking of upward propagating gravity waves. In contrast the summer echoes show a distinct peak at 86 km, approximately the height of the mesopause, with a half-power width of 2 km and a smooth S/N profile. This height is much greater than that predicted by Lindzen for the breaking of gravity waves, implying that the summer echoes are predominantly produced by a different mechanism to the winter echoes.

At the mesopause the Brunt-Väisälä frequency, which is inversely proportional to temperature, is a maximum. For high-frequency waves the dispersion relation is approximated by

$$m = \frac{N}{(\bar{u} - c)}, \tag{1.5}$$

where m is the vertical wavenumber (Fritts, 1984). This suggests that near the mesopause the increasing Brunt-Väisälä frequency is accompanied by an increase in the vertical wavenumber and decrease in the vertical wavelength. Since shorter vertical wavelengths are more rapidly damped, enhanced dissipation is likely to occur at the mesopause and may be responsible for the summer echoes (Van Zandt and Fritts, 1989)

A second mechanism which may be responsible for the summer echoes has been proposed by Balsley *et al.* (1983). They suggest that the summer echoes are primarily the result of shear instabilities produced by low frequency tidal motions near the mesopause. Tidal shears have been estimated to increase by a factor of two to three at and above the mesopause (Avery, as quoted in Balsley *et al.*, 1983). Balsley *et al.* report a diurnal variation in the summertime echo characteristics which lends support to a tidal interpretation. Further support is given by results presented by Fritts and Vincent (1987), who find a strong diurnal modulation in the momentum flux divergence and mean flow acceleration, which correlates with the phase of the diurnal tide.

This section has covered the principal processes by which gravity waves interact with the

environment through which they propagate. While mechanistic models are used to describe interactions of gravity waves with the mean flow, observations of individual wave interactions are difficult. Observations of gravity wave parameters, including momentum fluxes, provide some evidence of these processes. Studies of the climatology of atmospheric gravity waves and turbulence provide useful observational evidence of gravity wave processes.

1.4 THE LOWER THERMOSPHERE IN THE AURORAL ZONE

In this section the nature of the lower thermosphere in the auroral zones during both geomagnetically quiet and disturbed times is discussed. (The auroral zones are defined as the regions where the statistical probability of seeing an overhead aurora is largest. The regions form two approximately circular zones, of radius 22°, centred on the geomagnetic invariant poles). The auroral zone lower thermosphere has characteristics of both the mesosphere and the upper thermosphere. It is penetrated by upwardly propagating tides and gravity waves similar to the mesosphere and is pervaded by the same electric fields that drive the ionization in the upper thermosphere. The aspects of the lower thermosphere which are similar to the mesosphere are discussed in the previous section. The focus of this section will be the upper thermospheric characteristics which are most pronounced in the auroral-zone lower thermosphere during disturbed times.

The lower thermosphere is a complex region to model. In general thermospheric circulation models do not apply below about 120 km while mesospheric models have an upper boundary of about 85 km. Two thermospheric models which appear to have had some success in describing lower thermospheric wind observations will be outlined. However, there is a distinct lack of observational data from the lower thermosphere. Radar observations currently provide most of the data in this height region. The effectiveness of radar techniques when used to measure neutral winds in the presence of large electric fields, as found in the auroral zones, has been questioned. This point will be discussed.

In the quiet ionosphere ionization is produced by solar UV and EUV radiation. During the daytime local maxima in the vertical profile of the electron density define the D, E, and F region peaks (see Figure 1.6). At night rapid recombination at lower altitudes causes the disappearance of the D and E regions, leaving only the F-layer (above about 200 km).

In the disturbed ionosphere particle precipitation leads to enhanced ionization at heights dependent on the energy spectrum of the incoming particles. The auroral electron spectrum is relatively soft (of the order 5 to 10 KeV) and peak ionization rates occur between 100 and 130 km. During solar proton events the relatively hard proton spectrum (up to a few hundred MeV) produces peak ionization rates between 60 and 90 km (Ratcliffe, 1972; Vallance Jones, 1974).

Electric fields are generated in the magnetosphere, where the solar wind produces circulatory movements in the plasma. Figure 1.7 shows how the electric field maps down the magnetic lines of force into the auroral zone and polar cap regions. Here they drive a current system in the polar ionosphere. The currents are enhanced during disturbed conditions, when the strength and extent of the polar electric field increases and ionospheric conductivities are enhanced.

The electric field influences particle motions in a manner which is dependent on the gyro-frequency of the charged particles and the collision frequency. At heights above 200 km, where the collision frequency is low compared to the gyro-frequency, no net current flows since both the electrons and ions are driven in the same direction by the electric ($\mathbf{E}$) and magnetic ($\mathbf{B}$) fields. The plasma flows in the direction of the $\mathbf{E} \times \mathbf{B}$ force producing a convection pattern consisting of two oppositely directed circulation cells, as shown in Figure 1.8. The flow is anti-sunward across the polar cap and sunward in the dawn and dusk sectors of the auroral oval. Momentum is transferred from the ions to the neutrals via collisions causing the neutral wind to move with the plasma flow. This process is known as 'ion drag'.

The collision frequency increases with decreasing altitude, becoming greater than the ion gyro-frequency below 140 km and greater than the electron gyro-frequency below 80 km. Be-

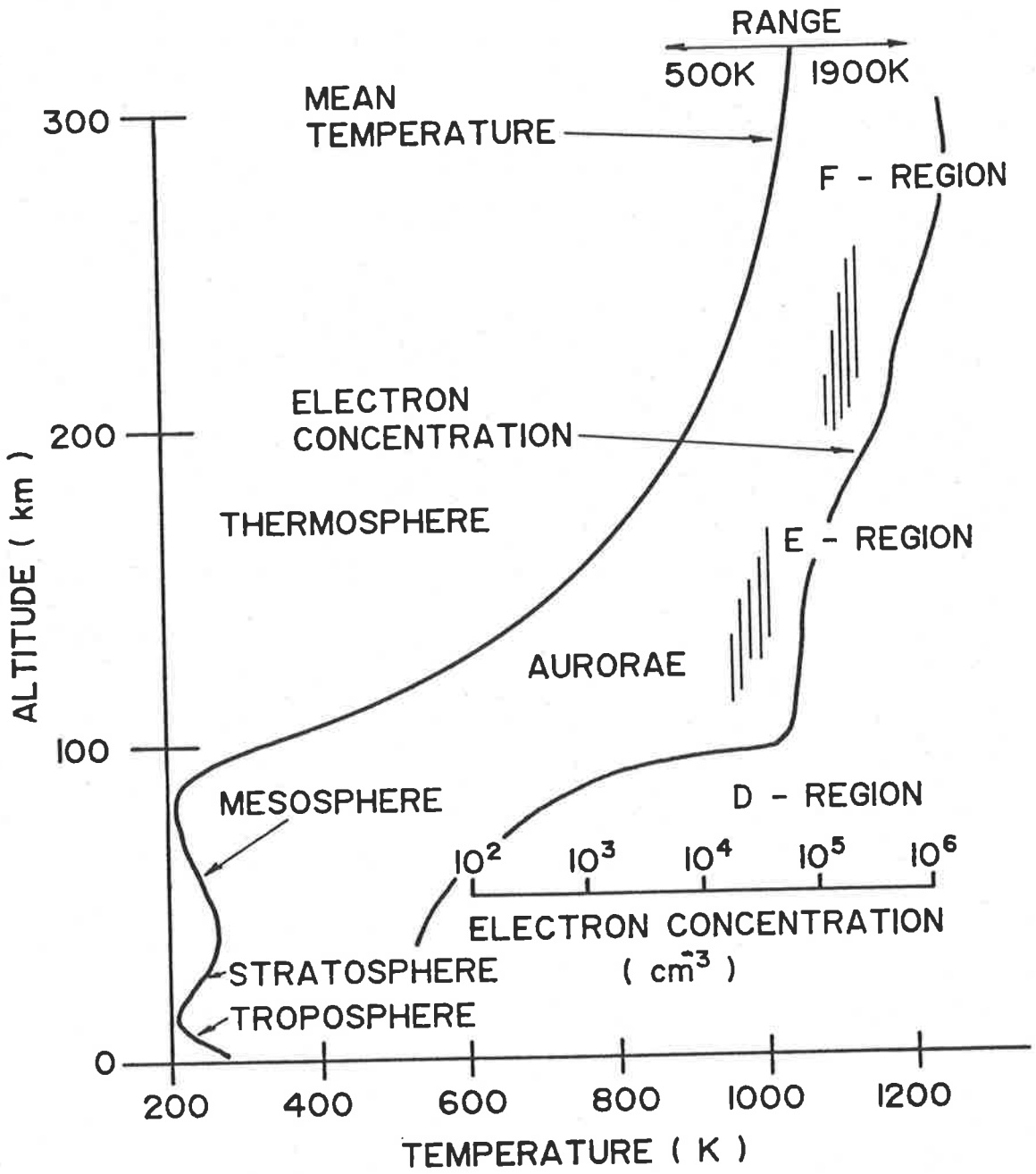

Figure 1.6: Vertical profiles of temperature and electron density define the regions of the earth's atmosphere (after Cole, 1987).

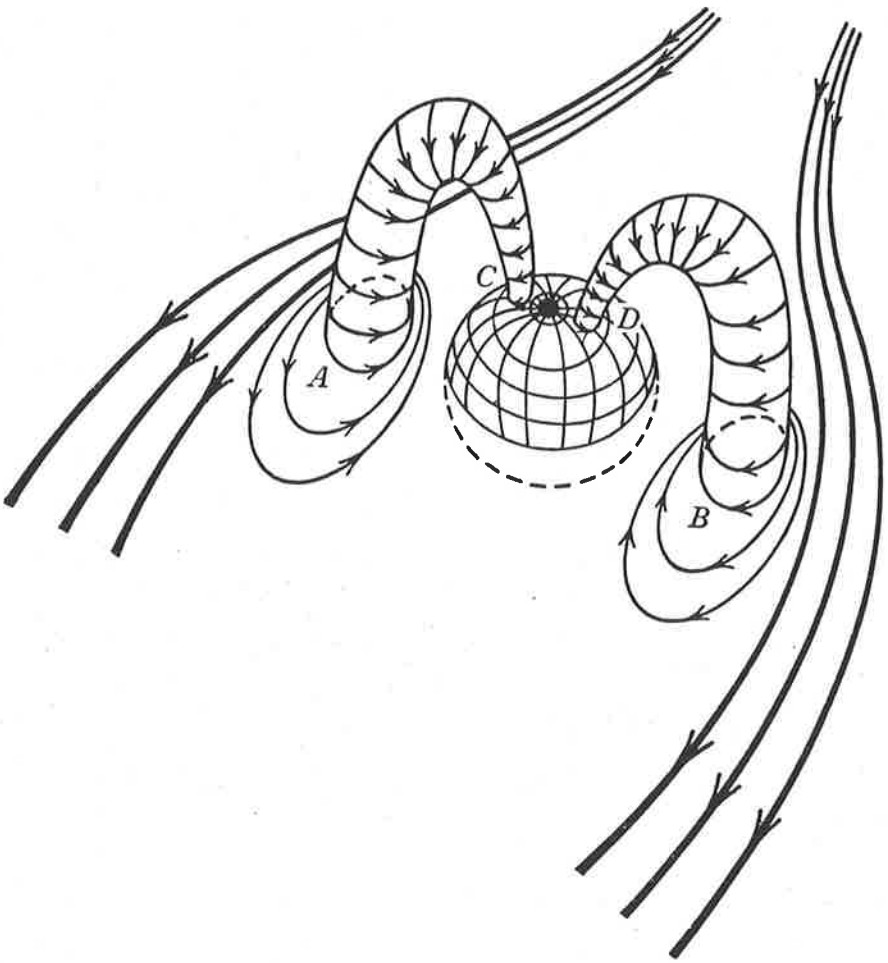

Figure 1.7: Circulatory motions of the plasma in the magnetosphere (at A and B) are mapped down to the ionosphere via the magnetic field lines producing a current system in the polar ionosphere (at C and D), (after Ratcliffe, 1972).

tween these two heights lies a region where electrons are driven by the electric field but the ions are not, and a current system is set up. As the collision frequency increases the drift direction of the charged particles shifts away from the direction of $\mathbf{E} \times \mathbf{B}$ and approaches a direction parallel to $\mathbf{E}$. At the height where the collision frequency equals the gyro-frequency of the charged particle, the particle will drift in a direction halfway between the $\mathbf{E} \times \mathbf{B}$ and $\mathbf{E}$ directions (Ratcliffe, 1972).

Ion drag is the dominant force acting on the high-latitude neutral atmosphere above about 150 km, but it is completely ineffective below 60 km. The upper mesosphere/lower thermosphere lies within a region of transition between these two extremes.

The response of the thermosphere to a geomagnetic substorm has been investigated by Fuller-Rowell and Rees (1984), using a three-dimensional model. The results suggest that ion drag is effective down to altitudes of 120 km. A comparison of the model response at altitudes of 120 and 240 km suggest three basic differences. Firstly, it confirms that during disturbed periods the flow at 240 km is in the $\mathbf{E} \times \mathbf{B}$ direction while at 120 km the winds are shifted toward the direction of $\mathbf{E}$. Secondly, the recovery phase of the substorm is found to proceed far more quickly at 240 km than at 120 km, since in the lower thermosphere kinematic viscosity is significantly less. Finally, during geomagnetically quiet times, ion drag continues to be effective in the lower thermosphere, while in the upper thermosphere the winds are driven in a general anti-sunward direction by the day-night pressure asymmetry.

A major source of heating in the lower thermosphere is the complex set of strong and often localised current systems which are set up in the auroral zone ionosphere. Joule dissipation of the currents produces heating rates, maximising between 120 and 150 km, which can exceed the heating due to solar radiation. Theoretical simulations of Joule heating in the auroral zones suggest that meridional circulation cells extending to mid-latitudes may be set up during periods of intense heating (Blanc and Richmond, 1980). Expansion of the heated region causes an upwards and equatorwards flow. Cooling and sinking occurs at mid-latitudes and a poleward

flow is established at lower altitudes.

Equatorward flows thought to be produced by a meridional circulation cell have been reported by Mazaudier and Bernard (1985). They use the Saint-Santin incoherent scatter radar to measure the meridional neutral winds using the assumption that the ion drift velocity parallel to **B** is identical to the neutral wind component along **B**. Observations were confined to the daytime. A study of four storms reveals that: above 150 km equatorward winds are only seen on disturbed days, down to 110 km winds tend to equatorward on disturbed days, and at 100 km the disturbance effects are hardly visible. Intensification of the equatorward flow during storm-times is found down to at least 120 km. The return poleward flows were barely detectable.

The ion drag model of Fuller-Rowell and Rees predicts equatorward winds in the morning hours, with an enhanced equatorward component persisting from about midnight until midday during disturbed conditions. It is therefore only in the afternoon and early evening hours that the ion drag model and the meridional circulation cell model conflict. The results of Mazaudier *et al.* show a strong equatorward component in the wind field during the afternoons of two of the four periods discussed. This suggests that on those occasions Joule heating was the principal forcing mechanism.

Meteor, MST, and partial reflection radars deduce the neutral wind velocity and directions from the motion of small scale irregularities in the refractive index. In the upper mesosphere/lower thermosphere the refractive index irregularities are due to corresponding irregularities in the electron density. Reid (1983) suggests that in the presence of electric fields the ionized irregularities will be driven mainly by the electric field rather than by the neutral wind. Reid calculates the drifts that occur in the presence of a moderately enhanced electric field (50 mV m^{-1} in the meridional direction and 10 mV m^{-1} in the zonal direction). Significant drifts of at least 10 ms^{-1} are induced down to altitudes of 90 km in the meridional direction and down to 100 km in the zonal direction. The drift velocity increases rapidly with altitude for

both components. These results suggest that in the auroral zones, during disturbed conditions, 'wind' velocities measured using radar techniques may depart from the neutral wind vectors.

An interesting comparison of concurrent meteor, auroral, and partial reflection radar observations is presented by Prikryl *et al.* (1986). It is usually assumed that meteor and partial reflection radars measure the neutral winds. In this experiment, meteor and partial reflection wind data between 90 and 100 km were compared with the auroral radar measurements of the $\mathbf{E} \times \mathbf{B}$ Hall drift of electrons around 105 km. During a disturbed period the meteor/auroral radar measured large equatorward flows around local midnight, while the partial reflection radar, situated 500 km further south (equatorward), measured only a small equatorward wind. Prikryl *et al.* conclude that meteor trails become decoupled from the neutral medium when the electric field is large enough, in this case around midnight, whereas the effect on the irregularities observed by the partial reflection radar is not as strong. They suggest the difference lies in the shape and density of the irregularities. The meteor trails are cylindrical and more ionized than the turbulent irregularities measured by the partial reflection radar. Prikryl *et al.* do not consider the effects of local heating to be significant and suggest that the 500 km separation of the facilities does not explain the difference in the observations.

The discussion so far suggests that down to at least 120 km altitude the ion drag force can drive the neutrals in the direction of the charged particles. The ion drag force increases during disturbed times when ionization and the electric field are enhanced. The increased electric field may also cause ionized irregularities to become decoupled from the neutral wind vector down to about 90 km, implying that at such times radar techniques no longer measure the neutral wind. These two mechanisms produce the same result: the measured 'winds' increase and shift away from the direction of $\mathbf{E} \times \mathbf{B}$ and towards the direction of $\mathbf{E}$ when the electric field strength is increased.

A correlation between radar 'wind' measurements and geomagnetic activity, has been observed at a number of high latitude sites. Meteor observations at College, Alaska (Hook, 1970),

and Syowa, Antarctica (Ogawa, 1986), show generally enhanced 'winds' during active periods. MST radar observations at the mesopause above Poker Flat, Alaska, find the zonal 'wind' component to be enhanced during a period of increased electrojet activity (Balsley *et al.*, 1982). In contrast Johnson and Luhmann(1985a), who analysed three summers of mesospheric data from the same site, found no consistent response to activity. Observations by Manson and Meek (1986), over a two year period, show a rather weak correlation between the 10 min to 1 h spectral component at 100 km and the Ap index. An increase in the diurnal variation of the wind, above 95 km, during periods of high Kp is seen in partial reflection radar data from Mawson, Antarctica (Phillips and Jacka, 1987). The data show a maximum northward component near dawn which is enhanced at times of high Kp. Figure 1.8 shows that the direction of plasma flow in the lower thermosphere at a particular site rotates 360° in a day, thus producing a diurnal component in the drift direction. At Mawson this direction is geographically northward around dawn, consistent with the observations.

In the case of radar measurements, it is not possible to distinguish whether the neutral winds are enhanced or the ions are becoming decoupled from the neutrals during active times. Optical measurements of the atomic oxygen λ558 nm emission can be used to determine the neutral wind in the lower thermosphere. In the auroral zones, and particularly during auroral substorms, the measured emission is principally from the visible aurora and hence the emission height is dependent on the energy spectrum of the incoming particles.

Fabry-Perot spectrometer measurements by Jones and Jacka (1985, 1987) estimate the emission height to be between 100 and 130 km. Night-time observations of the λ558 nm emission at Mawson, Antarctica, show the neutral winds to be enhanced during geomagnetically disturbed periods (defined as Ap $>$ 20). The neutral wind field is found to be well described by the 'ion drag' model of Fuller-Rowell and Rees, suggesting that ion drag may be an effective driving mechanism down to 100 km in the lower thermosphere.

Interest in the lower thermospheric region is increasing. The CEDAR (Coupling, Energetics

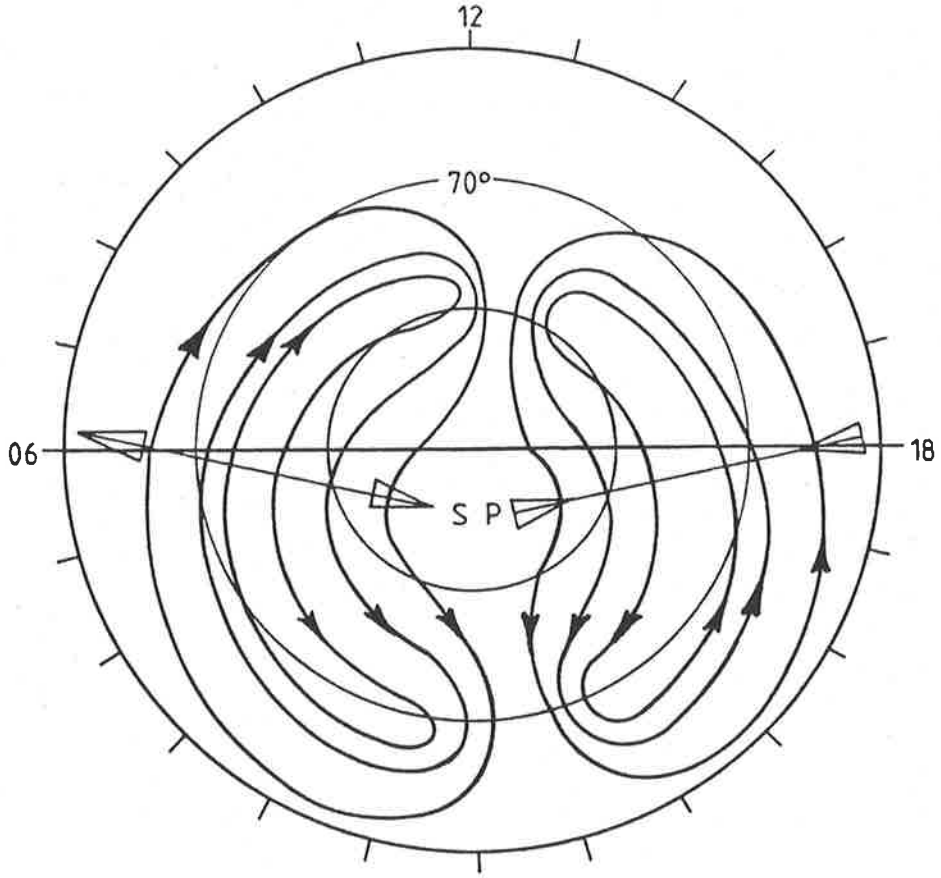

Figure 1.8: Equipotentials of the high latitude electric field. In the upper thermosphere plasma is convected roughly parallel to these, in the $\mathbf{E} \times \mathbf{B}$ direction which is indicated by the small arrows for the southern hemisphere. Large arrows indicate the approximate direction of the electric field, $\mathbf{E}$, across the dawn-dusk meridian. Plasma flow in the lower thermosphere is in a direction between $\mathbf{E}$ and $\mathbf{E} \times \mathbf{B}$. Coordinates are invariant latitude and magnetic local time (adapted from Heelis *et al.*, 1982).

and Dynamics of the Atmospheric Regions) committee organised a Lower Thermospheric Coupling Study (LTCS) workshop and observational campaign to look at the 70 to 140 km level. Some of the problems highlighted at the workshop included the removal of F-region and auroral contamination effects from λ558 nm Fabry-Perot determinations, and the need for comparing Fabry-Perot and radar determinations of winds (Romick, 1987). The latter is required to determine the effectiveness of radar observations in measuring the neutral wind in the auroral zone.

This section has looked at the effectiveness of the ion drag force and Joule dissipation of currents in driving the winds in the lower thermosphere. Measurements of the wind in the auroral zone lower thermosphere, using both radar and optical techniques, show the wind field to be generally enhanced during geomagnetically active times. In the case of Fabry-Perot observations the enhanced wind may be due to either Joule heating or ion drag, while for the radar measurements it may indicate that the neutral wind becomes decoupled from the reflecting irregularities.

1.5 GRAVITY WAVES GENERATED IN THE AURORAL ZONES

Gravity waves play an important role in the global redistribution of geomagnetic energy. Energy is deposited in the auroral zones giving rise to thermospheric perturbations which propagate away from the source region as travelling ionospheric disturbances (TID's). These are ionospheric manifestations of gravity waves and they have been categorised by Georges (1968) into large and medium scale waves. Large scale waves have horizontal speeds in excess of 300 ms^{-1} (approximately the speed of sound in the lower atmosphere) while medium scale waves have speeds less than 300 ms^{-1}. The phase speed of gravity waves generated in a region cannot exceed the speed of sound in that region. It follows that large scale TID's are generated in the thermosphere, while the more frequently occurring medium scale TID's are generated in both the lower and upper atmosphere.

The main thermospheric sources of gravity waves lie in the auroral zones and have been reviewed by Hunsucker (1982). The principal generation mechanisms are the effects of Joule heating, the Lorentz force, and particle precipitation. Theoretical studies of thermospheric gravity waves have been carried out by Chimonas and Hines (1970), Testud (1970), Francis (1975), Richmond and Matsushita (1975), Richmond (1978), Luhmann (1980), Waltersheid and Boucher (1984), Rees *et al.* (1984a, 1984b), and Mayr *et al.* (1984a, 1984b).

The generation of a broad spectrum of wavelengths accompanies geomagnetic energy input. Near the source region trapped modes are dominant and a rich spectrum of waves is present. Short period waves are largely dissipated within one wavelength of the source. Outside of the source region energy is transported globally by propagating modes. Waves may be freely propagating, reflected from either the base of the thermosphere or from the earth's surface, or they may be ducted between these two regions. Only long period waves propagate to mid and low latitudes where they are observed as quasi-monochromatic waves.

Transfer functions are used by Mayr *et al.*(1984a,b)to model the response of the thermosphere to time dependent sources. The propagating gravity waves are mainly launched as the source is turned on or off i.e. they appear as a transient response analogous to ringing in an electrical circuit. "Near the source, their pulse durations are typically of the order of 20 min and are determined, through the dispersion relation for gravity waves, by the horizontal dimension of the source (approximately 700 km)" (Mayr *et al.*).

Vertical wind measurements are sensitive to local heating and gravity wave motions. Since the mean vertical wind is approximately zero, perturbations in the vertical wind are more readily identified than are perturbations in the horizontal wind component. Fabry-Perot spectrometer observations of the F-region wind field show rapid upward motions, sustained for periods of 15 - 30 min, accompanying auroral disturbances (Wardill and Jacka, 1986; Rees *et al.*,1984a; Herrero *et al.*, 1984). The vertical winds in the lower thermosphere have been shown to reverse in a time scale of about 30 min. Upward winds were measured during the passage of a low altitude

auroral arc while downward winds were measured during a high altitude aurora (Peteherych *et al.*, 1985). These perturbations may be interpreted as manifestations of gravity waves.

In the auroral zones gravity waves are generated during auroral substorms. In the near field, the presence of both trapped and propagating modes may appear as impulsive disturbances in the velocity field.

Chapter 2.

THE SPACED ANTENNA PARTIAL REFLECTION TECHNIQUE

2.1 INTRODUCTION

The spaced antenna partial reflection (SAPR) technique provides a simple method of measuring horizontal wind velocity throughout the D-region and into the lower E-region of the ionosphere. Wind measurements determined using this technique were first reported by Fraser (1965, 1968) and have since been used at a number of mid and low latitude sites (Stubbs, 1973; Gregory and Rees, 1971; Vincent and Ball, 1981). A SAPR radar was installed at the high latitude site of Mawson, Antarctica (68°S, 63°E) during 1981 (Macleod and Vincent, 1985; Macleod, 1986), and another at Scott Base (78°S, 167°E), Antarctica in 1982 (Fraser, 1984).

2.2 INSTRUMENTATION

The SAPR radar was first operated at Mawson, Antarctica during the summer of 1981 / 82. During 1984, the receive and transmit antenna arrays were rebuilt and a modified system, including an on-line computer, was installed. The new system has operated almost continuously since July, 1984.

The SAPR radar operates in a pulsed mode at a frequency of 1.94 MHz, transmitting from a vertically directed array. Three receiving antennas are located at the apexes of an equilateral triangle, with sides of length 150 m. The receiving antennas detect weak echoes backscattered from irregularities in the refractive index. The fading of echoes is recorded at the three receivers, and the horizontal motion of the irregularities is deduced from measurements of time shifts between the fading records.

The layout of the SAPR radar at Mawson is shown in Figure 2.1. In order to conform to station requirements, the transmitting and receiving arrays lie within areas designated electrically active and electrically quiet, respectively. The transmitter is housed in a building located close to the transmitting array. The receivers, timing and control electronics and data logger are

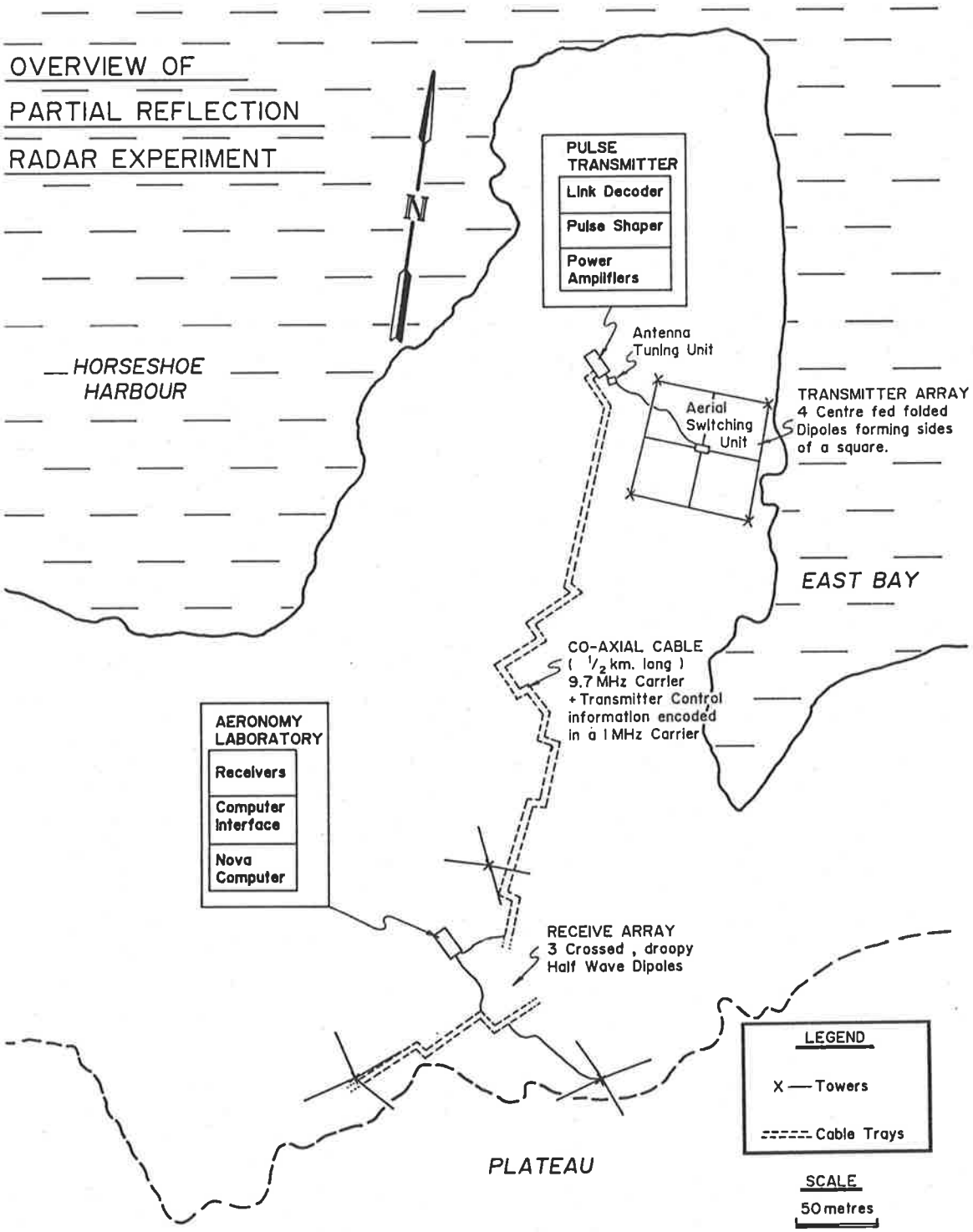

Figure 2.1: The layout of the SAPR radar at Mawson showing the relative positions of the transmitting and receiving arrays.

housed in the aeronomy laboratory, which is situated within the receiving array. A 500 m long coaxial cable carries transmitter control information and a 9.7 MHz carrier from the aeronomy laboratory to the transmitter hut. The carrier wave is fed to the transmitter at five times the transmitted frequency, to avoid direct feedback with the transmitter. The cable is secured to a cable tray for most of its length.

2.2.1 The Transmitter

The transmitter has a peak power of 5 kW and a pulse width of 30 μsec (giving a range resolution of 4 km). A block diagram of the transmitter is shown in Figure 2.2. The 9.7 MHz carrier and transmitter control signals are generated by the control electronics in the aeronomy laboratory. They are split at the transmitter interface electronics and the control signals decoded. The 9.7 MHz carrier is divided by five, amplified, then modulated with a 20 Hz Gaussian shaped pulse. The output is amplified to produce a Gaussian shaped output pulse with a peak to peak voltage of 1.6 kV into a 75 ohm load. The transmitter output is matched to the 600 ohm twin line feeders of the transmitting array at the antenna tuning unit (ATU) which is located outside the transmitter building.

The transmitting array consists of four, centre-fed, half-wave, folded dipoles which are suspended 10 m off the ground from four towers. The array forms a square with sides of length one half wavelength. The transmitted beam has an ideal polar diagram of width $\pm 20°$ at the half power points. The SAPR radar can transmit both right and left-handed circularly polarised waves, corresponding to the ordinary and extraordinary magneto-ionic components. An aerial switching unit (ASU) lies at the centre of the array and is connected to each dipole by a half wavelength open feeder. The polarisation of the transmitted wave is set by introducing a $\pm\frac{\pi}{2}$ phase shift between the dipole pairs.

The transmitter is usually set to transmit the extraordinary component at Mawson, as operation in this mode generally results in stronger reflections from heights below the E-region.

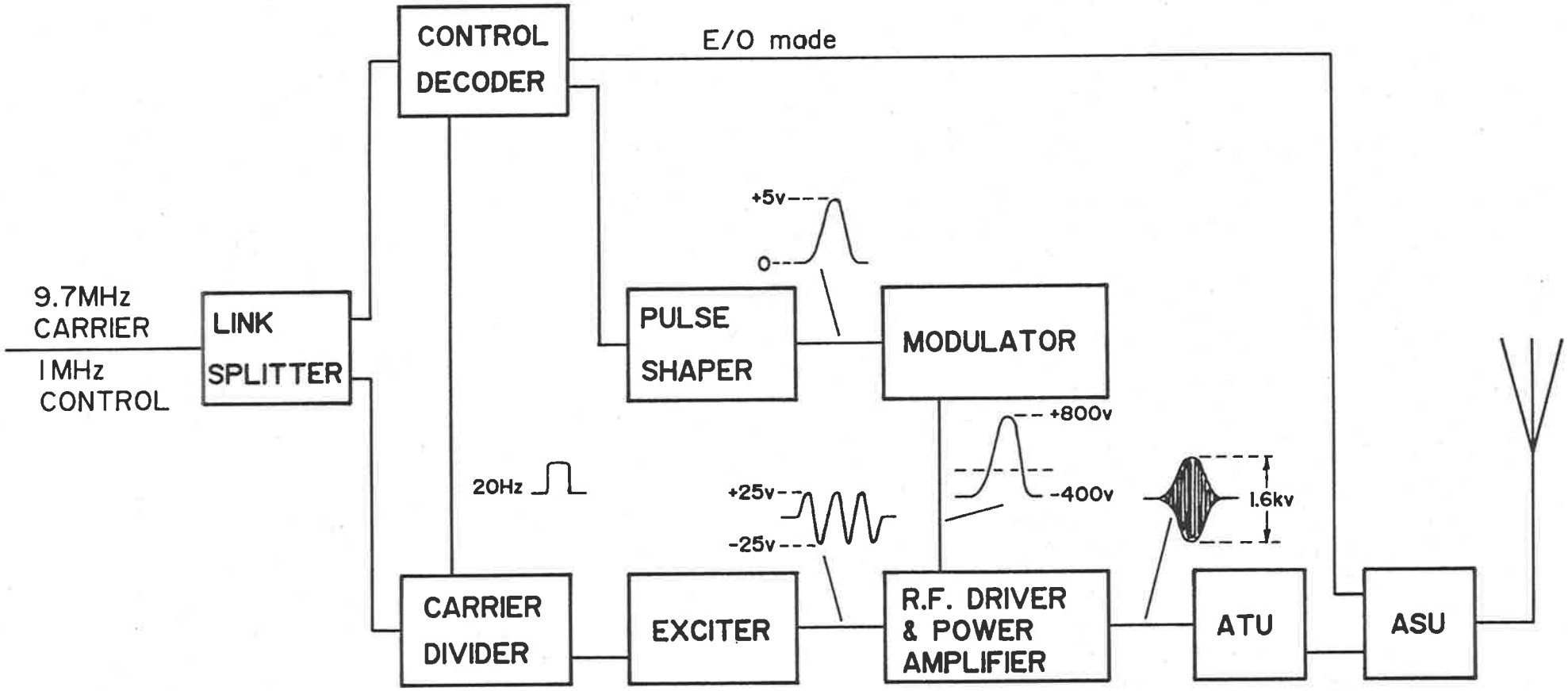

Figure 2.2: Block diagram of the SAPR transmitter at Mawson.

2.2.2 The Receivers

The three receiving antennas each consist of two crossed, half-wave, droopy dipoles which are centre fed and tuned to be resonant at 1.94 MHz. Balun boxes located at the top of each receive tower match the balanced lines, which form the antenna, to the unbalanced coaxial feed lines. The coaxial cables run from the receive towers to the receiver chassis, which is located inside the aeronomy laboratory. The sense of polarisation of the received wave is matched to that of the transmitted wave by introducing a $\frac{\pi}{2}$ phase shift between the crossed dipole pairs.

The receivers have a gain of 100 dB and a bandwidth of 25 kHz. The receivers are two channel, recording both the in-phase and quadrature components of the signal. The signal to noise ratio is improved by a factor of 8 by coherently integrating the complex waveform over 8 consecutive pulses (Vincent, 1984b). The pulse-repetition frequency is 20 Hz and the effective sampling rate after preintegration is 2.5 Hz. The height range covered by the radar produces a large dynamic range of echo strengths which is accommodated by sampling over three-overlapping height ranges (usually 70 - 90 km, 80 - 100 km, and 90 - 110 km). The receiver gains are set appropriately for each height range. On occasions when low reflections are apparent a start height of 60 km may be used. A block diagram of the receivers is shown in Figure 2.3.

2.2.3 Data Logging

Data are acquired over a height range (20 km) for 2 min out of every 5 min. On-line analysis is carried out by the Nova 2 computer during the remaining 3 min. The analysed wind data, correlation parameters and receive antenna signal-to-noise ratios are monitored continuously on a VDU. If either the signal is too weak, or any of a number of analysis criteria are not satisfied for a particular height, no wind measurement is obtained and an error code is displayed. Data are recorded on 7.5 inch floppy discs which hold 5 days data.

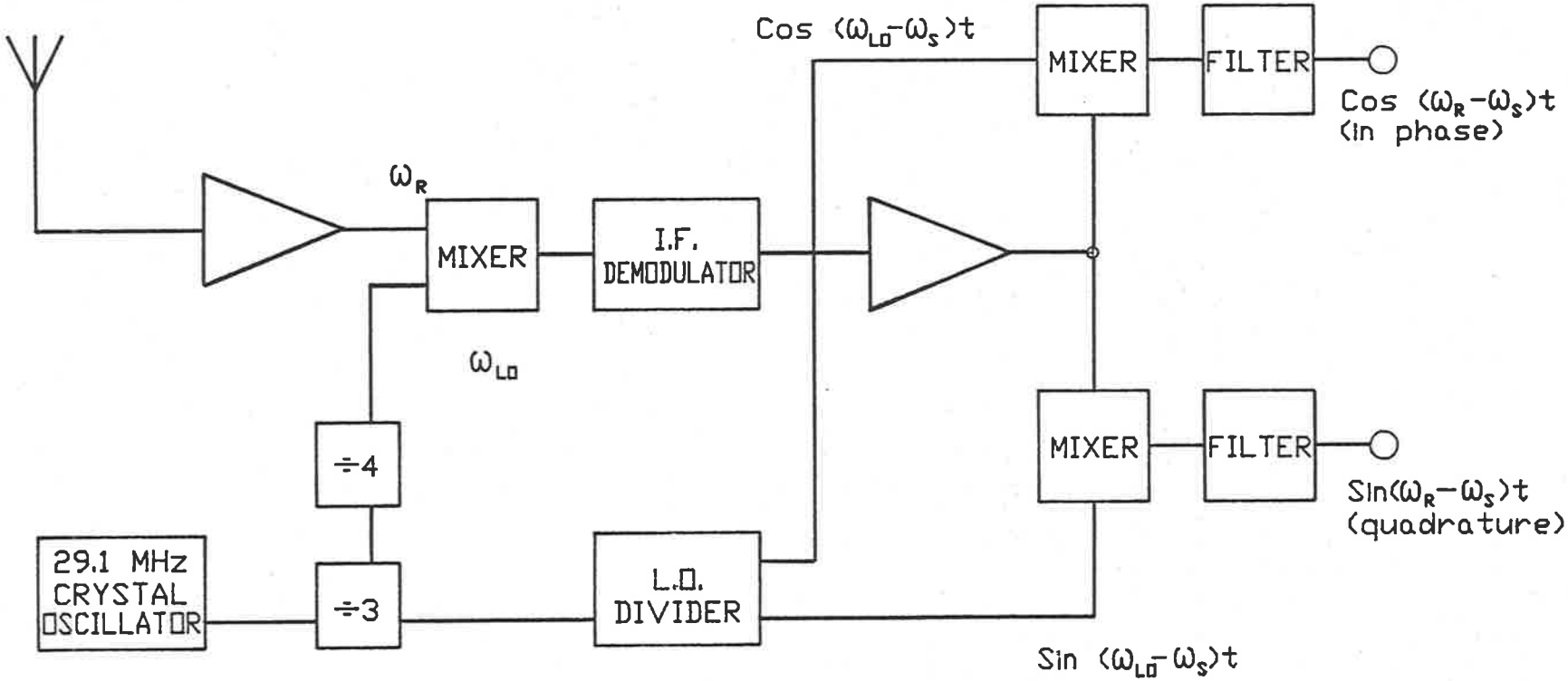

f_R = 1.94 MHz (received)
f_S = 1.94 MHz (standard)
f_{LO} = 2.425 MHz

Figure 2.3: Block diagram of the SAPR receivers showing the steps involved in recording the in-phase and quadrature components of the signal.

2.3 OPERATION DURING 1985

The SAPR radar operated almost continuously throughout 1985 with a total downtime of only 2 weeks. Routine work on the antenna arrays was carried out during the summer of 1984/1985 by the author and the 1984 expeditioner who installed the system, Andre Phillips. The receiving array was tuned by trimming the antenna wires which had stretched since they were erected the previous summer. Balun boxes were installed on top of each tower to match the coaxial feed lines to the antenna wires. The two antenna towers which are situated in close proximity to buildings were extended to improve the received signal-to-noise ratio. It was found unnecessary to extend the third tower as it is situated in a relatively quiet position 75 m from the nearest building (Figure 2.4)

During the 1985 winter season the experiment was operated and maintained by the author without any dedicated support staff. Some technical assistance was given by the electronics engineer from the Ionospheric Prediction Service, Mark Loveridge. The main hindrances to the operation of the SAPR radar at Mawson are the persistent strong winds (averaging about 35 km/hour) and blizzards. Blizzard conditions were experienced for 32 days during 1985, with winds up to 170 km/hour and drifting snow.

Data acquisition was substantially reduced during blizzards because drifting snow carried static charge which produced excessive noise in the receivers. The data acquisition rate remained unimpaired however, on occasions when the receiving antenna wires remained above the drifting snow. Blizzards often damaged sections of the antenna arrays or caused electrical short circuits in the feeder lines. Bad weather also caused faults to develop in the exposed connectors on the ATU and balun boxes.

Regular transmitter overhauls were carried out in the first few months of 1985, when several valves were replaced and blown transistors found in the shaping circuit. Work was carried out to improve the RF shielding of the transmitter control signals which are fed down the cable from the aeronomy laboratory. A low pass filter and 5.82 MHz trap were installed which reduced in-

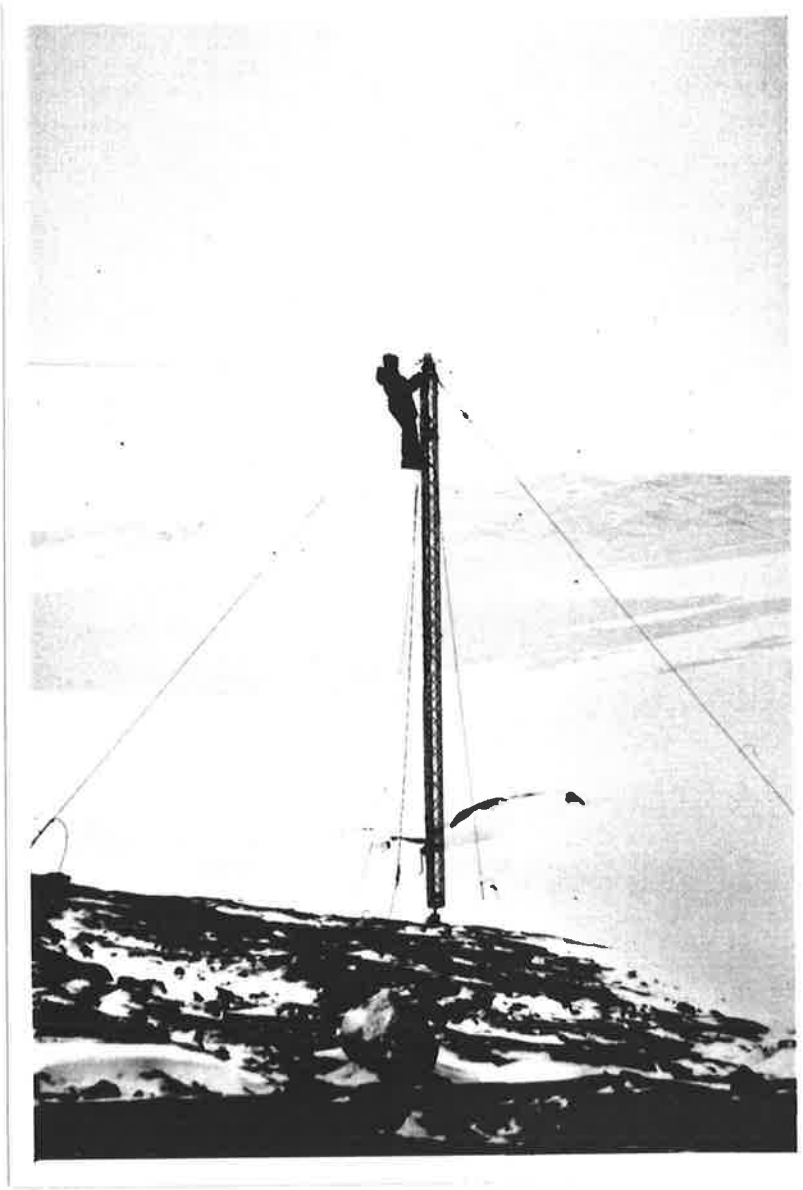

Figure 2.4: The author repairing one of the three receiving antennas which is situated in an electrically quiet location approximately 75 m from the nearest building on the edge of the plateau.

terference to the station communication receivers. Throughout the year the transmitter output was checked monthly and tuned to produce a clean output pulse of maximum voltage.

External cables which run to the antenna arrays and along the 0.5 km line to the transmitter building were maintained throughout the year. Worn cables were often found to be responsible for reduced receiver performance or noise on the transmitter control line. Cables are secured to cable trays or towers where possible, otherwise they are layed on the ground and covered by rocks. There were two occasions during the year when ground cables within the receiving array were severed by vehicles.

The SAPR radar is one of the most 'efficient' experiments operated at Mawson. High time resolution data are obtained over a range of heights with little operator intervention. The major problems encountered during the year were associated with the harsh environmental conditions experienced. Generally the experiment has proved capable of withstanding such conditions and with the features of low cost and simplicity, it has been proved most worthwhile.

2.4 THE FULL CORRELATION ANALYSIS

The full correlation analysis (FCA) is used to determine the velocity of the ground diffraction pattern formed by the interference of radio waves reflected from irregularities in the ionosphere. The diffraction pattern moves with a velocity of twice that of the reflecting region due to the so called 'point source' effect (Briggs, 1980). The FCA is well described by Briggs (1984).

The ground diffraction pattern consists of a randomly changing, two-dimensional moving pattern which can be described by a spatial and a temporal autocorrelation function. The spatial correlation function can be approximated by a family of similar ellipses. The ellipse for a correlation value of 0.5, which is often referred to as the characteristic ellipse, is used as measure of the scale of the irregularities in the random pattern. At Mawson, three parameters are recorded to describe the size, elongation and orientation of the characteristic ellipse for each wind-data point.

The temporal autocorrelation function describes the variation of the diffraction pattern with time, as measured by a fixed observer. The temporal correlation function is assumed to have the same functional form as the spatial correlation function and the time taken for the temporal auto correlation function to fall to 0.5 is calculated in the analysis.

The 'true velocity' of the diffraction pattern, Vt, is defined as "the velocity of an observer who so adjusts his[/her] motion to obtain the most slowly decreasing auto-correlation function i.e. the slowest possible rate of fading" (Briggs, 1980). An 'apparent velocity', designated Va, can be calculated from the distance between the receivers and the average time delay for maximum cross correlation between pairs of receivers. The velocity Va "will in general be too large and its direction ϕ_a will be incorrect due to the neglect of random changes and anisometry" (Briggs, 1980). The difference between Vt and Va indicates the size of the correction applied to the data in allowing for random changes and anisometry. The larger the correction, the larger is the uncertainty in the true velocity as determined by the FCA. Briggs recommends that data should be rejected if the correction is large, and the following rejection criteria are suggested.

$$\text{Va} > 3 \times \text{Vt}$$

$$\text{Va} < 0.5 \times \text{Vt}$$

$$|\phi_a - \phi_t| > 40°$$

Further rejection criteria recommended by Briggs are-

a) the mean signal is either very weak or so strong that the receivers are saturated most of the time

b) the fading is very shallow

c) S/N ratio < -6 dB

d) the fading is too slow

e) the cross correlation functions are oscillatory

f) the percentage time discrepancy (PTD), which is the sum of the time displacements taken in pairs around the triangle of antennas, is greater than 20% of the sum of the absolute

time delays around the circle (i.e. added without regard to sign).

The final criterion was introduced in order to reject cases where the wrong maximum had been used in the cross-correlation analysis. A recent study by May (1988) has shown that if the PTD limit is set too low then statistical fluctuations may cause many records, for which the identification of the maximum is quite correct, to be rejected. May used a PTD limit of 30%, but he suggested that "consideration should be given to relaxing the condition still further". The value of 30% was adopted in this work as it was considered a reasonable compromise between the values recommended by Briggs and May.

2.5 THE NATURE OF THE SCATTERERS

2.5.1 Introduction

The nature of the irregularities responsible for the partial reflection of HF radio waves has been discussed in the literature since the partial reflection technique was first used in 1953 (Gardner and Pawsey, 1953). The technique was originally applied to the determination of the electron density in the D-region, using the so called differential absorption method, and later to measurements of mesospheric winds. Despite continued use of the technique the nature of the structures which cause the echoes is not fully understood (Hocking and Vincent, 1982a; Manson and Meek, 1984).

In the lower ionosphere, variations in the electron density are generally assumed to be the principal cause of variations in the refractive index which produce scatter at HF and VHF (Belrose *et al.*, 1972; Rastogi *et al.*, 1982; Hocking and Vincent, 1982a; Manson and Meek, 1984). A comparison of the electron density profile, as measured by a rocket borne Langmuir probe, with simultaneous HF partial reflection observations have been reported by Hocking and Vincent (1982a). It was found that the heights of observed partial reflection echoes could be related to features in the electron density profile, namely ledges of increasing and decreasing electron concentration and a region of irregular electron density fluctuations.

Irregularities in the neutral atmosphere are imparted to the ionized component and result in irregularities in the refractive index. These appear to be generated by two basic mechanisms: turbulent mixing of the vertical gradient of refractive index and the occurrence of stable, horizontally-stratified laminae of sharp gradients in the refractive index (Royrvik, 1983). There is experimental evidence in the literature of both types of scattering, with a number of authors having successfully modelled results assuming turbulent (or volume) scattering, and others Fresnel scattering. Before embarking on a discussion of these observations and results, an outline of the principal forms of turbulence is presented.

2.5.2 The Role of Turbulence

Turbulence may be defined as "any set of zero-mean motions which are too random to describe by concepts such as waves, or any ordered phenomena" (Hocking, 1981). The effects of turbulence in the atmosphere are to deposit mechanical energy as heat, and to increase the rate of diffusion. The following discussion is based on the work of Hocking (1981).

Turbulence is generated in large eddies by any of a number of processes including rotation started by wind shear, thermal processes, and the breaking of gravity waves. The large scale motions generate smaller scale motions which in turn produce still smaller motions until limited by viscosity. The effects of gravity cause the larger scale motions to become anisotropic whereas eddies of tens and hundreds of meters in size are isotropic.

The energy spectrum of atmospheric turbulence is readily divided into four sub-ranges according to eddy size. The largest scale eddies fall into the buoyancy range where buoyancy effects are dominant and the eddies are anisotropic. In this range energy not only propagates down the scales but is also lost in the generation of incoherent gravity waves. Smaller scale eddies lie in the inertial range of turbulence, where the turbulent energy just propagates down from larger to smaller scales. At the bottom end of the scale is the viscous range where energy is dissipated at wavelengths too small to be maintained against the effects of viscosity. The

Tschen range is a transition region between the viscous and the inertial ranges.

Typical values for the transition scales between the turbulent sub-ranges in the atmosphere are shown in Figure 2.5. Radar backscatter for an incident wavelength λ is produced by volume scattering from irregularities of size $\frac{\lambda}{2}$, and from Fresnel reflection at sharp horizontally extended height gradients in electron density (Thrane *et al.*, 1987). The latter may be produced when highly localised, isotropic turbulence acts to deform a pre-existing gradient of refractive index (Bolgiano Jr., 1968). It is seen from Figure 2.5 that MF radars ($\lambda \sim$100 to 150 m) are likely to observe turbulence in the inertial sub-range throughout the mesosphere whereas VHF ($\lambda \sim 6$ m) observations in this sub-range may be limited to lower altitudes. Scatter from turbulence in the viscous sub-range will generally be weak as the turbulence is heavily damped.

VHF radars can be used to determine the turbulent structure of the atmosphere. The SOUSY-VHF radar has been used for such studies in Germany and the results have been reported by Czechowsky *et al.* (1979) and Röttger *et al.* (1979). Three characteristic features of the structure of the turbulence in the mesosphere are noted: intermittent sheets of a few hundred metres in thickness, cloud-like layers over a height range of a few kilometres and blobs which occur sporadically. During summer, at heights below 70 km, blobs and sheets with short lifetimes predominate (Röttger *et al.*, 1979), while above 80 km the majority of structures are cloud-like with thicknesses of 3 to 10 km (Czechowsky *et al.*, 1979).

2.5.3 The Nature of Scatterers as Determined by Observations

Radio backscatter from the middle atmosphere is dependent on the turbulent structure of the neutral atmosphere, the temperature gradient, the electron density and the total electron concentration. The turbulent structure, in turn, is related to dynamic processes such as the breaking of gravity waves and the presence of wind shear. As a consequence, the scattering irregularities vary quite abruptly with height. (This can be understood in a broad sense by consideration of the stability of the atmosphere, as determined by the temperature gradient,

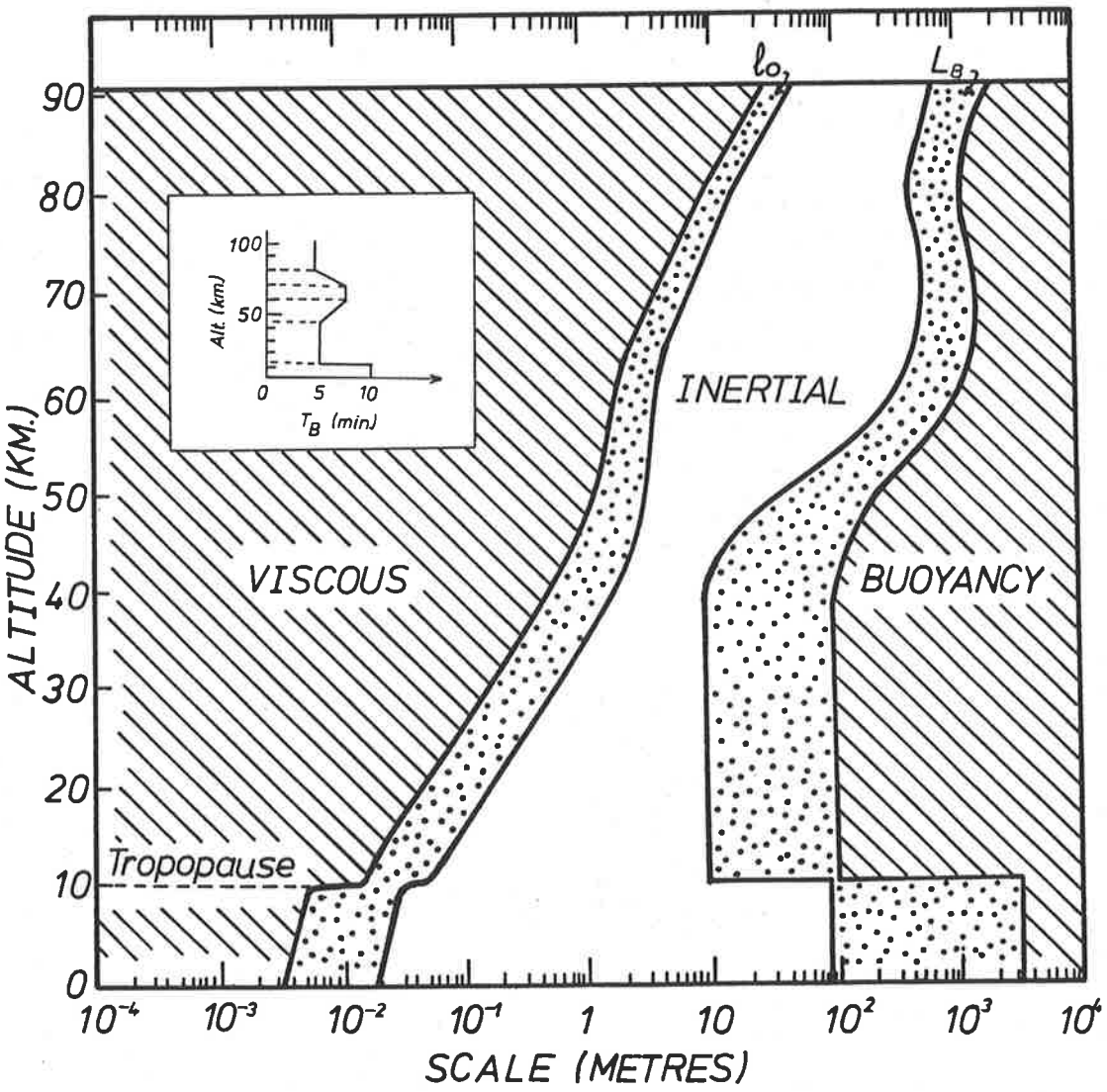

Figure 2.5: Plot showing typical values for the transition scales between the turbulent sub-ranges throughout the middle atmosphere (after Hocking, 1985).

and the influence that this has on the turbulent structure.) The results of experiments reported below reveal the general properties of the scattering irregularities and the variation of these with height.

A common finding of observations of radio scatter from the lower ionosphere is that echoes are generally observed to come from preferred heights. Simultaneous soundings at 3 and 41 MHz (Royrvik, 1985) and 2 and 6 MHz (Hocking and Vincent, 1982b) show the preferred heights on each occasion to be similar at the compared frequencies, at heights up to 85 and 90 km respectively. This suggests that the scattering regions contain a range of Fourier components and that the mechanisms responsible for the echoes at the different frequencies are closely related (Royrvik, 1985).

The mean angular spread of MF echoes tends to increase with increasing altitude, with quite a sudden transition reported to occur at about 80 km. Gardner and Pawsey (1953) showed that the strength of the echoes below 80 km could be substantially reduced, and echoes above 80 km enhanced, by replacing a vertically directed receiving array with a horizontally directed array. This showed that there was a substantial off-zenith component at the higher altitudes. Similar results were found by Vincent and Belrose (1978) and Hocking (1979) who compared the power received from arrays of very different beamwidths. Vincent and Belrose estimated that the off-vertical angles of scatter were less than 10° for altitudes below 80 km and of the order 15° to 20° for altitudes above 80 km. These results were obtained in Ottawa during winter and they are in good qualitative agreement with similar results obtained in Adelaide by Lindner (1975). The values measured at Adelaide were smaller than those measured at Ottawa at all heights, with off-vertical angles of less than 5° being measured at heights below 80 km.

Quasi-specular reflections are produced by Fresnel scatter from irregularities of horizontal extent greater than one Fresnel zone ($=\sqrt{\lambda z}$, where λ is the radio wavelength and z the height of scatter) and vertical extent less than about $\frac{\lambda}{8}$ (Hocking and Vincent, 1982a). Scatter from wide off-zenith angles suggests the scattering irregularities are isotropic and most likely generated by

isotropic turbulence.

Theoretical calculations of the ratio of the reflection coefficients at 2 and 6 MHz have been compared to the measured ratio of observed power at these frequencies (Hocking and Vincent, 1982b). Calculations were carried out for the cases of both Fresnel scatter from a sharp boundary and for isotropic volume scatter from inertial range turbulence. Results suggest that scatter from below 76 - 80 km is Fresnel-like at both frequencies but that scatter from above 80 km contains a significant contribution from turbulent scatter. Above 90 km the 6 MHz scatter was very weak suggesting that scales of 25 m are within the viscous sub-range at this altitude.

Similar conclusions regarding the nature of the scatterers have been reported by Royrvik (1985) and Thrane *et al.* (1981). Royrvik showed that measurements of the absolute scattering cross section at 3 and 41 MHz compared well with theoretical values predicted by assuming turbulent irregularities as the scattering mechanism. Thus Royrvik attributed the scattering irregularities to either pure turbulence or turbulence acting on a gradient in the refractive index. High latitude results reported by Thrane *et al.* (1981) showed that the intensities of partial reflection echoes are consistent with computations based on volume scattering from ionospheric structures as measured by a sounding rocket. This once again suggests that scattering is due to isotropic turbulence at all heights.

Recent work undertaken as part of the Middle Atmosphere Program/Winter in Northern Europe campaign (MAP/WINE) provides good evidence for both volume and Fresnel type scattering of partial reflections in the winter middle atmosphere (Thrane *et al.*, 1987). A comparison was made between data from the SOUSY MST radar, a partial reflection radar and ion probe measurements. Falling sphere and foil cloud observations gave high time resolution measurements of the wind field. A number of interesting results were obtained. Firstly, height regions producing radar echoes were found to coincide with regions of significant turbulence in 70% of the cases examined. Wind and temperature field measurements revealed that turbulence

tends to be associated with regions of gravity wave saturation.

A second result of the work by Thrane *et al.* was the identification of wind corners, a mechanism by which Fresnel reflections could be produced. Wind corners are defined as thin layers (typically less than 0.5 km thick) where there is both a rapid change of wind direction with altitude and a minimum in the wind-speed vertical profile. It was found that 80% of the observed wind corners were associated with partial reflection echoes but that less than half of these were associated with turbulence. It was therefore concluded that a wind shear could produce gradients in electron density sufficiently strong to produce observable partial reflections, and that this basic mechanism could also be active outside of the auroral zone.

Specular reflections from wavelike undulations in the lower E-region (at about 100 km) are also found to produce fading by the interference of different sets of fringes (Briggs, 1977; Guha and Geller, 1973). The large scale undulations are travelling and display characteristics expected for gravity waves at this level (Vincent, 1972). Just what the measured velocity from such reflections relates to will be discussed in the next section.

To sum up, it appears that there is a range of possibilities regarding the nature of the scatterers and the mechanisms responsible for partial reflections. There is general agreement that turbulence produces radio scatter in the presence of a gradient in the electron concentration. There is less agreement on the mechanism responsible for Fresnel scattering.

2.6 SOURCES OF ERRORS

A number of potential sources of error are inherent in the estimation of wind velocity using the SAPR technique. There are measurable sources of error associated with the height of observation, instrumental errors which can be minimized, statistical errors and a large source of potential error based on the question "what velocity are we measuring?". Each of these error sources will be discussed in this section.

The height of observation is determined from the echo delay, based on the assumptions that

radio waves travel at their free space velocities and that reflections are confined to the zenith. The first assumption is valid for waves well below the height of total reflection. An increase in the electron concentration leads to reduction of the wave group velocity and eventually the reflection of the wave when the group velocity becomes zero. At heights close to the height of total reflection retardation causes the virtual height (i.e. that derived on the assumption that the free space velocity applies) to exceed the true reflection height. Fraser and Kochanski (1970) show that most of the retardation occurs within the last kilometre of the true path. The effect of pulse retardation is generally ignored below about 100 km (Fraser, 1968; Gregory *et al.*, 1982).

The second assumption of no off-zenith reflections introduces a potentially larger uncertainty in the height of reflection than that due to pulse retardation. Reflections from an off-zenith angle of 20° (the half-power width of the Mawson transmitting array) would cause the scatterers to appear at a height 5 - 6 km higher than the true height. Contamination from off-zenith reflections is most likely to occur above 85 km where the scatterers may contain a large quasi-isotropic component (see section 2.1). Fraser and Kochanski (1970) suggest that this source of error will be reduced by the use of the correlation analysis. Off-zenith components will produce a ground pattern which is poorly correlated over distances comparable to the dimensions of the spaced receiver system, and will thus be rejected by the FCA. Fraser and Kochanski conclude that the measured drifts may be assumed to indicate drifts within one pulse width (4 km) of the indicated height.

The size of the triangle formed by the receiving antenna array can lead to an underestimate of the velocity if it is too small. The measured 'true' velocity tends to increase as the size of the triangle increases and tends to a limit at the correct velocity, when the triangle size is approximately equal to the scale of the diffraction pattern (Golley and Rossiter, 1970). The so-called 'triangle-size effect' will lead to an underestimate of the velocity as there is no compensating tendency for the measured velocity to be large when the pattern size is small (Stubbs, 1973). Stubbs and Vincent (1973) recommend an antenna spacing of 160 m for SAPR work in average

D-region conditions. A comparison of meteor and SAPR measurements by Stubbs shows the drift velocities measured using the SAPR technique to be on average 10% smaller than the meteor drifts, when a triangle spacing of approximately 190 m is used. Stubbs attributes this discrepancy entirely to the large triangle-size used thus it is likely to be an overestimate of the error introduced by this effect. The SAPR at Mawson conforms to the recommended receiver spacing for D-region conditions and apart from this no further consideration is given to this possible source of error.

The statistical errors involved in the determination of wind speeds using the SAPR technique have been calculated by May (1988). A comparison of two sets of independent wind determinations was made using two sections of the large Buckland Park array, located near Adelaide. The measured wind speeds, in the height range 70 to 90 km, had values generally lying between 70 and 100 ms^{-1}. The rms difference between simultaneous pairs of observations gave a statistical error distribution, which was strongly peaked between 10 - 15 ms^{-1}. This value is an indication of the statistical variance inherent in SAPR measurements of the wind velocity.

The greatest source of potential error lies in the uncertainty as to what velocity is being measured by the SAPR method. The possibilities are the velocity of turbulence carried by the neutral air, ionization, ionized irregularities, or atmospheric wave motions (Briggs, 1977; Vincent *et al.*, 1977). During the 1950's and 60's a high priority was given to addressing this question and experiments were carried out to compare wind measurements from the SAPR method with measurements from other techniques including meteor radar, VHF radars, and various rocket techniques (Kent and Wright, 1968; Fraser and Kochanski, 1970; Manson *et al.*, 1973; Stubbs, 1973, Stubbs and Vincent, 1973; Briggs, 1977; Vincent and Stubbs, 1977). Results of these studies suggest that the SAPR method does in general measure the neutral wind. One observed exception, however, is found in measurements made in the vicinity of the equatorial electrojet. Here, the SAPR technique is found to measure the drift of electrons rather than the

neutral velocity (Briggs, 1977).

In the D-region, it is generally accepted that the SAPR method measures the neutral air velocity, one component of which will be the perturbation velocity associated with gravity waves (Briggs, 1977; Vincent and Ball, 1977; Manson *et al.*, 1973,1976). Indeed the SAPR technique has been used extensively to measure gravity wave parameters (section 1.3). In the E-region, large scale gravity waves produce undulations in the reflecting surface, and simulation models suggest the measured velocity should be the translational motion of the reflecting surface (Guha and Geller, 1973) i.e. the horizontal component of the gravity wave phase velocity. Observations suggest, however, that the velocity measured by the SAPR in the E-region is in fact the velocity of the neutral air (Vincent, 1972), as is the case in the D-region.

There are two theories as to why the SAPR method measures the neutral air velocity in the presence of large scale gravity waves which undulate the reflecting surface at the base of the E-region. The first suggests that if gravity waves propagate isotropically, then their phase velocities will cancel out and drift results will on average measure the background wind. An alternative explanation is that wave-induced irregularities will be dominated by those waves which have reached their critical level. Since a critical level is defined as the height at which the horizontal phase velocity of the wave matches the neutral air velocity, measurements of the phase velocity will in fact give the neutral air velocity (Hines, 1968; Vincent, 1972).

A source of error which may be introduced by gravity wave motions, is the effect of density and pressure perturbations associated with the passage of a wave (Fraser, 1968, Fraser and Kochanski, 1970). Fraser suggests that pressure wavefronts moving through the ionized irregularities may produce spurious motions in the ground-diffraction pattern which will be different from the phase velocity of the wave. A final possible error source is the misinterpretation of time variations in absorption and reflection coefficients as indicating motions of the scatterers. Patches of absorption could mask reflections from higher altitudes, so that the motion of these patches would be attributed to the motion of the reflecting irregularity. There have been no

reported investigations of this effect.

Despite the conclusion that the SAPR method generally measures the motions of the neutral atmosphere, the question of what velocity is being measured is considered to introduce the greatest uncertainty in 'wind' measurements determined in this work. As discussed in section 1.4 the presence of enhanced electric fields in the auroral zone may have a similar effect on SAPR drift measurements in the vicinity of the auroral electrojet, as has been found near the equatorial electrojet. This question will be discussed further in this work, as it is considered to be of fundamental importance to the interpretation of the results.

Chapter 3.

THE FABRY-PEROT SPECTROMETER

3.1 INTRODUCTION

The Fabry-Perot spectrometer (FPS) is used to measure the Doppler width and peak position of airglow and auroral atomic emission lines, from which the temperature and line of sight velocity of the emitting species may be deduced. Fabry-Perot spectrometers have been used extensively since the mid-1950's to infer thermospheric temperatures (e.g. Armstrong, 1956; Turgeon and Shepherd, 1962; Killeen and Hays, 1983) and more recently for the determination of wind velocities (e.g. Armstrong, 1969; Hays and Roble, 1971, Wilksch, 1975; Hernandez and Roble, 1976; Hernandez, 1982). The Mawson instrument is a development of an instrument used at Mt Torrens, a field station near Adelaide (Wilksch, 1975; Jacka *et al.*, 1980 and Cocks *et al.*, 1980), and it was installed in Antarctica during 1980. Routine observations commenced in 1981, and it has been operated every year since then, with the exception of the 1982 and 1987 winters.

An outline of the instrument and the basic principles of operation is presented here, which is based on more detailed descriptions given by Jacka (1984) and Wilksch (1975). The operation of the FPS during 1985 and the procedures adopted for data analysis are described, along with a critical discussion of the data.

3.2 INSTRUMENTATION

The Mawson instrument is a dual, separation-scanned FPS which may be operated over a broad range of wavelengths and has the capacity for both night-time and daytime observations. In this work the operation of the FPS was restricted to night-time observations of the λ558 nm atomic oxygen emission from the lower thermosphere. The instrument is used to determine the line of sight component of the wind. Observations were confined to the zenith allowing measurements of the vertical component of the wind to be made.

3.2.1 Overview

The FPS is located in the aeronomy laboratory of the Mawson base. Light enters the system via a roof mounted periscope which is shown in Figure 3.1. The optical system is shown in Figure 3.2. The periscope is driven in steps of 0.1 degree of zenith angle and 1 degree of azimuth angle. An optical relay comprising several lenses is incorporated below the periscope to accommodate the very high roof of the laboratory (~4 m). Various light sources may be introduced into the optical path below the optical relay for the purposes of calibration.

The Fabry-Perot etalons and detector optics are suspended from a steel frame which is mounted on a concrete block and seated on bedrock. They are thus mechanically isolated from the periscope and optical relay. An insulated and temperature controlled cabinet surrounds the spectrometer. The low resolution etalon is used for daytime observations and maybe swung out of the optical path for night-time observations. A field stop carrier mounted between the low and high resolution (HR) etalons allows a selection of six field stops. A filter wheel carrying up to six interference filters is mounted above the photomultiplier.

All routine operations are performed from the operator's console which is mounted on an observation deck. A viewing dome allows the operator full view of the sky (and periscope), so that auroral activity and observing conditions are readily monitored. A theodolite is also mounted within the observation dome to allow the position of auroral forms to be determined.

3.2.2 The Etalons

The high and low resolution etalons consist of 150 and 50 mm diameter plates respectively. The low resolution etalon is only used for daytime observations and will not be discussed further here. The plates of the HR etalon are of fused silica and the coatings are of a 13-layer all-dielectric type. The reflective finesse after ageing was 27 at λ546 nm and 33 at λ632 nm, and the defect finesse of the plates in operation is 40 (the reflective and defect finesse are defined in section 3.3).

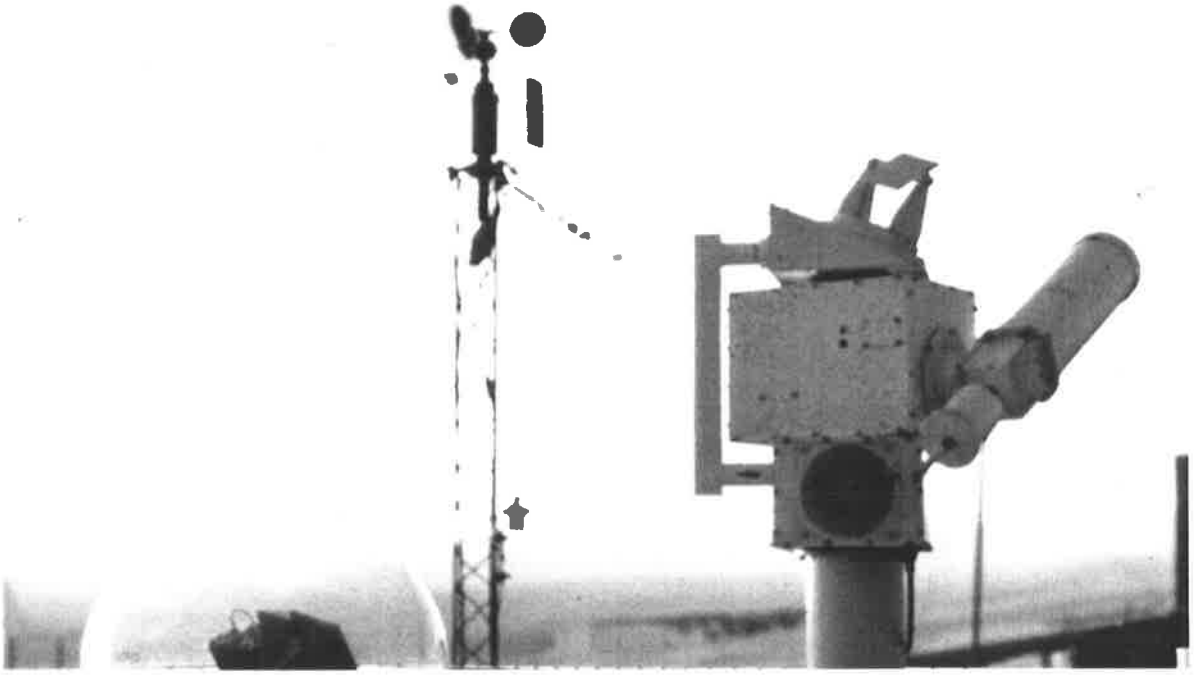

Figure 3.1: The dome (*left*) and periscope (*right*) of the FPS as viewed from the roof of the aeronomy laboratory. Photograph by M. Conde.

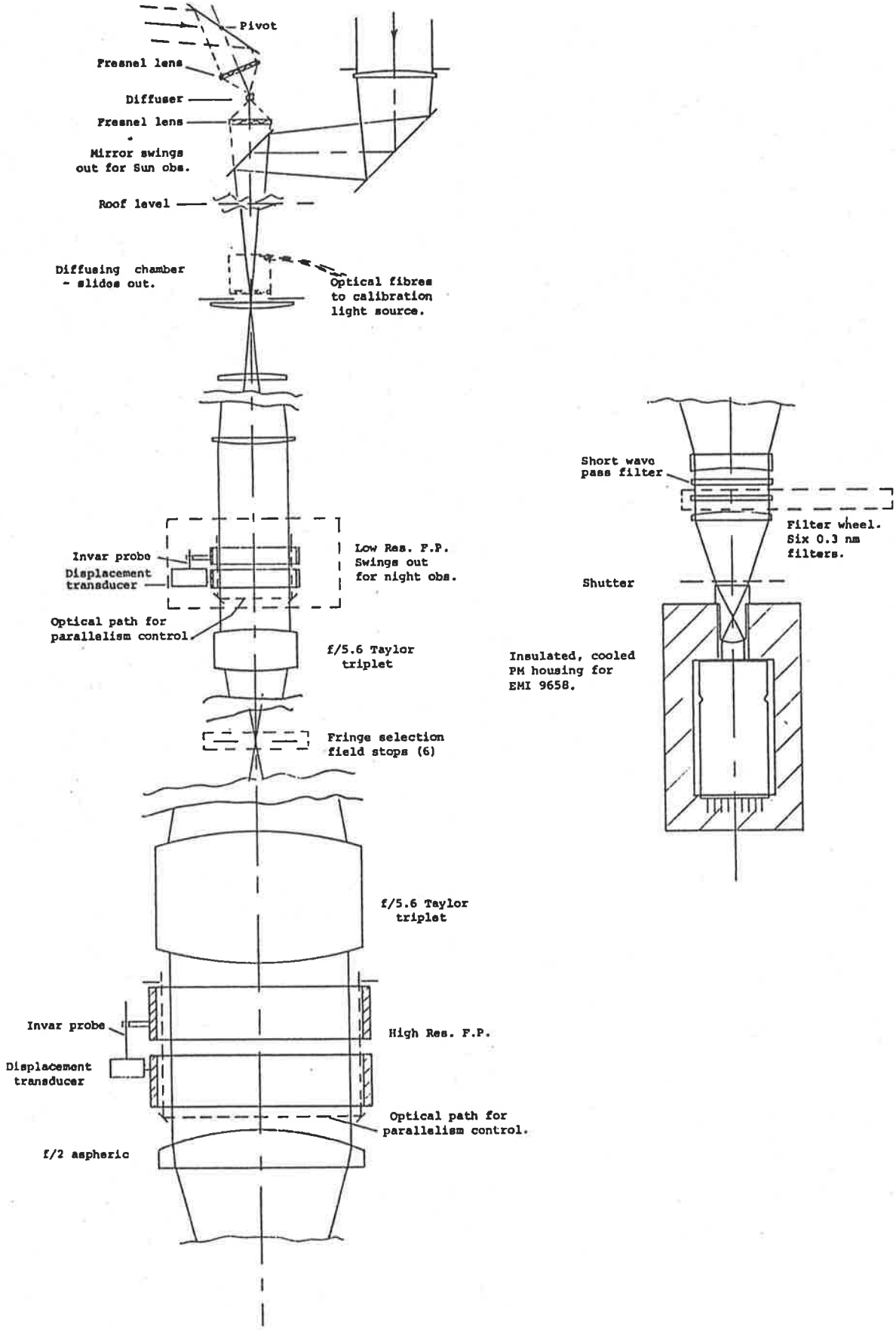

Figure 3.2: The optical system of the Mawson Fabry-Perot spectrometer (not to scale).

The etalon plates are mounted within "meehanite" rings and supported by PZT 5H piezoelectric tubes, with an expansion coefficient of ~1nm/V. This setup allows fine control of plate separation. Large variations in plate separation are achieved by means of three steel support screws driven by stepper motors. The maximum plate separation is 25 mm. Temperature within the etalon chamber is controlled to within $\pm 5 \times 10^{-3}$ °C

3.2.3 Parallelism Control

Departures from plate parallelism should not exceed the size of plate defects. Plate parallelism is servo-controlled and employs the method of Ramsay (1962), which is illustrated in Figure 3.3. The system is applied across each of two orthogonal diameters of the etalon. A beam of near infrared light passes down the etalon space on one side, returning up through the space on the other side, where it is detected by a PIN diode. The transmitted intensity is maximised when the optical distances AB and CD are equal.

The direction of any departure from parallelism is sensed by applying a small amplitude (~3 nm) and ~1 kHz three-phase perturbation or 'wobble' to one plate. This produces an oscillatory component in the transmitted intensity and PIN diode output, which is amplified and passed through a phase sensitive detector which in turn applies a correcting voltage to the piezoelectric tubes in a negative feedback loop.

3.2.4 Separation Control

The etalon is scanned using a stepped saw-tooth waveform with a period of ~6 sec. Accurate control of plate separation is achieved via a servo-controlled system. A capacitance displacement transducer measures variations in the geometric separation of the plates. The amplitude of the output signal is proportional to departures of the separation from some arbitrary zero and the phase indicates the direction of displacement. A barometric correction signal, produced by a pressure transducer within the etalon chamber, is added to this output signal to ensure that the operating order is unaffected by pressure fluctuations. The resulting signal is compared with

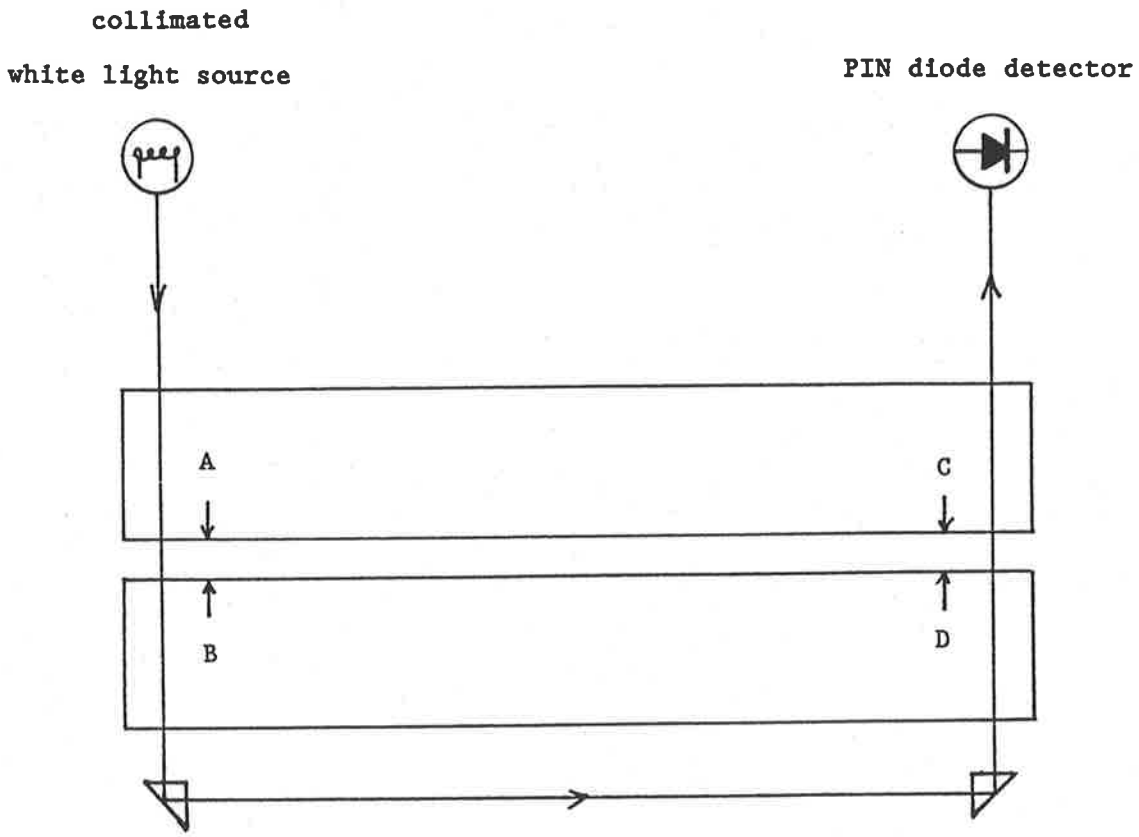

Figure 3.3: A schematic of the plate parallelism control system.

the scan waveform to produce an error signal which controls the piezoelectric tube voltage, thus completing the feedback loop.

3.2.5 Photon Detection

Intensity is measured by an EMI 9658A photomultiplier with an S20 photocathode. The photocathode is deposited on a multi-pyramidal form impressed into the inside surface of the front window, to increase the effective quantum efficiency of the photomultiplier. The photomultiplier is cooled to ~-30°C by the use of a Peltier junction cooler to reduce the dark counts. Dark counts are further reduced by the use of magnetic defocussing. A photomultiplier pulse counting system is employed for night observing.

3.2.6 Data Acquisition

The data acquisition system comprises three microprocessors; one displaying accumulated data on a CRO or plotter, one operating the data recording facility and one controlling data acquisition including generation of the scan waveform and setting of the observation program. The three microprocessors access a common block of memory having 256 channels which may be addressed as one block or two separate blocks of 128 channels. Generally, the instrument scan-range is set so that a single peak of the emission feature is recorded on 128 channels. The position of the peak is then determined in terms of channel numbers. The distance between two successive peaks, or the number of channels representing one order, can be measured by increasing the scan range and recording two peaks of the emission feature on 256 channels.

A profile of the emission feature (a line profile) is acquired by scanning the instrument a number of times and recording the accumulated pulse counts in each channel. A total pulse count of at least 10^4 counts is required to produce a reasonable SNR profile.

Data are recorded as ASCII characters along with data indicating the state of certain instrument parameters at the time of observation. These include periscope zenith and azimuth angles, date, start and stop times, filter number, number of scans and scan speed.

Various observing modes are possible. In the simplest mode a single spectrum is acquired in 128 or 256 channels with the instrument scanning for a preselected number of scans. When the acquisition is completed the operator may then choose to record, discard, or add to the accumulated profile. Alternatively the user may preset the instrument to record a set number of profiles of a single source (either the sky or a calibration source) for a preselected number of scans.

During 1984, modifications were made to the data acquisition system to allow a sequence of sky/calibration source or sky/sky observations to be carried out and recorded. The number of scans required for each of the sky and calibration profiles being preset independently. This is referred to as the 'automatic' mode of operation.

3.3 PRINCIPLES OF ANALYSIS

The passage of a collimated beam through an etalon consisting of perfectly flat, parallel plates produces a transmission versus frequency variation described by the Airy function. The Airy function is approximately periodic, with a 'period' which varies slightly with frequency; variations in the period are caused by variations in the phase change upon reflection of the etalon plate coatings and by variations in the refractive index of the medium between the plates. The ratio of peak spacing to peak width of the Airy function defines the reflective finesse. For an imperfect etalon, where the plate separation varies across the plates, the distribution of values of effective plate spacing about the mean spacing may be described by a defect function. The ratio of the peak spacing to the peak width of the defect function then gives the defect finesse. The effect of using a finite aperture is described by the aperture function. The convolution of the Airy function, the defect function and the aperture function defines the instrument function.

Observations of light from a source with a small spread in wavelength yields a recorded function which is a convolution of the source function (intensity versus wavelength) and the instrument function. For a separation scanned spectrometer the recorded profile is a function

of the separation and may be interpreted as a spectrum. If the instrument function is known, the source function is obtained by deconvolving the instrument function from the recorded profile. Alternatively, if the source function is known, the instrument function may be determined by deconvolving the source function from the recorded profile. Often it is necessary to adapt the instrument function obtained at one wavelength for use at another. The defect and aperture functions are independent of operating wavelength, however the Airy function changes scale with wavelength and must be changed accordingly.

Once the source function at the wavelength of interest is obtained, the line profile width and position are determined by fitting a Gaussian function to the source function in the Fourier transform domain. The noise dominated components are removed by truncation of the series and the power spectrum of the instrument function is used as the weighting function for the least squares fit. The variance of the set of residuals, viz. the goodness of fit parameter chi-squared, is minimized by using a grid search procedure to vary three parameters: the line width, centre position and strength. Successive iterations are used to locate local minima for each parameter in turn, which are then used to determine the emission temperature, line of sight component of the wind, and emission intensity respectively.

The chi-squared parameter is the ratio of the estimated variance of the fit to the dispersion of the data about the parent distribution. If the fitting function is a good approximation to the parent function, then the chi-squared parameter should approach unity (Bevington, 1969). A number of factors may cause distortions of the observed profile including large variations in drift, departures in instrument parallelism and variations in the emission intensity. Such distortions are reflected in corresponding large values of chi-squared, thus such profiles may be rejected by setting an appropriate upper limit on this parameter (usually 15 or 20). An estimate of the random noise superimposed on the signal is also derived, following the method of Bevington, which gives an estimate of the standard error in each of the three parameters.

3.3.1 Calibration

The λ546 nm spectral line emission of the isotope Hg 198 is used as a reference emission because of its spectral purity and narrow half-width. The emission is produced in a discharge tube which is excited by RF oscillations and kept near ambient temperature. The spectrum of the λ546 nm emission is assumed to be Gaussian with a half-width which may be determined from the operating temperature (approximately 300 K) and atomic mass of the isotope. In this way the source function of the calibration source may be derived.

The instrument function at the calibration wavelength is determined empirically by deconvolving the source function of the λ546 nm emission from the calibration profiles. The Airy function at the calibration wavelength is then replaced with that at the observation wavelength to give the instrument function at λ558 nm. A high signal to noise ratio instrument function may be obtained by summing a number of λ546 nm emission profiles, which is usually done by summing all the calibration profiles obtained over a night.

Observations of the Hg 198 source are also used to set the scale for conversion from number of channels to wavelengths and to determine the instrument drift. The number of channels representing one order, or a change in optical plate separation of one half wavelength, is determined at the start of each night by scanning over two peaks of the λ546 nm emission. The instrument drift is monitored by making regular observations of the Hg 198 source throughout the observing period. Any drift in the peak position of the λ546 nm emission is then attributed to variations produced within the instrument itself.

3.4 OPERATION DURING 1985

The FPS is a sophisticated instrument that usually requires a full time operator if it is to be used to full capacity. Unfortunately this was not possible in 1985 and, because of problems encountered during the first half of the year, the FPS was only operated from July until mid October. Observations became less feasible beyond this time as the hours of darkness decreased.

A total of 22 nights intensity and temperature data and 14 nights vertical wind data were obtained.

During the autumn of 1985, attempts to commence operation of the FPS proved unsuccessful as the plates of the HR etalon could not be made parallel. Over the following months a few problems were identified with the assistance of a technical officer with the Department of Meteorology, Paul Chesworth. The major problem was that one of the three stepper drives used to produce large changes in plate separation had jammed, placing a large tilt on one of the plates. Once this situation had been corrected it was necessary to set up a fringe viewing system with a helium/neon laser in order to set the plates of the HR etalon approximately parallel before the parallelism control system could be used.

The first observations of the nightglow were carried out in August when the λ630 nm emission was recorded. The instrument drift was monitored and an overheating problem in the floor of the cabinet isolated and rectified. A bulk separation change was carried out at the beginning of September in order to set the plate separation of the HR etalon to that required to optimize measurements of the λ558 nm emission (the instrument had been set to observe the λ630 nm emission in 1984).

Regular night-time observations of the λ558 nm emission commenced on 15th September, and a summary of operation is given in Table 3.1. The FPS was initially run in automatic mode, alternating between observations of the sky and calibration source. However it is unnecessary to calibrate after each profile and since doing so significantly reduces the time resolution of the data, a semi-automatic mode of operation was later adopted. In this mode a sequence of sky/sky profiles was obtained with the instrument in automatic mode. This sequence was interrupted, after usually five or six sky profiles had been obtained, and the instrument manually set to observe the calibration source. The instrument would then be returned to automatic mode. Although the instrument could be left unattended between calibrations, better results were obtained if the profile-acquire time was manually varied throughout the observing period to

Table 3.1: Days of operation of the FPS during 1985 showing: the instrument drift over the night, mode of operation, an indication of when wind data was calculated (days resulting in no wind data are marked with a 'x') and comments on the performance of the instrument.
LSC = laboratory source carrier and
FW = filter wheel.

Day	Range of Drift (channels)	Mode of Operation	Wind Data	Comments
258	32	auto 20 min/profile	x	Long acquire times and and large drift
259	21	auto 20 min/profile	x	" "
260	21	auto 13 min/profile	x	" "
263	12	auto 20 min/profile	x	Pressure transducer switched off. 0156 UT reset central-scan voltage.
264	31	auto 12 min/profile	x	2032 UT calibration profile drifted out of scan range, instrumnt not reset.
265	25	auto 5 min/profile		1940 UT reset central-scan voltage
268	55	semi-auto		Large drift after 2137 UT
271	-	auto 175min/profile	x	Very long acquire times since data acquisition control incorrectly set
272	51	semi-auto	x	Large drifts resulting from field stop carrier being driven out of position by circuit transients
273	44	semi-auto	x	Field stop carrier disconnected.
277	19	semi-auto		2221 UT reset central-scan voltage
278	24	semi-auto		
279	15	semi-auto		Parallelism out producing broad instrument function, reset 2107 UT.
280	8.8	semi-auto/auto		Changed calibration technique to drive LSC and FW separately
281	5.5	semi-auto		
282	Power failure	- no power	from	1000 to 1340 UT
284	13	semi-auto		Parallelism out-2111 to 2211 UT 2247 UT reset central-scan voltage
285	9.5	semi-auto		
286	2.3	semi-auto		
287	7.5	semi-auto		
288	3.8	semi-auto/auto 6 min/profile		
289	5.9	semi-auto		
290	6.2	auto 6 min/profile		

accommodate the large variations in emission intensity accompanying variations in auroral conditions.

The main problems encountered during the observing period were associated with transients in the field stop carrier (FSC) control circuitry. These caused the FSC to be driven out of position a number of times over the evenings of days 272 and 273. The FSC drive subsequently jammed. Once freed and repositioned, the control line was disconnected as a temporary solution to the problem.

The FPS was fully operational for a period of 33 days. Weather conditions prevented observations on 11 nights. Of the remaining 22 nights, instrumental problems prevented wind determinations on 2 nights, and the combination of large instrument drift and long acquire times lead to poor wind determinations on 8 nights. The latter were not included in the wind analysis. Altogether, reliable wind measurements were obtained on approximately 50 %, and temperature and intensity measurements on 66 % of the nights within the observing period.

3.5 THE DATA AND METHODS OF ANALYSIS

The data obtained using the FPS show evidence of large vertical winds which will be discussed in Chapter 4. There have been very few measurements of vertical winds in the lower thermosphere and none of these show vertical winds as large as those presented here. For this reason a detailed discussion of the analysis procedure and data is given, with particular emphasis on identifying sources of error or bias which may lead to an over-estimate of the vertical wind.

3.5.1 Determination of the order of interference

The order of interference, or optical plate separation in half-wavelengths, is determined using an iterative procedure. A first estimate is given by the geometric plate spacing as measured with a micrometer. A more accurate estimate of the operating order was determined from the relative peak positions of a number of emission lines with wavelengths covering a range of 86 nm. The emission lines used are listed below.

Hg 198 546.07532 nm

He-Ne Laser 632.81646 nm

Atomic oxygen 557.7345 nm

Neon 621.72813 nm

The operating order was found to be between 24955 and 24958 at λ558 nm.

3.5.2 Choice of instrument function

The instrument profiles for ~~over~~ the 14 nights over which wind data were obtained showed some variation due to two main sources. Firstly, on the nights when the instrument was operated at one order less then the usual operating order, part of the low-wavelength tail of the calibration profile was just out of the scan range of the instrument. As a result, the instrument function calculated from the shortened calibration profiles was slightly asymmetric. This effect was most severe on days 280 and 290. Secondly, a broadening of the instrument function resulted when departures in plate parallelism were greater than the size of the plate defects, resulting in a broadening of the defect function. This was the case on days 284 and 279. The source of asymmetry in the instrument function will only affect the calibration profiles, and not the observation profiles, whereas departures in parallelism will cause a broadening of both the calibration and observation profiles.

The effect on data analysis of using different instrument functions was investigated firstly by analysing the data from each night using the instrument function appropriate to that night and secondly by analysing the data using the instrument function calculated for day 286. The instrument function from day 286 was originally chosen as a reference since on this night neither of the sources of instrument function distortion was apparent. In addition the instrument drift over the night was the smallest measured, indicating that the instrument was most stable on this night. Subsequent results supported this choice, as analysis using the instrument function of day 286 generally resulted in smaller values of the chi-squared parameter than those obtained

using the instrument function from other nights.

Values of peak position and temperature obtained by analysing the data from each night with the two instrument functions, were compared for each data point. The variation in the difference between these two parameters for each night are listed in Table 3.2. The variation in terms of wind speed corresponding to the variation in peak channel is also given. The differences were greatest on days 279, 280, 285, and 290, when the instrument functions were distorted as discussed above.

Table 3.2: The difference in peak position and temperature produced by analysing the data from each night by firstly using the instrument function appropriate to that night, and secondly by using the instrument function obtained on day 286.

Day	Difference in peak channel (channels)	Equivalent Velocity (ms^{-1})	Difference in temperature (K)
265	.04 - .10	1.7 - 4.4	10 - 20
268	.03 - .05	1.3 - 2.2	2 - 8
277	.04 - .06	1.7 - 2.6	10 - 17
278	.04 - .07	1.7 - 3.0	14
279	.04 - .15	1.7 - 6.5	45 - 53
280	.06 - .36	2.6 - 15.	5 - 35
281	.00 - .03	0.0 - 1.3	11 - 17
284	.01 - .02	0.4 - 0.8	26 - 39
285	.03 - .13	1.3 - 5.7	9 - 21
287	.00 - .01	0.0 - 0.4	0 - 3
288	.07 - .13	3.0 - 5.7	14 - 26
289	.00 - .02	0.0 - 0.8	11 - 20
290	.20 - .42	8.7 - 18.	17 - 60

Wind velocity is determined from the relative peak positions of the calibration and sky line profiles and is therefore unaffected by sources of bias in the peak position. It is thus only variations in the difference in peak position which may affect the results. For most nights, this variation was less than the equivalent of 2 ms^{-1} in wind velocity. On days 279, 280, and 290 when variations of up to 18 ms^{-1} appeared to occur, individual data points associated with large differences were examined. In cases where the error limits calculated in the least-squares fitting procedure did not account for the variations, the data points were rejected.

The temperature, on the other hand, is determined here from an absolute measurement and

is therefore affected by sources of bias. The differences in temperature were therefore considered to represent a source of uncertainty in the measurements and were used to place an error limit on the temperature measurements where this error exceeded the temperature error calculated in the least squares fit.

The data were generally analysed using the instrument function from day 286. An exception was the profiles obtained before 2111 UT on day 279 when the instrument function was broadened for a number of hours due to departures in parallelism. In this case, an instrument function calculated from the calibration profiles obtained within this period was used to analyse the data.

3.5.3 Summation of Profiles

Profiles were generally acquired over a period of 6 min when the FPS was operated in semi-automatic mode. In the auroral zones the λ558 nm emission is predominantly an auroral emission (see section 4.2) and as such it is subject to very large variations in intensity which are dependent on the incoming particle flux. Profiles acquired when the emission intensity was high had a correspondingly high signal to noise ratio (SNR) and those obtained during periods when there was no visible aurora often had a very poor SNR. Where possible, the acquire time was reduced when the emission intensity was high, in order to improve the time resolution of the data. At the other extreme summation of successive low SNR profiles was carried out during analysis.

The criterion used to determine when the SNR was unacceptably low was based on the method used by Wilksch (1975). This method uses the ratio of the power in the fundamental Fourier component to the average noise power, which is referred to as the 'power ratio'. This parameter is shown by Wilksch to be well correlated with derived statistical uncertainties in the wind and temperature measurements, such that the latter increase rapidly as the power ratio decreases below about 10^3. Wilksch concludes that the power ratio should exceed 10^3 for good

results.

In accordance with this criterion, summation of two low SNR profiles was carried out -

a) when two successive profiles both had power ratios less than 10^3 and

b) when no calibration had been carried out between the two sky profiles.

If summation of the two profiles resulted in a profile which still had a power ratio less than 10^3 then further summations were carried out if the above criteria were once again satisfied.

3.5.4 Estimation of the Drift Curve

The results of peak position determinations for both calibration and sky profiles are plotted as a function of time for the observations from each night. An instrument drift curve is then determined, by carrying out a linear interpolation between the peak channels of the calibration points. The drift curve is then shifted in the direction of the 'y' axis until the average distance between the drift curve and observation points is zero. This is equivalent to setting the mean vertical velocity over the night to zero, where the velocity is given by

$$v = \frac{v_o \, \Delta p}{M \, C} \tag{3.1}$$

where,

v_o is the velocity of light

Δp is the shift in peak position

M is the order at the observation wavelength

C is the number of channels representing one order at the observation wavelength.

The drift curves obtained on days 280, 285 and 286 show the variation in shape of typical drift curves (Figures 3.4a,b,c). On day 280 the drift curve is roughly parabolic, on day 285 it is monotonically increasing, and on day 286 it is rather irregular but covers a relatively small

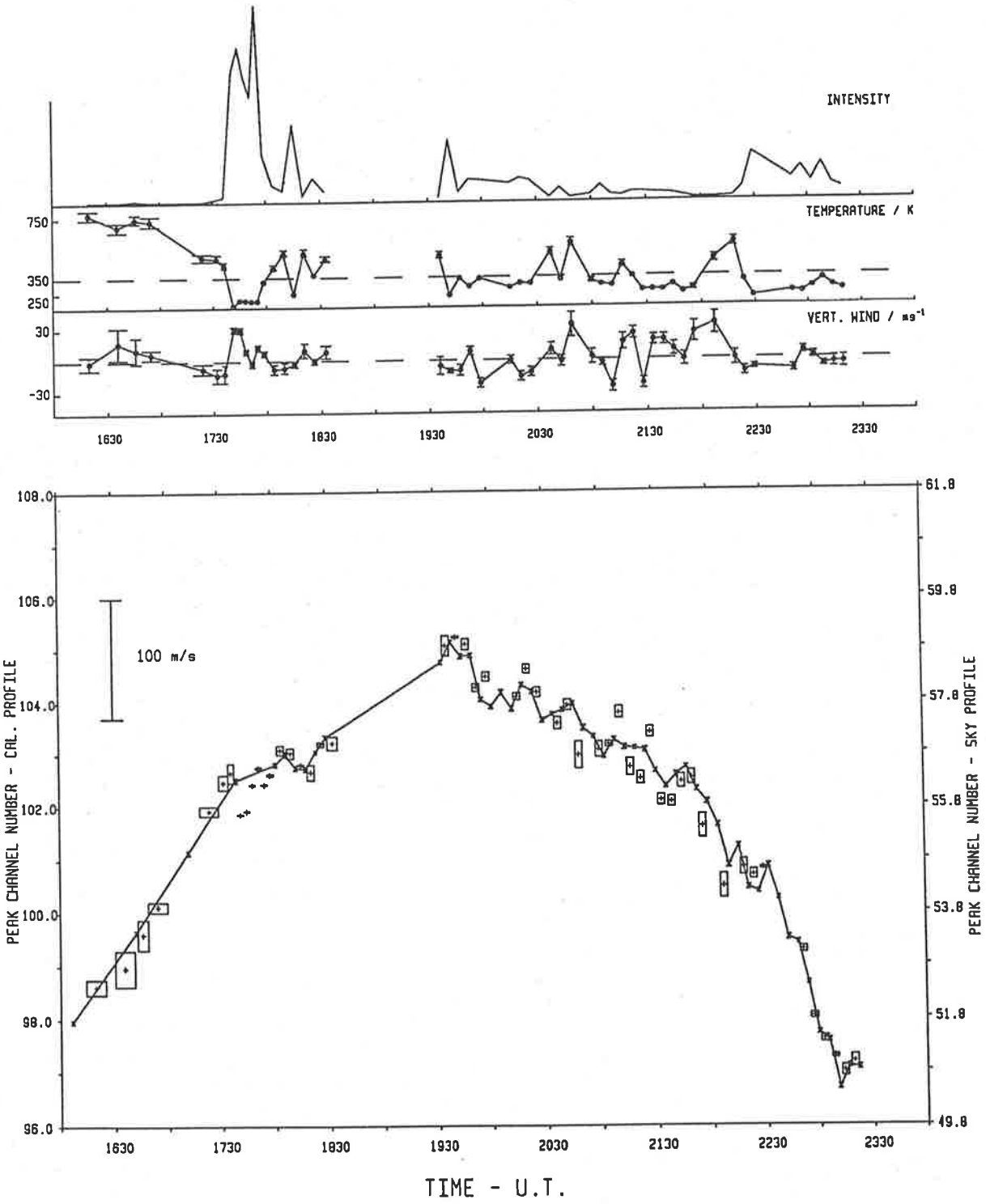

Figure 3.4: (a) Day 280 *top:* Plot of relative intensity of the λ558 nm emission, Doppler temperature and vertical wind (positive upwards) versus time. *bottom:* Peak positions of the calibration and λ558 nm or sky profiles plotted against time. The peak position of the sky profiles are marked with a cross and a rectangle marks the error bounds where these exceed the dimensions of the cross. The peak channels of the calibration profiles are joined by line segments and the resulting curve is referred to as the drift curve.

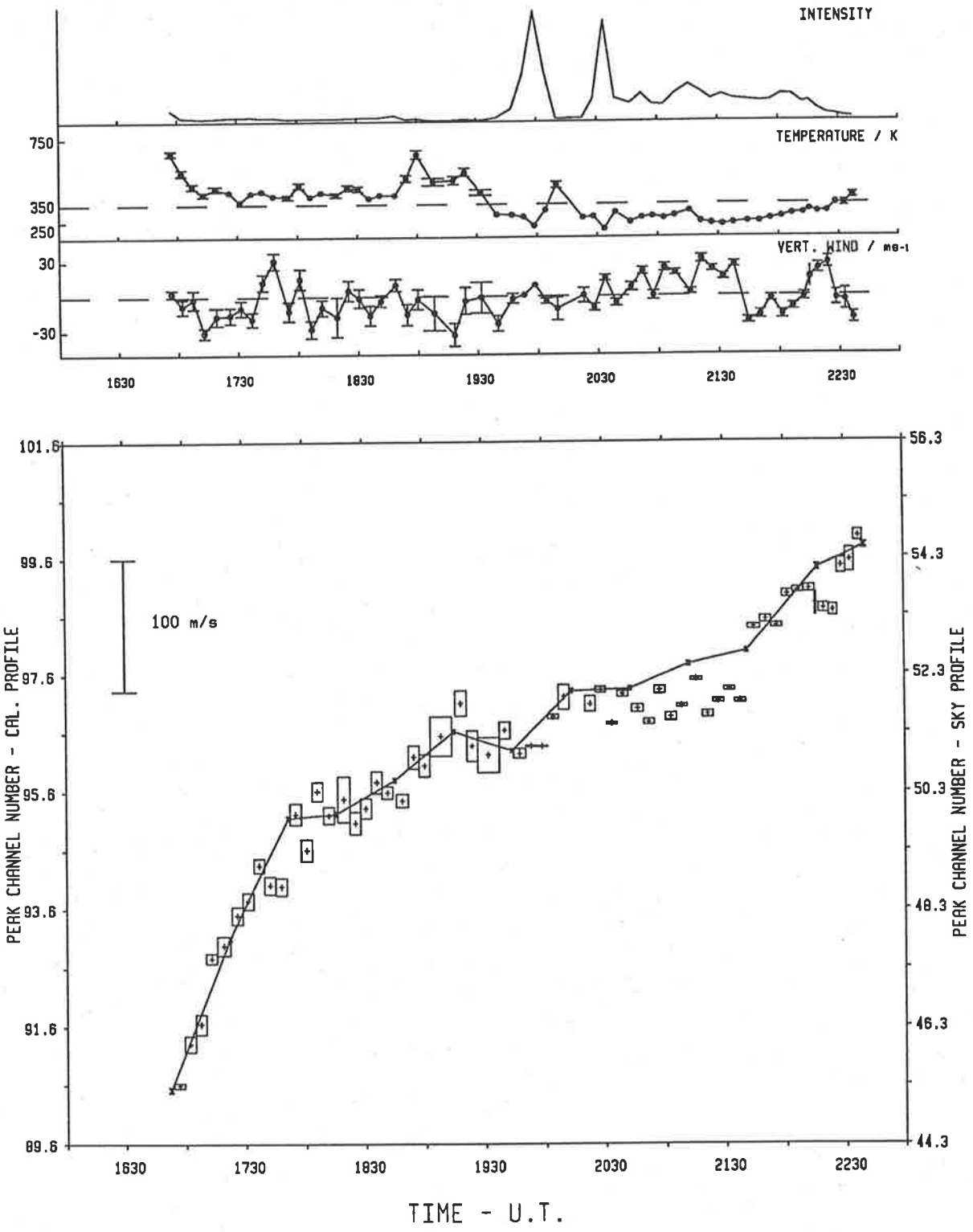

Figure 3.4: (b) Day 285 As for Figure 3.4(a).

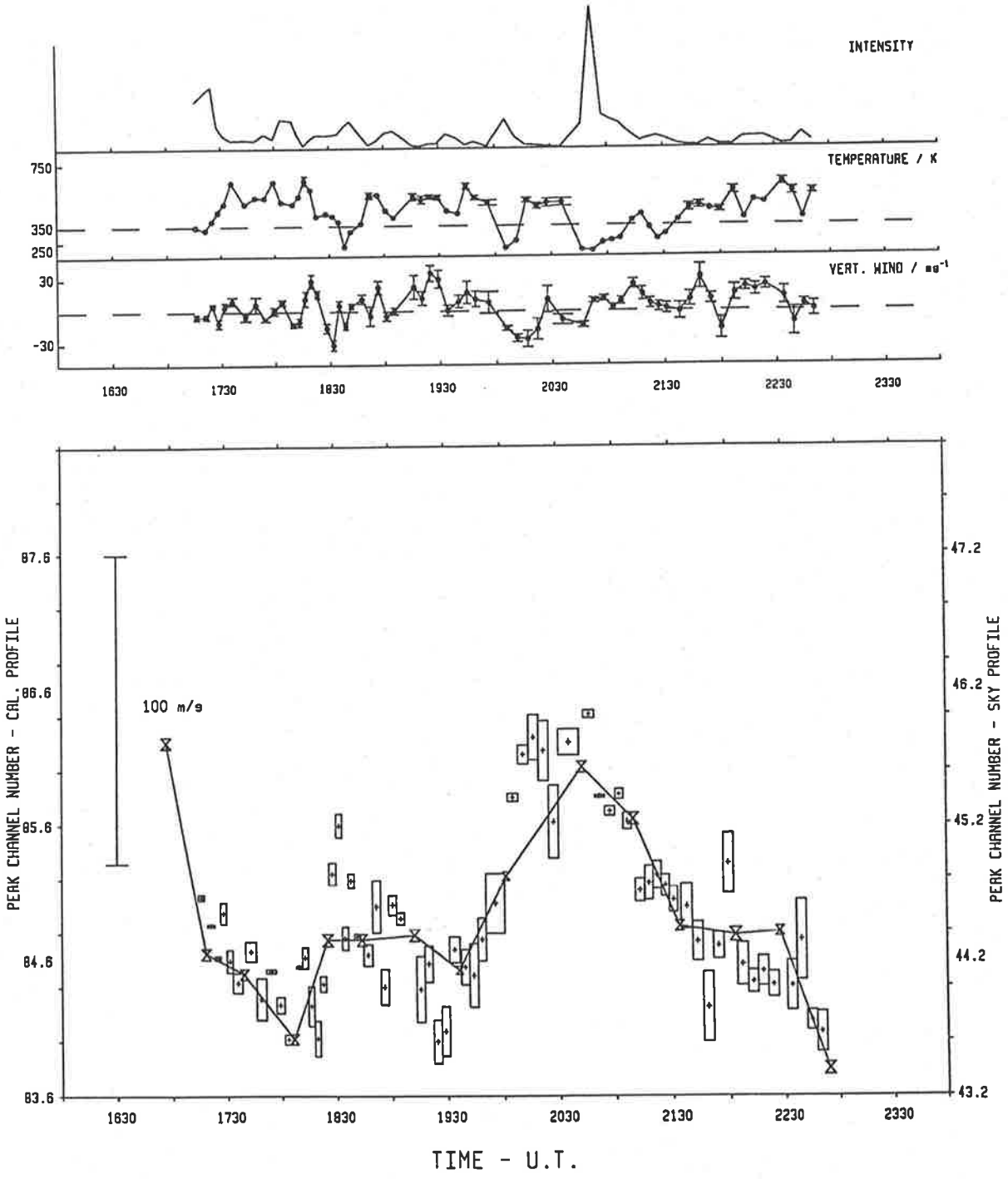

Figure 3.4: (c) Day 286 As for Figure 3.4(a).

range of channel numbers. Temperature variations are likely to produce smooth variations in the instrument operating parameters which determine the general shape of the drift curve on days 280 and 285. Sudden changes in the gradient of the drift curve (and in some cases direction of the drift) are likely to be caused by sudden temperature fluctuations produced by movement of the LSC and filter wheel during calibration. Small mechanical vibrations introduced during calibration are more likely to produce sudden jumps in the drift curve, however this does not appear to be a common occurrence.

The application of a linear interpolation between the calibration peak channels results in a drift curve which gives a reasonable fit to the observation points. There are a few cases, e.g. between 2000 and 2145 UT on day 286 (Figure 3.4c), when a polynomial or spline curve may have given a better fit to the data and slightly reduced the wind values, but generally this is not the case. Where large wind values or significant trends in the wind data were measured, e.g. on day 280 at 1740 UT (Figure 3.4a) and on day 285 from 2030 to 2140 UT (Figure 3.4b), the drift curves were examined to check that the winds were not a consequence of instrument drift.

3.5.5 Day-to-Day Variations in the 'Zero Wind' Velocity

The correction which is applied to the drift curve in order to set the mean vertical velocity over a night to zero, shows some variation from day-to-day. The value of the correction, in channel numbers, is given in Table 3.3 for the observations from each night. The size of the required correction varies between operating orders, by the difference between the number of channels corresponding to one order at λ558 nm and the number of channels corresponding to one order at λ546 nm (here about 5.6 channels). This is seen in the corrections calculated for the days on which the instrument was operated at one order less than usual, which are marked

with an asterisk. The value of the correction used on day 286 is compared with that calculated

Table 3.3: The variation in the correction applied to the drift curve (in channels) and corresponding variation in the mean vertical or 'zero' velocity between nights. Values are compared with those obtained on day 286. The days on which the instrument was operated at one order less than usual are marked with an '*'.

Day	Correction (channels at λ558 nm)	Difference in the 'zero' velocity estimate (ms^{-1})
265	39.47	-3.5
268	40.07	-8.7
277	40.13	-6.1
278	40.45	7.8
279	40.35	3.5
280	*46.27	13
281	*46.73	33
284	*45.38	-26
285	*45.49	-21
287	40.42	6.5
288	40.40	5.7
289	40.61	15
290	*46.82	24

for each other night, and the corresponding difference in the estimated mean vertical velocity determined (Table 3.3). The variation amounted to less than 10 ms^{-1} on most nights, with larger excursions measured on the nights when the instrument was operated at the lower order and on day 289.

Day-to-day variations in the estimated mean-vertical velocity, or equivalently in the relative positions of the λ558 nm and λ546 nm line profiles, are most likely associated with variations in the voltage range used to drive the piezoelectric stacks when scanning. The central-scan voltage and scan range must be manually adjusted at the start of each night in order to enable two peaks of the calibration source to be observed, from which the number of channels corresponding to one order is calculated. It is then manually reset before observing and is usually not varied throughout the observing period (a note has been made in Table 3.1 of the few occasions when it was varied). On the days when the instrument was operated at a lower order, the voltage range over which the piezoelectric stacks were driven was approaching the limits of the usable range. It is therefore likely that either non-linearities in the separation transducer, or non-

linearities in the piezoelectric stacks which are not fully compensated for by the servo-system, caused the observed variations on these days. The largest variation between two successive days occurred between days 281 and 284, when the estimated mean-vertical velocity appeared to vary by 59 ms^{-1}. This variation may be attributed to a power failure, which occurred on day 282 and lasted for 3 and a half hours, and may have affected the operating characteristics of the piezoelectric stacks and separation transducer.

In summary, it is suggested that the day-to-day variations in the mean zero velocity are mainly caused by variations in the operating characteristics of the separation transducer and piezoelectric stacks. Since the central-scan voltage and scan range are not generally varied throughout the observing period it is unlikely that any systematic variations in the wind measurements, throughout a particular night, will result. There is also no evidence of such variations in the data. This source of error could however be reduced in future, if care is taken to accurately reset the central-scan voltage to the centre of the operating range at the start of each night.

3.5.6 The Effect of Variations in Emission Intensity

The Mawson FPS was specifically designed to cope with the large variations in emission intensity which accompany optical aurora. The instrument takes 6 sec to complete a scan and each profile is usually obtained by summing over at least 30 scans. If the emission intensity is either uniformly increasing or decreasing throughout the time required to acquire a profile, the resulting profile will be asymmetric. However, variations in the auroral λ558 nm intensity generally occur on a time scale smaller than the profile-acquire time and larger than the scan time thus variations in emission intensity will usually be very effectively averaged out.

In order to investigate whether there was any evidence of such distortion, the observed profiles were plotted along with the convolution of the best-fit Gaussian curve and the instrument profile. Deviations of the observed profile from the best-fit profile, or the residuals, were also

plotted. Approximately 100 profiles were examined in this way and of these only one, which is plotted in Figure 3.5a (iv), showed evidence of distortion which could be attributed to variations in the emission intensity. This profile gave a chi-squared value of 29, so it was rejected by the analysis, however it is presented here as an illustration. The distorted profile was obtained during the recovery phase of an auroral substorm and shows an enhancement at the base of the profile on the lower side of the scan range. This suggests that the emission intensity was decreasing throughout the acquisition period. The value of the vertical wind determined from the distorted profile was 38 ms^{-1}, an increase of $\sim$40 ms^{-1} from the previous measurement.

Profiles obtained on either side of the distorted profile are also presented in Figure 3.5a, however, these show no signs of distortion due to intensity variations. The profiles obtained on day 280, when a sudden decrease in temperature and increase in intensity and vertical velocity were measured, were also examined (Figure 3.5b); once again there is no evidence to suggest that variations in intensity are responsible for the sudden increases in the vertical wind. Thus, although it is possible for variations in the emission intensity to distort profiles and produce large apparent velocities, such profiles are a rare occurrence and would routinely be rejected during analysis.

3.5.7 Other Causes of Profile Distortion

The main feature in most of the residual curves is a decrease in the residuals towards the end of the scan. A slight asymmetry in the instrument function, which is a result of not having the calibration peaks at the centre of the scan, is responsible for this effect. Such deviations do not significantly affect the analysis but cause the curve resulting from the convolution of the best-fit Gaussian curve with the instrument function to be slightly distorted.

A second feature which is apparent in some of the profiles is a symmetric enhancement of the residuals on either side of the base of the Gaussian curve. This is most likely due to slight contamination of the lower thermospheric λ558 nm emission with the F-region emission.

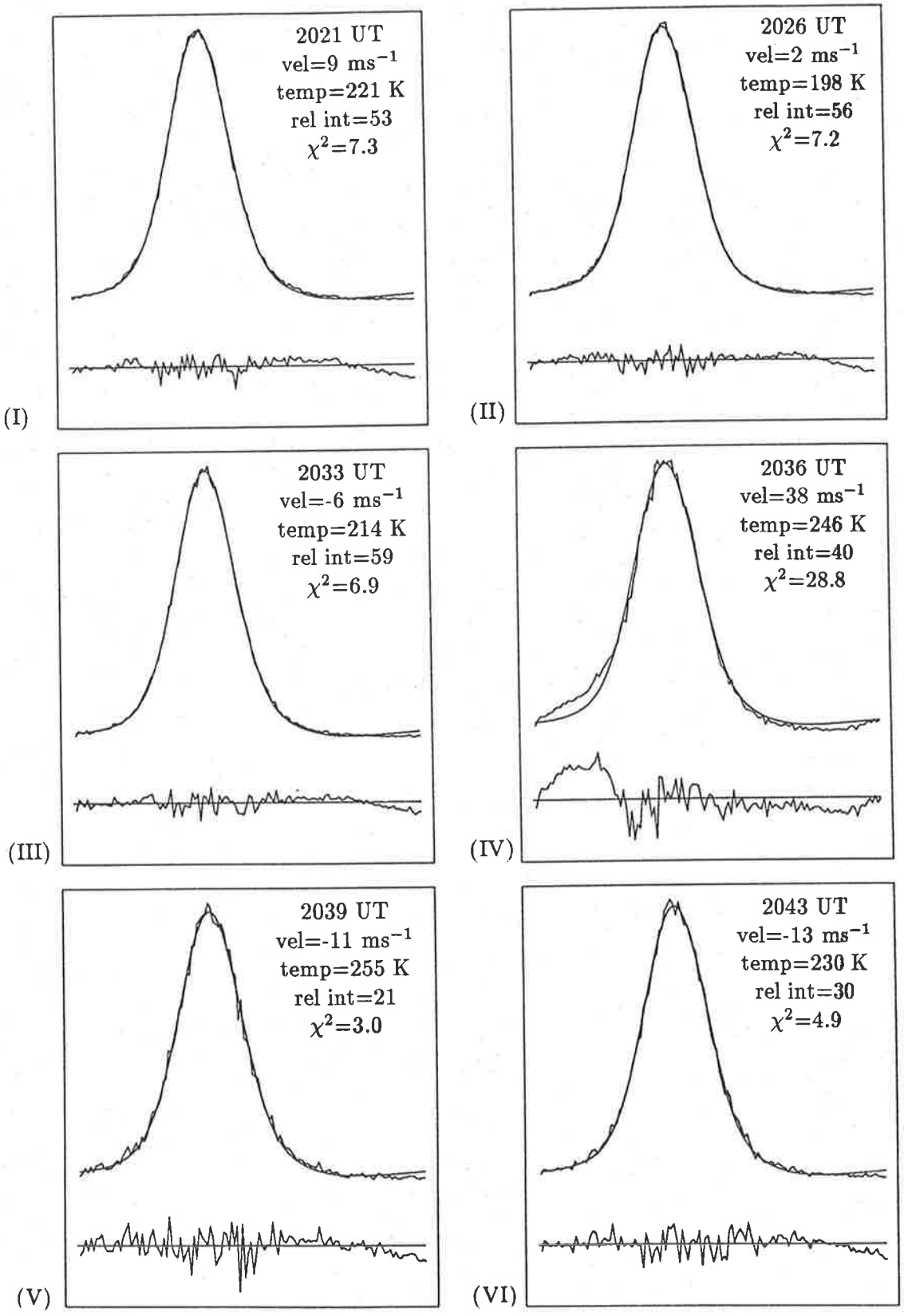

Figure 3.5: (a) Day 281 A sequence of six profiles recorded in succession. The recorded profiles are plotted against the convolution of the best-fit Gaussian curve and the instrument profile. The residuals, which are expanded to a scale ten-fold that of the data, are plotted below each profile . The values of the vertical velocity, temperature, relative intensity, and chi-squared parameter determined from each profile are listed.

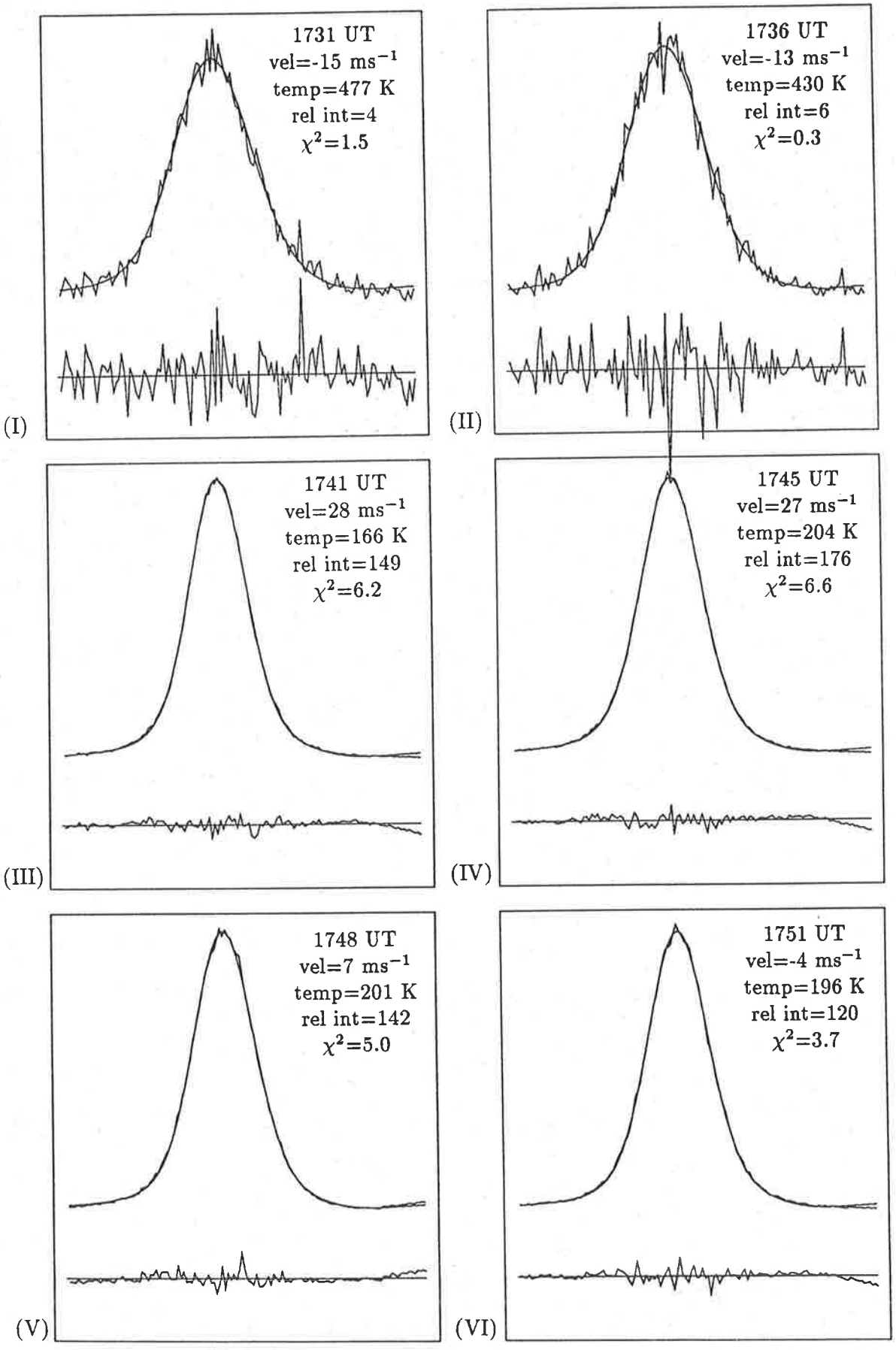

Figure 3.5: (b) Day 280 As for Figure 3.5(a).

Again this effect will not affect the wind data but may produce a slight enhancement in the temperature measurements which is not considered to be significant compared with the large range in temperatures determined from the λ 558 nm auroral emission.

3.5.8 Discussion

A degree of scepticism has, in the past, surrounded measurements of large vertical winds in the lower thermosphere. This point is illustrated by the fact that a previous report, finding vertical winds of tens of metres per second, was treated with so much scepticism when verbally presented in 1971 (Peteherych and Shepherd, 1971) that the results were not published until 1985 (Peteherych *et al.*, 1985).

Several possible sources of bias and error in the vertical wind measurements have been discussed including: a source of bias associated with the choice of instrument function, a source of error associated with the estimation of the drift curve, day-to-day variations in the 'zero' velocity estimate, and errors associated with acquiring profiles in conditions of varying emission intensity. The fourteen nights of wind data have been examined individually and the sources of error have either been: incorporated in the error estimates, explained in terms of variations in the instrument operating parameters, or found unlikely to significantly affect the results over the periods of interest.

Chapter 4.

VERTICAL WINDS DURING AURORAL EVENTS

4.1 INTRODUCTION

In the auroral zone lower thermosphere small-scale winds may be generated by a number of mechanisms including particle precipitation, Joule heating, and gravity waves. Heating effects are a principal generation mechanism for gravity waves (Hunsucker, 1982) and thus, in the source region, it may not be possible to distinguish between motions resulting from local heating and motions resulting from the passage of gravity waves. In this chapter the direct response of the vertical wind to auroral events is examined and the results are interpreted in terms of the heating associated with such events.

The FPS data set lends itself well to the study of small scale vertical winds which are likely to be associated with local heating events. The field of view of the FPS is 0.67° (with a 3 mm field stop) so the instrument observes a region of diameter $\sim$ 1.3 km at 110 km. The instrument is capable of acquiring high time resolution data during auroral events, when a sampling period as short as 2 min may be used. The vertical wind, Doppler temperature, and λ558 nm intensity are derived from the observations. The temperature may be used to determine the emission height if a temperature-height profile is assumed. The emission intensity indicates the presence of overhead aurora. In addition, the relationship between the measured temperature and intensity gives some information on the relative importance of heating effects and variations in the energy spectrum and flux of precipitating particles, in producing variations in the measured temperature.

4.2 THE λ558 nm EMISSION

The λ558 nm emission results from a transition from the ^{1}S to ^{1}D states of atomic oxygen. The O(^{1}S) upper state is metastable with a radiative lifetime of about 0.8 sec. In determining the kinetic temperature of a region from the Doppler broadening of an emission line, the emitting

species is assumed to be in thermodynamic equilibrium with its environment. The collision frequency decreases with altitude having a value of 5 s^{-1} at about 200 km (U.S. Standard Atmosphere, 1976); thus the $O(^1S)$ atoms will be well thermalised before radiating at heights below about 200 km.

The λ558 nm emission is found in the nightglow and in the aurora. The nightglow emission comes from a thin layer at around 97 km, with a secondary emission layer in the F-region which contributes about 10 % (Hernandez, 1976; Thomas and Donahue, 1972). The λ558 nm auroral emission has the strongest emission intensity of any single feature in the visible aurora. The auroral emission is dependent on the flux and energy of the precipitating particles. The particle energy determines the emission height and the particle flux determines the emission intensity at a given height.

In the nightglow there are two main processes responsible for the production of $O(^1S)$; the direct Chapman reaction and the indirect, two-step Barth mechanism. The relative importance of these mechanisms is discussed by McDade and Llewellyn (1986) and Bates (1981). The process(es) by which $O(^1S)$ is excited in the aurora is(are) not completely understood. Current evidence indicates that indirect excitation is most important, with $N_2(A) + O$ favoured as the dominant excitation process (Gerdjikova and Shepherd, 1987; Henriksen and Egeland, 1988).

It is expected that when aurorae are present the auroral λ558 nm emission will completely dominate the nightglow emission. Temperatures obtained from observations of the λ558 nm nightglow emission generally lie in the range 160 to 200 K (Hilliard and Shepherd, 1966; Hernandez, 1976). In the present data set observations which resulted in temperatures within this range were all associated with at least some level of auroral activity. Thus there appear to be no measurements of uncontaminated nightglow among the present observations and so only the auroral emission will be discussed further.

Most of the aurorae observed during the period studied are classified as Type-c or normal aurorae according to the International Auroral Atlas (International Union of Geodesy and

Geophysics, 1963). Type-c aurorae appear green or whitish in colour because their intensity is below the visual colour threshold. The height of the lower border of these auroral forms varies from 114 km for weak aurora to 95 km for very strong aurorae (Chamberlain, 1961 as quoted in Vallance Jones, 1974) and the luminosity most frequently extends between 20 and 40 km vertically (Currie and Weaver, 1955 as quoted in Vallance Jones, 1974). Measurements made by firing a rocket into a broad diffuse aurora showed the peak λ558 nm emission to be at an altitude of just above 100 km, with the intensity dropping to half at about 140 km (Sharp et al., 1979). The $O(^1S)$ atoms are collisionally deactivated at altitudes below about 85 km (Zwick and Shepherd, 1973).

The height distribution of the emission intensity is dependent on the energy of the precipitating particles and is similar to the height distribution of the ionization rate (Vallance Jones, 1974). Figure 4.1 shows the height distribution of the ionization rate associated with the precipitation of approximately mono-energetic electrons for a range of incident energies (Rees, 1963). Higher energy electrons penetrate to lower altitudes and produce a much sharper peak in the ionization rate than lower energy electrons which produce a broader peak at higher altitudes.

Temperature and velocity determinations are made by measuring the total emission along the observing line of sight, so the Doppler shift and Doppler broadening depends on the distribution of the volume emission rate along this line of sight. The measured velocities are a result of the physical motion of individual atoms. Rapid variations in the emission height will result in an averaging of the Doppler velocities over a large height range. However it is not possible for an 'apparent' velocity (i.e. a velocity which is not representative of any physical motion) to be generated in such a manner.

4.2.1 Determination of the Emission Height

The principal emission height is estimated by comparing the measured Doppler temperatures with temperature profiles obtained from rocket measurements. Temperature measurements

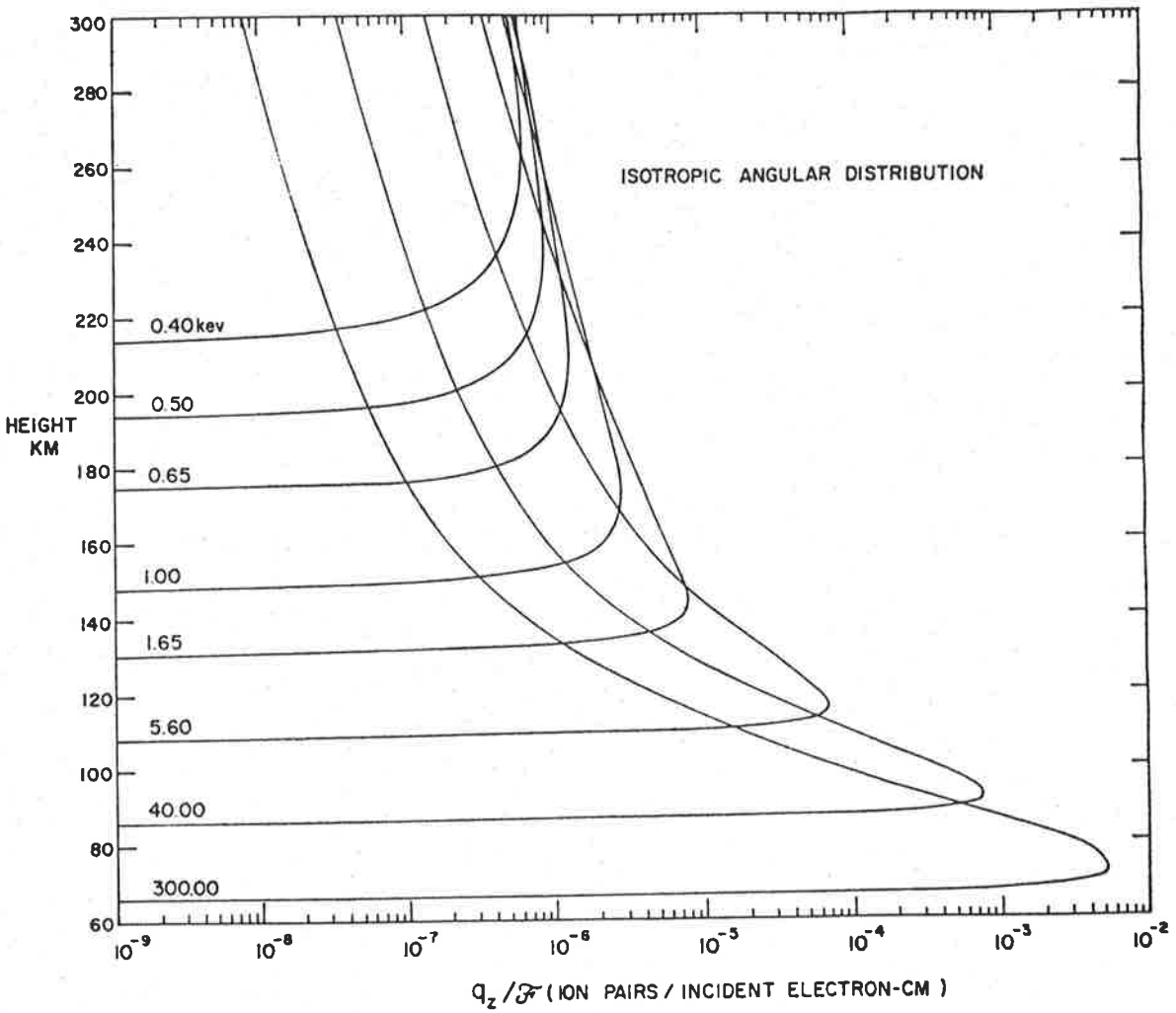

Figure 4.1: Model predictions of typical ionization curves for a range of incident energy levels for the case of an isotropic incident beam (after Rees, 1963).

have been made using a piezoelectric accelerometer on board rockets launched from Esrange, Sweden, during the Energy Budget Campaign (Philbrick et al., 1985). Rocket flights were made during both major (salvo A2) and moderate (salvo B) geomagnetic storm conditions and the temperature profiles are plotted in Figure 4.2. Temperatures from the U.S. Standard Atmosphere, 1976 (USSA 76) are also plotted.

The two salvo flights give a good indication of the variation in temperature which may be expected in the auroral zones during geomagnetically disturbed times, while the USSA 76 profile gives an average. Allowing for the temperature variations between the three sets of data the following conclusions are drawn:

1)Temperatures greater than 350 K have only been measured at altitudes greater than 114 km and

2)temperatures less than 250 K have only been measured at altitudes below 110 km. These limits are used to assign an approximate emission height to the FPS wind measurements from the values of the corresponding Doppler temperature.

4.2.2 All-Sky Camera Photographs

Auroral activity is determined from all-sky images in addition to FPS measurements of the zenith intensity of the λ558 nm emission. The all-sky camera produces black and white images of the whole sky at 1 min intervals. The camera was maintained by the author and operated on most clear nights throughout the winter. The FPS intensity measurements indicate the presence and intensity of overhead aurorae whereas the all-sky camera images are used to determine the presence of aurorae anywhere in the sky.

A series of four all-sky camera photographs, taken over 4 min is shown in Figure 4.3. The third and fourth photographs show a strong rayed arc. The rays lie parallel to the magnetic field lines and the point of convergence defines the magnetic zenith (the magnetic zenith appears to be almost overhead in the photographs). The lower border of the dominant form is clearly

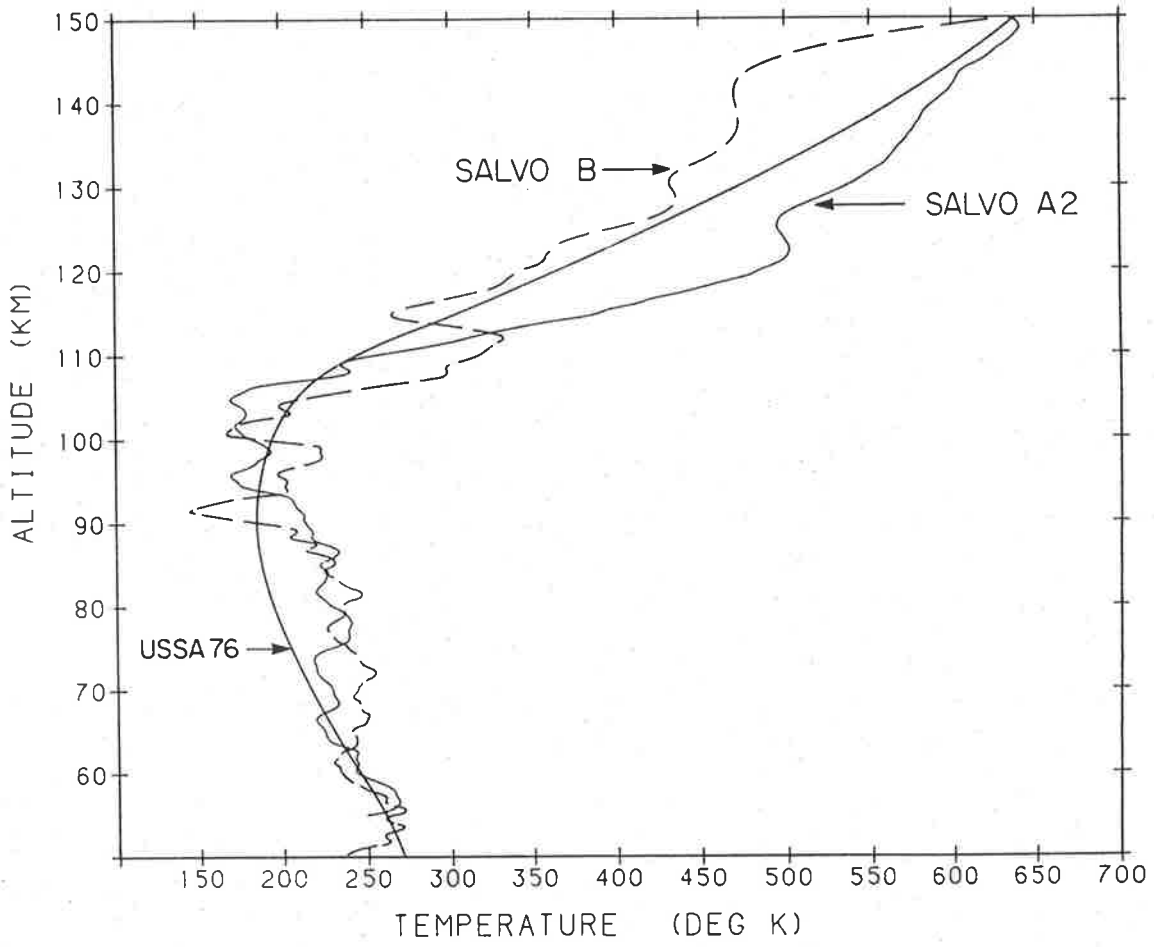

Figure 4.2: Temperature profiles determined from density measurements with a piezoelectric accelerometer during both major (salvo A2) and moderate (salvo B) geomagnetic storm conditions. A significant increase in temperature between 110 and 150 km is attributed to the effects of Joule heating during the period of larger geomagnetic activity. Temperatures from the U.S. Standard Atmosphere, 1976 (USSA 76) are also shown. (After Philbrick *et al.*, 1985).

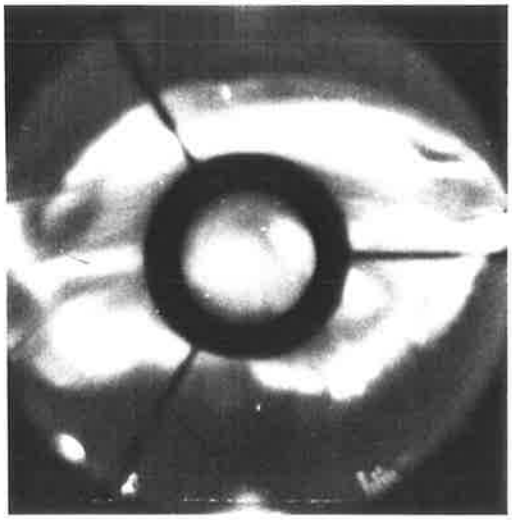

(I)

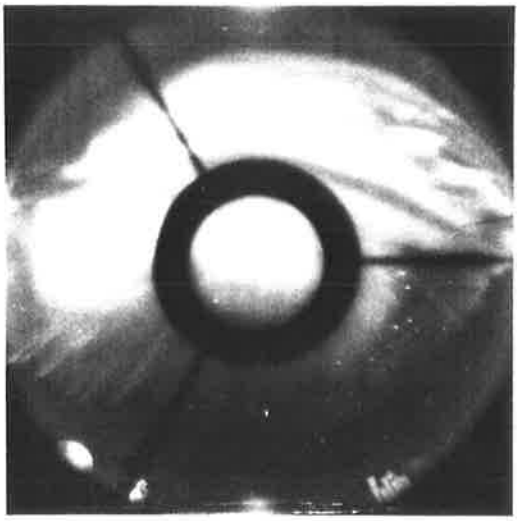

(II)

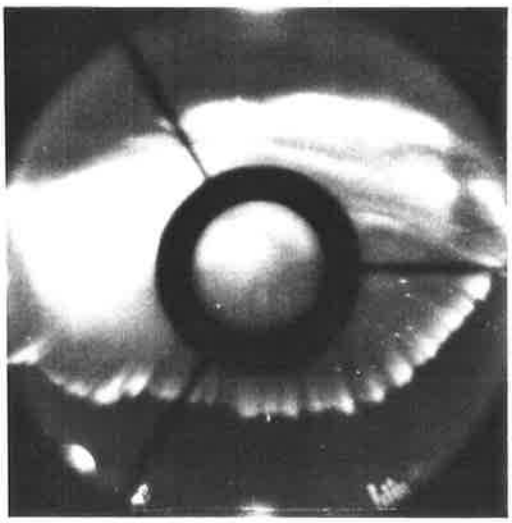

(III)

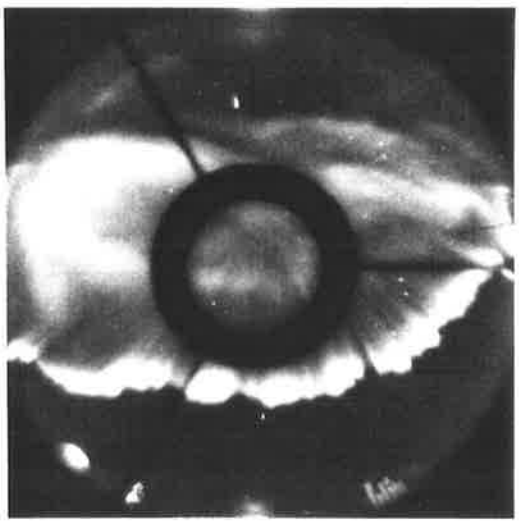

(IV)

Figure 4.3: A series of four all-sky photographs taken at one minute intervals from 1753 to 1756 UT on day 279. Photographs III and IV show a strong rayed arc. The rays lie parallel to the magnetic field lines and the point of convergence defines the magnetic zenith (which is almost overhead in these photographs).The curve formed by the termination of the rays defines the lower border. The lower border of the dominant form is clearly identifiable in photographs III and IV. The principal emission height of the aurora was less than 110 km as determined from Doppler temperature measurements using the FPS.

identifiable in photographs 4.3 (iii) and (iv). The intensity is seen to increase towards the bottom of the rays maximising in the vicinity of the lower border. The λ558 nm emission temperature, averaged over 3 min 24 sec and covering the period shown, was determined using the FPS and found to be 227 $\pm$ 3 K. Thus the peak emission of the aurora shown was inferred to be at a of height of less than 110 km.

4.3 THE INVERSE TEMPERATURE-BRIGHTNESS RELATION

The inverse temperature-brightness relation (ITBR) describes the tendency for auroral brightness and temperature, as inferred from observations of optical emissions, to be inversely related. This relationship has been studied by Hilliard and Shepherd (1966) who have explained the relationship as follows:

"the inverse relationship is crudely interpreted as following the atmospheric density curve; that is, that a uniform excitation per atom exists down to some cutoff height determined by the particle energy. This cutoff height thus determines both the auroral brightness and the observed temperature", and further that "while the inverse relation is in effect, auroral brightness (and temperature) changes result primarily from changes in the particle energy spectrum rather than changes in flux. This systematic relationship also seems to preclude the existence of major temperature changes through auroral heating at those levels."

Hilliard and Shepherd show that although the inverse relationship generally holds, points may lie on different curves for different events, with changes in the curve often occurring at the same time as magnetic bays.

A plot of temperature versus intensity is given for all the FPS data obtained over the 14 days of observations (Figure 4.4a). The plot shows that high intensity points are associated with low temperatures and that high temperatures are associated with low intensities. However it is not obvious that the ITBR holds throughout the data. Similar plots were drawn for individual auroral events from which it was found that the ITBR relation often held. Figure 4.4b shows

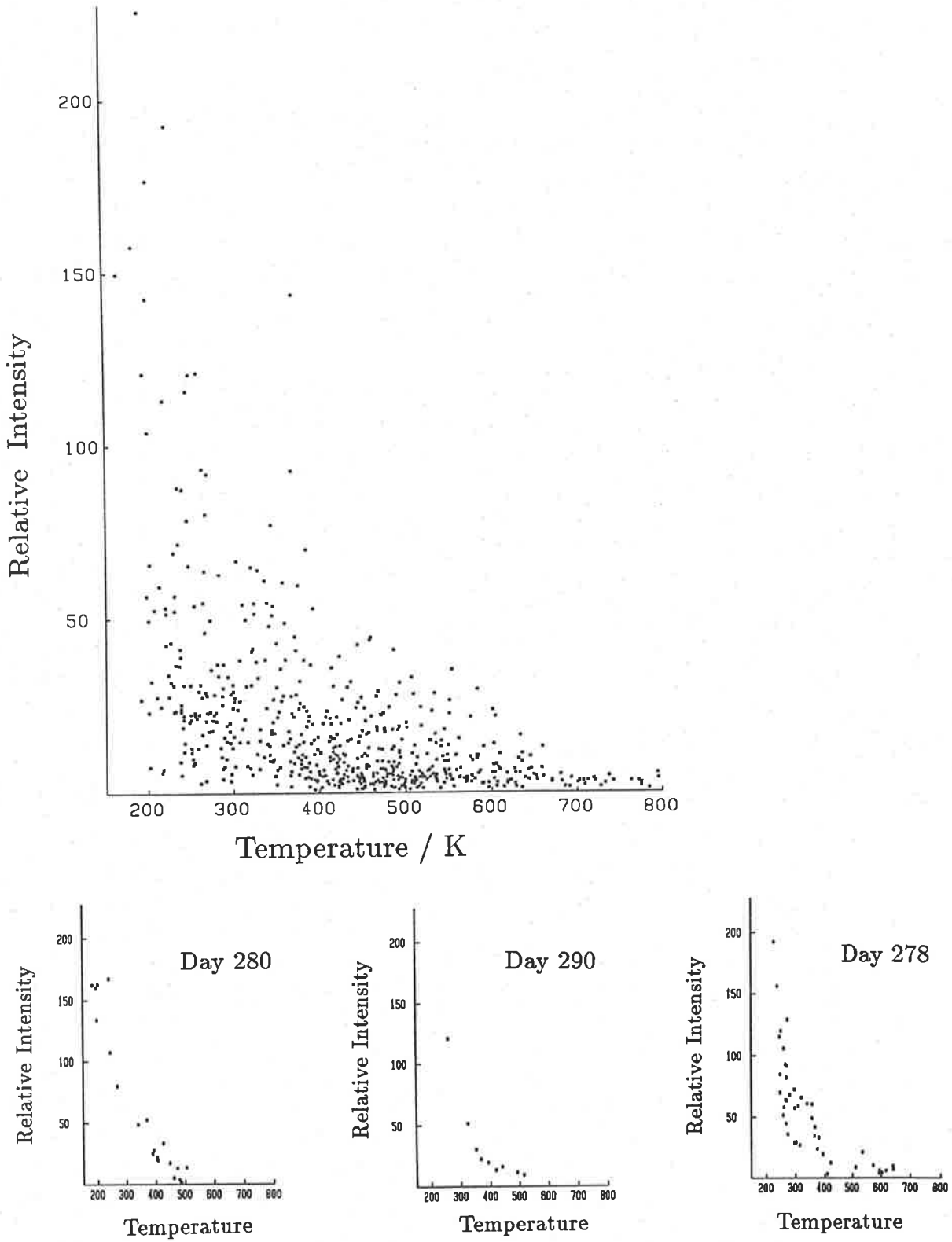

Figure 4.4: The intensity of the $\lambda 558$ nm emission versus temperature for *top:* all the FPS data obtained over the 14 nights of observations which resulted in wind measurements, and *bottom:* for three intervals of two hours in duration which coincided with auroral substorms occurring on days 280, 290, and 278. The points lie close to a simple curve suggesting that the ITBR holds for these intervals. The plot on the right however shows that this is not always the case as the points appear to lie on two different curves. The event described by this plot occurred on day 278 at about 2000 UT and it was a particularly intense and long duration event.

the intensity versus temperature curves for three such events occurring on days 280, 290, and 278. The points generally form a simple curve, however the third example shows that this was not always the case as the points appear to lie on two different curves. The event on day 278 was a particularly intense and long lasting event and will be discussed further in section 4.6.

4.4 CROSS-CORRELATION ANALYSIS

Auroral events typically occur on a time scale of tens of minutes and often recur on a time scale of hours. In order to investigate the effects of individual auroral events on the vertical wind the data were divided into a series of 2 hour intervals with an overlap of ~~half an~~ one hour. The wind data were then cross-correlated with both the intensity and temperature respectively for each two hour interval in turn. The intensity and temperature data were also cross-correlated. However, in light of the ITBR it proved more appropriate to cross-correlate the intensity and inverse temperature.

The significance of the results was determined by plotting the correlation coefficients against lag, up to a lag of $\pm$ 20 min. If a sharp maximum or minimum occurred within this interval then the correlation was considered significant. If the maxima or minima showed a broad peak or if there were larger extreme values within the interval plotted, then the correlation was considered not to be significant.

4.4.1 Correlation of Intensity and Temperature

A negative correlation between the intensity and temperature is apparent by visual inspection of the data. Such a relationship is clearly seen in the data of days 286 and 287 which are plotted in Figure 4.5. Plots of the correlation coefficient versus lag are shown for the two-hour intervals for which some level of auroral activity was apparent on these two days. These plots are considered to show a significant correlation between the intensity and inverse temperature at a lag of close to zero in each case.

A total of 47 two-hour intervals from the 14 days data were analysed. Of these, 40 intervals

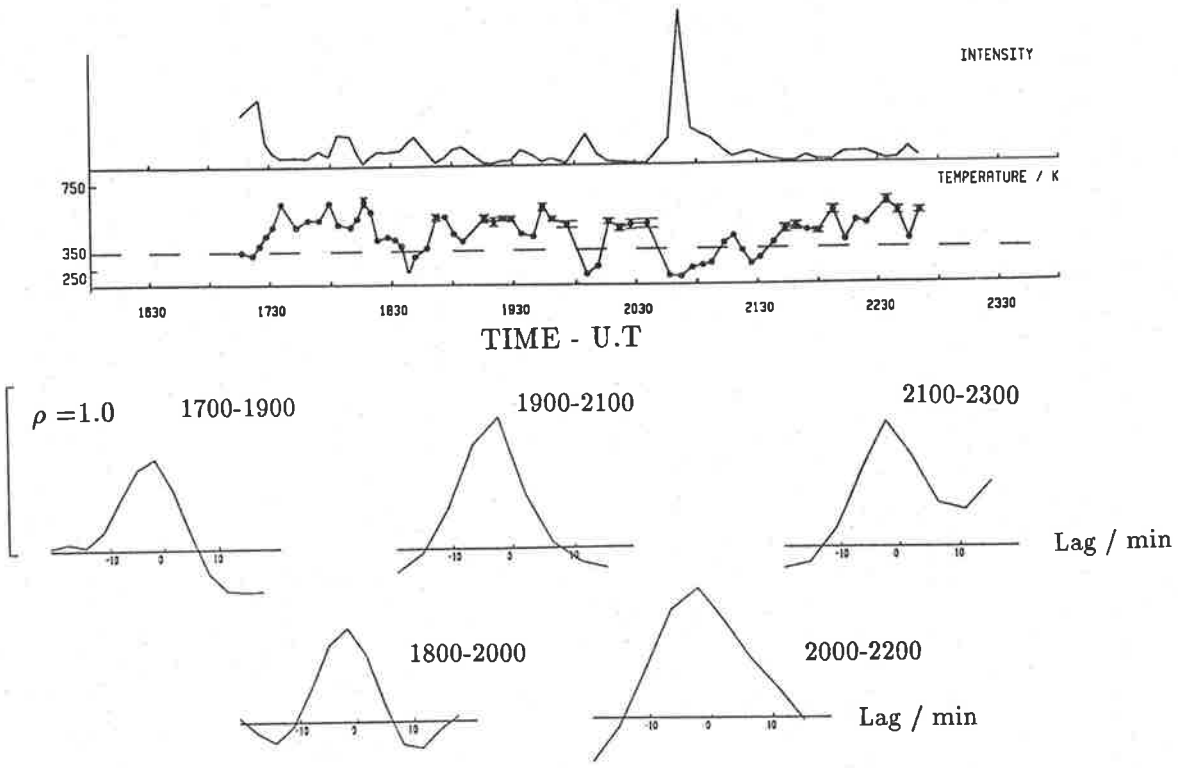

Figure 4.5: (a) Day 286 *top:* Plot of relative intensity of the λ558 nm emission and Doppler temperature versus time showing a negative correlation between these two quantities. *bottom:* Results of cross correlating the intensity and inverse temperature over all the observations which have been divided into two-hour intervals with 60 min overlap. The value of the correlation coefficient, ρ, is plotted against the lag in minutes. The five curves are considered to show a significant correlation between the intensity and inverse temperature.

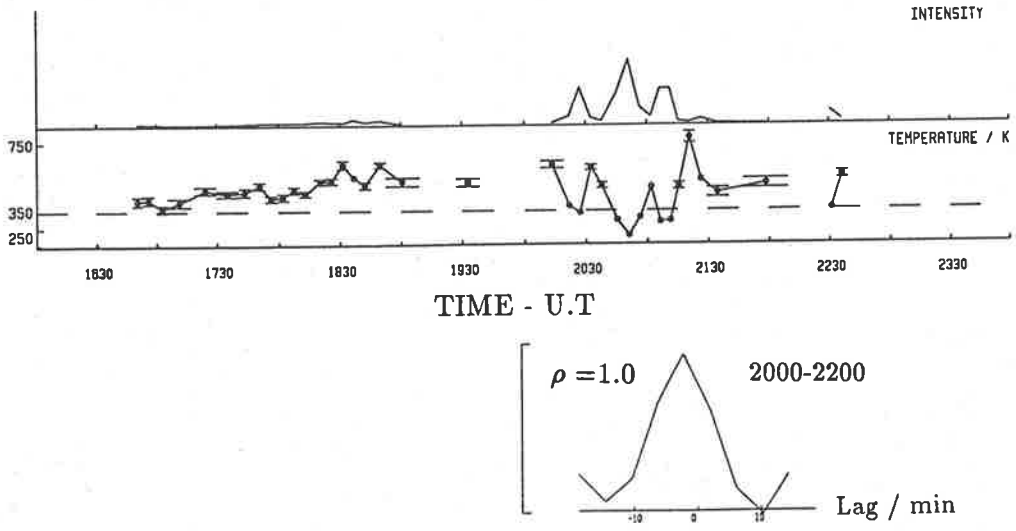

(b) Day 287 *top:* As for Figure 4.5a. *bottom:* Results of cross correlating the intensity and inverse temperature over the interval 2000 to 2200 UT which is the only two hour interval for which some level of auroral activity was present on this day. The plot of the correlation coefficient versus lag is considered to show a significant correlation between the intensity and inverse temperature.

showed a positive correlation between the intensity and inverse temperature, 4 showed a negative correlation and 3 showed no significant correlation. Two of the three intervals showing no correlation occurred on day 287 between 1630 and 1900 UT when the emission intensity was low (Figure 4.5b). The intervals resulting in a negative correlation were similar. Of the intervals resulting in a positive correlation 36 showed the maximum correlation to occur at approximately zero lag. In four cases the maximum occurred at a lag of $\pm$ 4 to 7 min which was equal to the time resolution of the data in these cases and thus not significantly different from zero.

The results are summarised by plotting the value of the maximum intensity obtained over each interval against the value of the maximum positive or negative correlation coefficient for that interval (Figure 4.6). Intervals showing strong peaks in the intensity also showed a strong positive correlation between the intensity and inverse temperature. Poor or negative correlations were only obtained when the intensity over the interval was low.

These results show that the intensity is positively correlated with the inverse of the temperature throughout most of the data, with the strongest correlation occurring at a time lag of zero. A stronger test of the relation between the intensity and temperature is applied by plotting the intensity against temperature, for which it is found that the data points often form a simple curve for individual events, although this is not always the case. When the data do lie on a simple curve with negative slope the ITBR is said to be satisfied. During times when the ITBR is satisfied the primary cause of variations in the measured temperature is variations in the energy spectrum of the precipitating particles. During times when the ITBR does not hold then variations in the temperature due to atmospheric heating and/or variations in the intensity due to variations in the flux of the precipitating particles are likely to be significant.

4.4.2 Correlation of Wind with Intensity and Inverse Temperature

A significant correlation between the wind (positive upwards) and either or both the intensity and inverse temperature, were measured on 12 of the 47 two-hour intervals examined. It was

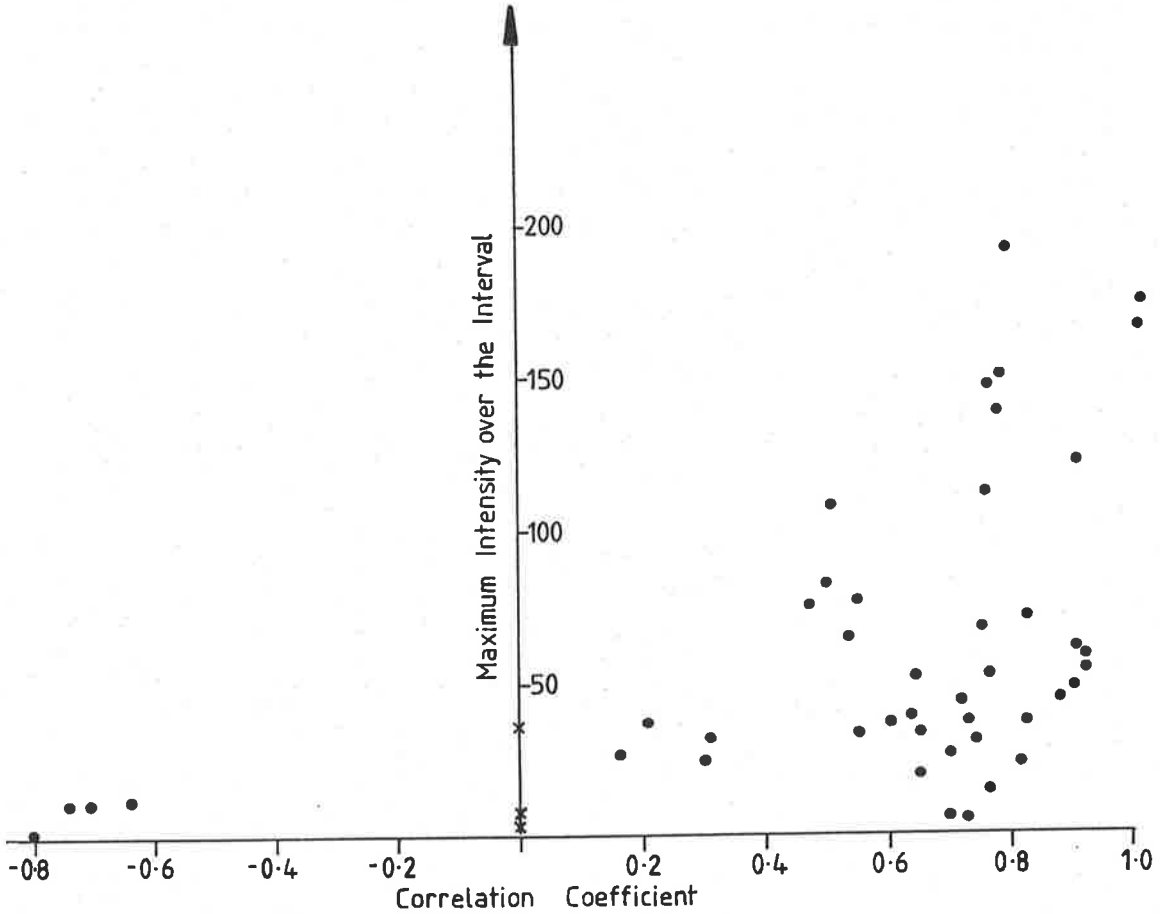

Figure 4.6: Summary of the results of cross-correlating the intensity and inverse temperature over 14 days data which have been divided into a total of 47 two-hour intervals which overlap by 30 min. The value of the maximum relative intensity measured over each two-hour interval is plotted against the maximum positive or negative correlation coefficient obtained at approximately zero lag for that interval. No significant correlation is indicated by a cross on the vertical axis. Intervals showing large peaks in the intensity also show a strong positive correlation. Results showing negative or no significant correlation were associated with intervals of low relative intensity.

found that if a positive correlation resulted when the wind was cross-correlated with intensity, then either a positive correlation or no significant correlation was found when the wind was cross-correlated with inverse temperature and similarly for a negative correlation. These findings are consistent with the results of the previous section which showed that the intensity is positively correlated with inverse temperature throughout most of the data.

The results of cross-correlating the vertical wind with both the intensity and inverse temperature are summarised in the following table.

Table 4.1: Summary of the results of cross-correlating the vertical wind and temperature and the vertical wind and intensity. The results are classified as class I or class II as defined below.

Measured Correlation	No. of Intervals	Class
1. Positive correlation between wind and intensity	2	
2. Positive correlation between wind and inverse temperature	4	I
1. and/or 2.	5	
3. Negative correlation between wind and intensity	7	
4. Negative correlation between wind and inverse temperature	3	II
3. and/or 4.	7	

The data were divided into two groups according to the sign of the correlation between the wind with intensity and wind with inverse temperature: class I included data from intervals which resulted in a positive correlation between either or both wind and intensity or wind and inverse temperature, and class II included data from intervals which resulted in a negative correlation between either or both wind and intensity or wind and inverse temperature. The maximum relative intensity over the interval for the class I data ranged from 55 to 174 whereas that for the class II intervals ranged from 13 to 150. Thus the class I data appear to be associated with higher intensity events than do the class II data.

To further investigate the difference between the class I and II data the intensity was plotted against temperature for each point in each of the two classes separately, as shown in Figure 4.7 a and b respectively. A clear difference between the two data sets is apparent. The class I data

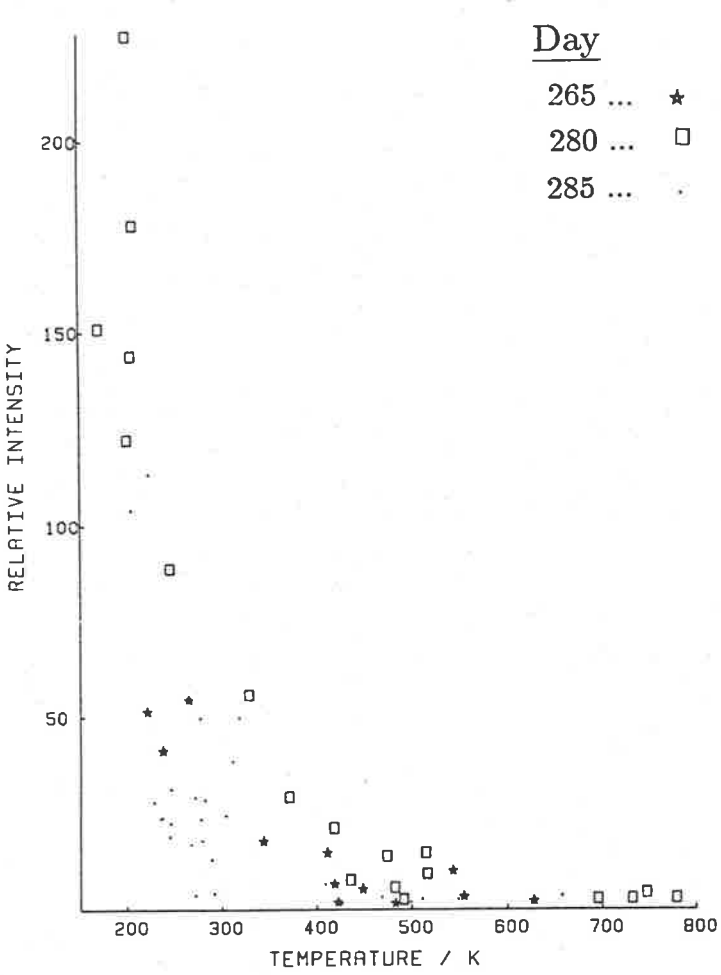

Figure 4.7: (a) Relative intensity of the λ558 nm intensity versus temperature for points lying within intervals classified as class I. (Class I intervals result in a positive correlation between the wind and intensity and between the wind and inverse temperature). The different symbols represent different days.

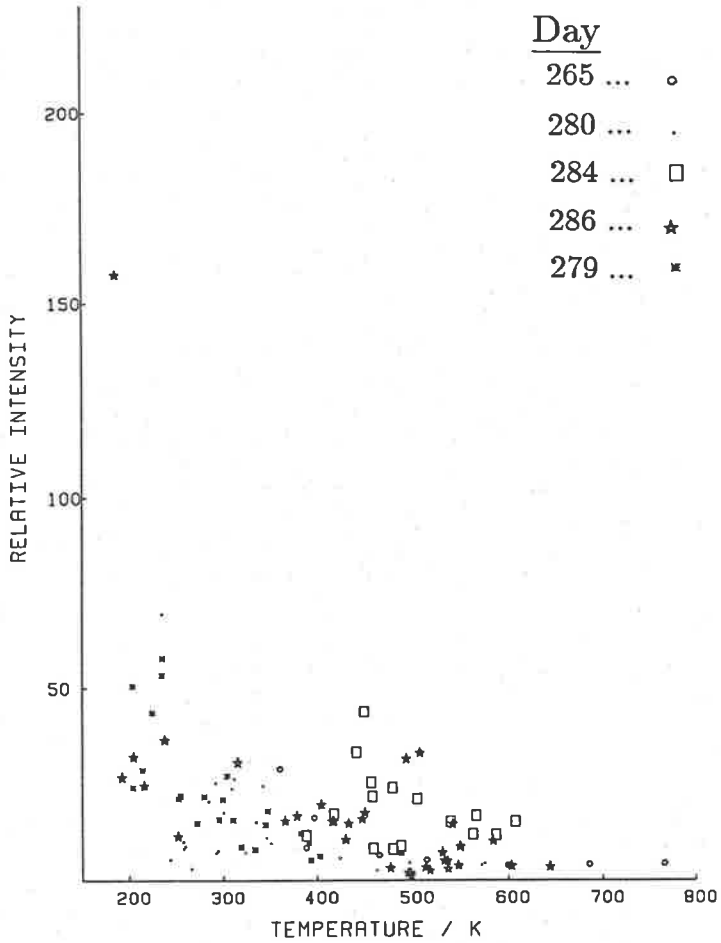

(b) Relative intensity of the λ558 nm intensity versus temperature for points lying within intervals classified as class II. (Class II intervals result in a negative correlation between the wind and intensity and between the wind and inverse temperature).

consists of intervals for which the ITBR relation holds with the points corresponding to each day generally lying close to a simple curve. Each interval contains points associated with temperatures less than 250 K (emission height less than 110 km) with a large proportion of the data having temperatures less than 350 K. The class II data on the other hand do not obey the ITBR. A large proportion of these points are associated with temperatures greater than 350 K (emission height greater than 114 km).

4.5 D-REGION IONIZATION INFERRED FROM THE SAPR RADAR DATA

The presence of strong D-region ionization may be inferred from the return heights and strengths of the SAPR echoes. During particle precipitation events the presence of enhanced ionization in the D-region will cause the SAPR data acquisition to be limited to the lower levels. Absorption of the transmitted wave is the most likely cause of the observed effect, although a second possibility is that the signal is being totally reflected at lower heights and thus not reaching the higher levels.

In the auroral zones, D-region electron concentrations have been observed to increase up to 10^6 cm^{-3} at 90 km (Hargreaves, 1980). This is much greater than the electron density of 4.68×10^4 cm^{-3} corresponding to a plasma frequency of 1.94 MHz (the operating frequency of the SAPR radar). It is thus possible that total reflection of the transmitted wave may occur at heights below 90 km. However an appreciable increase in electron density has been observed down to 85 km during auroral events (Devlin *et al.*, 1986). The electron-neutral collision frequency equals 1.94 MHz at about 79 km (Banks and Kockarts, 1973) so non-deviative absorption will maximise at this height. Deviative absorption will also be significant at heights just below the level of total reflection. Thus it is most likely that absorption of the transmitted waves at low heights is the cause of the absence of return echoes from higher altitudes during auroral events. Such events will be referred to here as 'absorption events'.

There were 17 days for which both SAPR data and FPS intensity and temperature measure-

ments were obtained. Over these days enhanced ionization in the D-region was evident on 10 occasions covering 8 days. These events caused the maximum acquisition height to be reduced to between 82 and 102 km. The absorption events lasted for periods of 30 min to 2 h with a faster recovery usually seen at the lower heights.

Absorption events are clearly seen in Figures 4.8 a and b. On day 280 there is no data obtained with the SAPR radar at heights above 98 km during a maximum in the intensity and minimum in the temperature, which occurred around 1740 UT, and only weak signals obtained between 86 and 98 km. Shortly after the start of the event the return echoes below 86 km appear to be enhanced. On day 286 there is no data obtained above 88 km coinciding in time with a peak in the λ558 nm emission and low emission temperatures which occurred around 2045 UT. Again strong return signals are obtained at heights below 88 km shortly following the start of the event.

[On both occasions there also appears to be an enhancement in the high level echoes (those above 98 km) immediately prior to the event. It is suggested that these may be due to strong off zenith reflections produced from a region of enhanced ionization associated with the approaching disturbance. A rough calculation shows that reflections from a region a horizontal distance of 50 km away and at a height of 100 km would produce echoes at an apparent height of 110 km, consistent with the observations]

Intervals showing evidence of enhanced ionization in the D-region and those which have been classified as class I or class II have been compared and the following comments are made:

Class I events occurred on three separate days. On two of these the class I events coincided with absorption events.

Class II events occurred over five separate days. On two of the five days class II events coincided with absorption events, on one day the class II event preceded an absorption event, and on two days there were no absorption events.

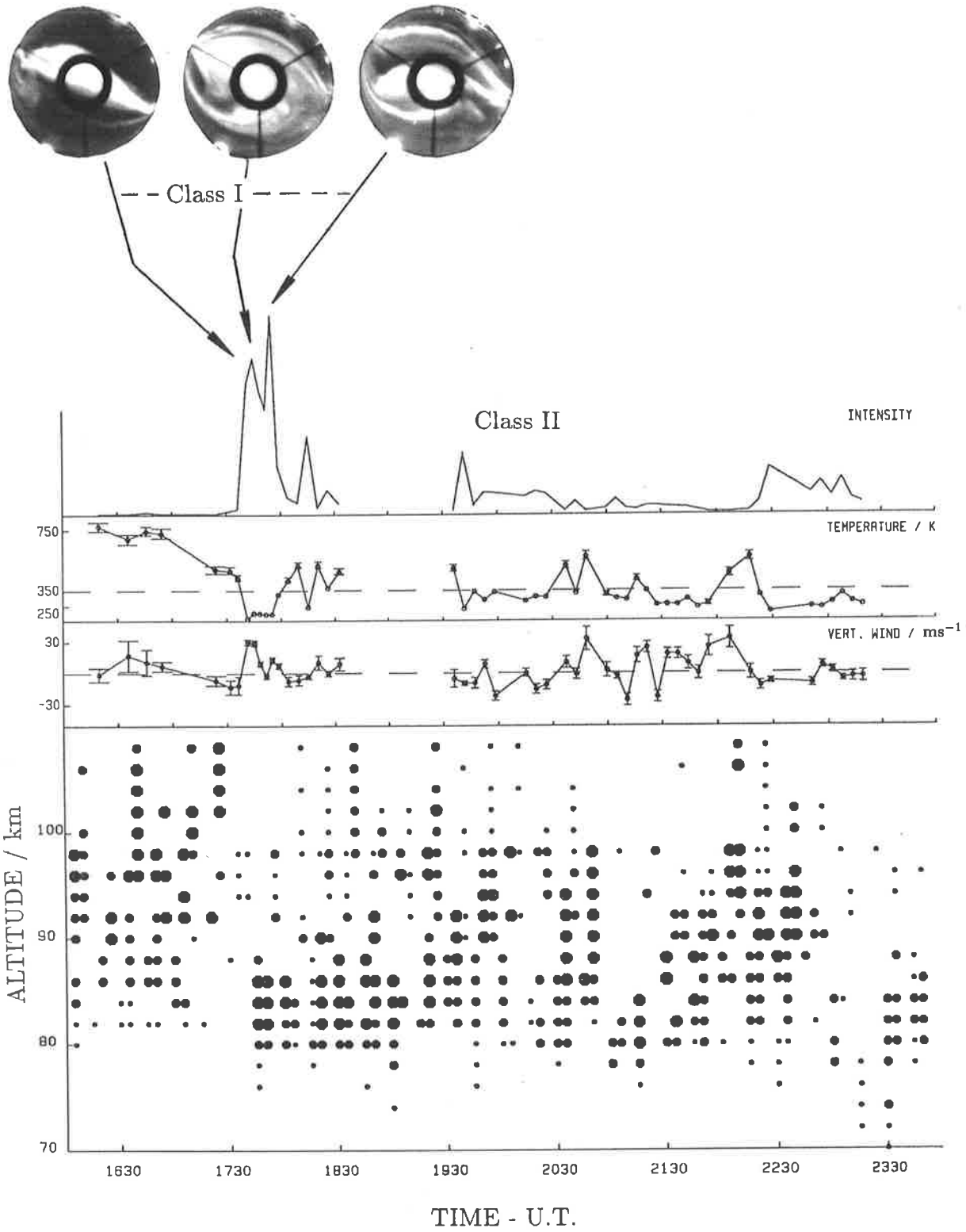

Figure 4.8: (a) Day 280 *top:* All-sky camera photographs showing auroral activity. *middle:* Plot of relative intensity of the λ558 nm emission, Doppler temperature and vertical wind (positive upwards) versus time. *bottom:* Height and time coordinates of echo returns from the SAPR radar. The relative strength of the return signals is indicated by the size of the symbols.

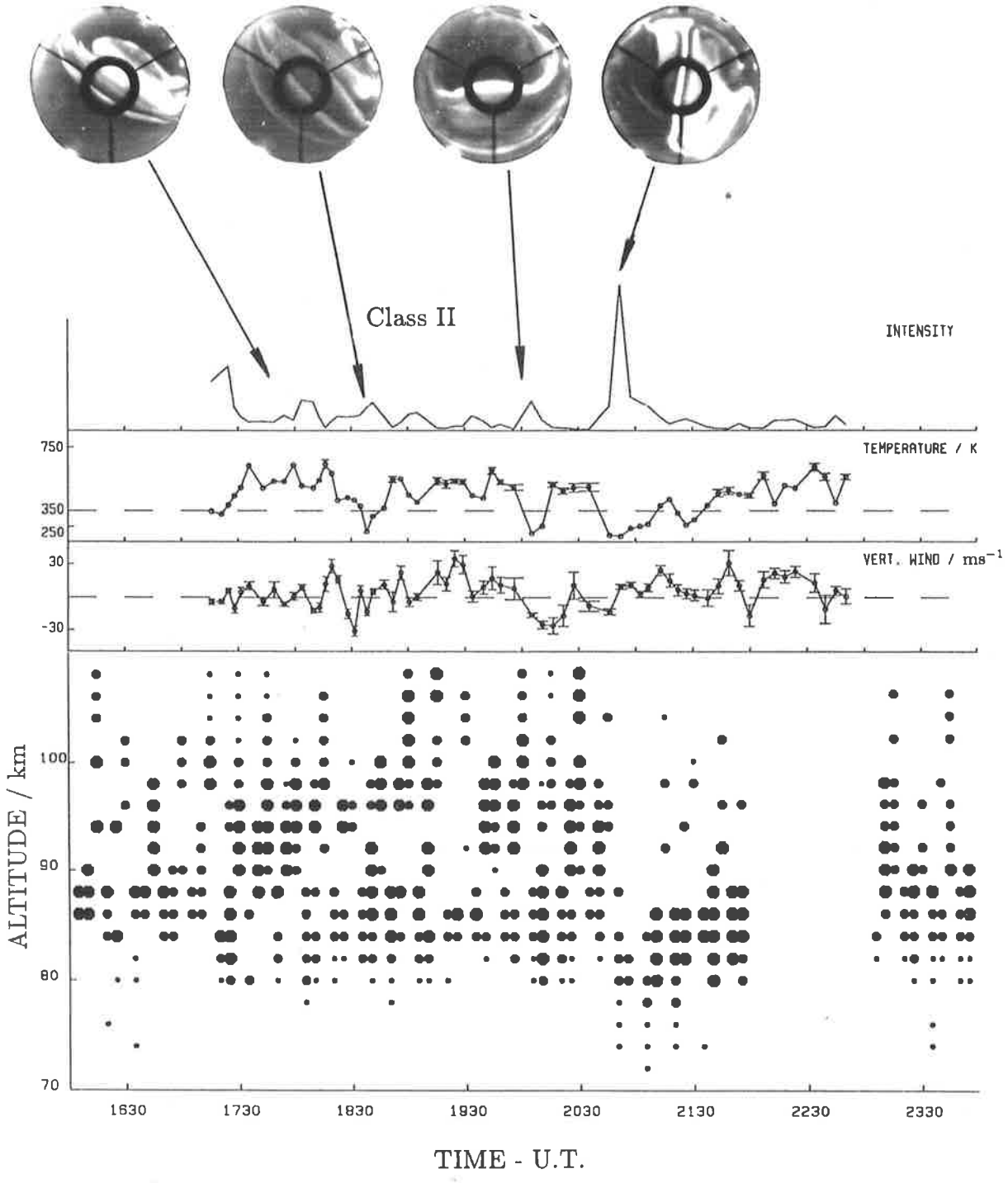

Figure 4.8: (b) Day 286 As for Figure 4.8(a). Note: the SAPR radar was not operating between 2200 and 2300 UT.

4.6 DESCRIPTION OF INDIVIDUAL EVENTS

The class I intervals tended to coincide with well-defined auroral events whereas the class II intervals were generally associated with extended periods of moderate auroral activity. From a total of five class I intervals two pairs of these were overlapping and therefore described single auroral events. These two events, which occurred on days 280 and 285, will be examined along with a third major event which occurred on day 278 and showed some similarities to the other two although it did not result in a significant correlation between the wind and the other parameters. Of the total of seven class II intervals, two pairs of these were overlapping thus there was a total of five isolated intervals. One of these intervals, which occurred on Day 286 will also be examined.

A large auroral disturbance which occurred at about 1740 UT on day 280 resulted in the strongest measured λ558 nm intensity over the 14 days of observations (Figure 4.8a). The peak in intensity was accompanied by measured temperatures of 166 to 204 K, thus the principal emission height was less than 110 km during this event. A sudden increase in the vertical wind of 41 ms^{-1} occurred at the start of the event with the wind attaining an upwards velocity of 28 ms^{-1}. This large upwards velocity was sustained for two measurements (approximately 6 min) after which the vertical wind reversed direction in the following two measurements.

Two high intensity events occurred in close succession on day 285 and were followed by a period over which a continuous level of moderate intensity emission was measured (Figure 4.9). Temperatures of less than 250 K were associated with the high intensity peaks, the temperature remaining less than 350 K for the following 2 hours and less than 250 K for almost half of this time. The vertical wind increased steadily for about 90 min following the first intensity peak, reaching a maximum value of 32 ms^{-1} towards the end of the period. Following the maximum an oscillation in the vertical wind of period approximately 50 min was evident.

A very large and long duration auroral event was observed on day 278, beginning at 1954 UT (Figure 4.9). The intensity was largest at the start of the event but remained at a high level

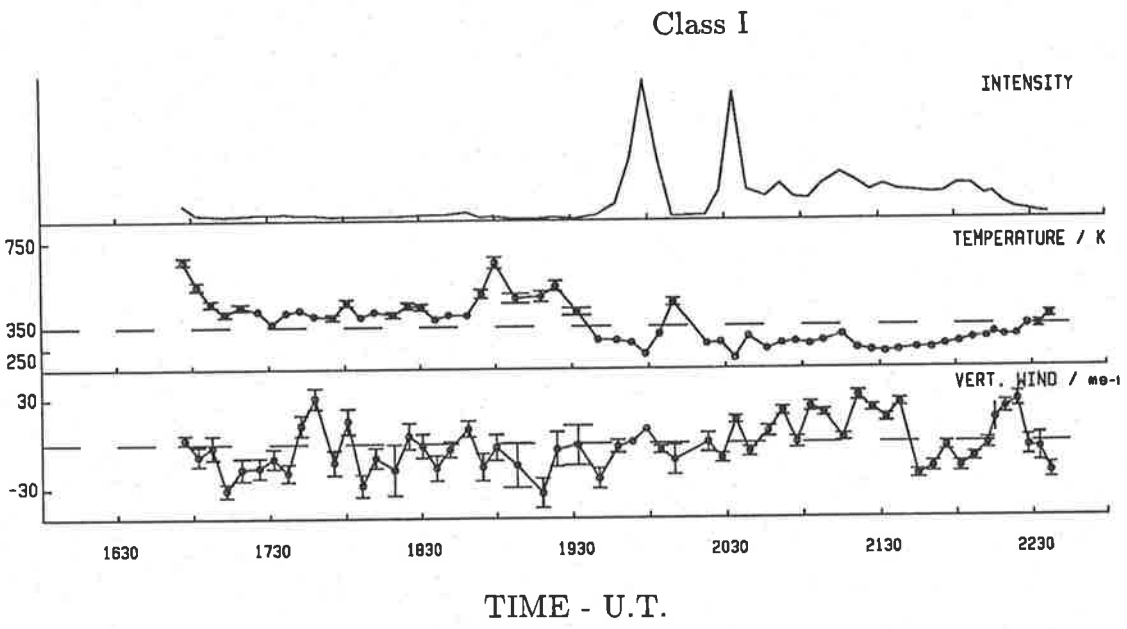

Figure 4.9: (a) Day 285 Plot of relative intensity of the λ558 nm emission, Doppler temperature and vertical wind (positive upwards) versus time.

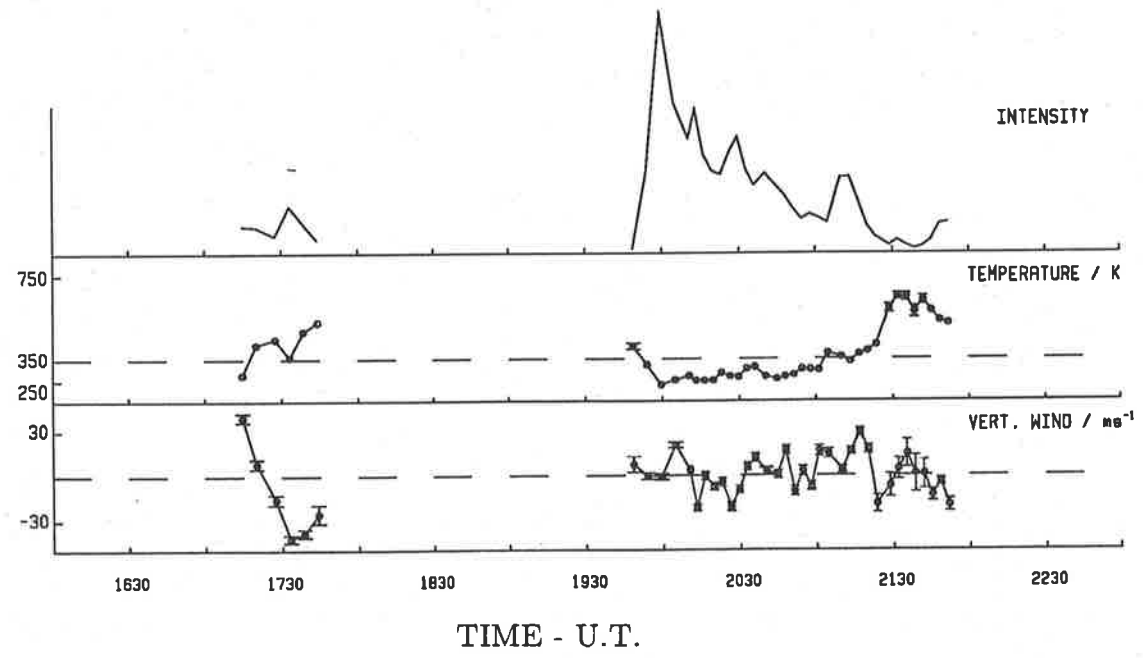

Figure 4.9: (b) Day 278 As for Figure 4.9(a).

for approximately 40 min, then fell to a moderate level with a secondary peak at 2110 UT. The measured temperature was less than 250 K for most of the first 20 min and was less than 350 K for the following 50 min. The vertical wind increased to 18 ms^{-1} shortly after the start of the event then decreased to -23 ms^{-1} after which it showed a generally increasing trend over the following hour, attaining an upwards velocity of 27 ms^{-1}. Following the maximum an oscillating component was then apparent in the wind field of period between 20 and 30 min. The intensity versus temperature plot for this event appeared to lie on two curves as shown earlier in Figure 4.4b.

On day 286 a moderate level of auroral activity was present throughout the night with the class II interval between 1800 and 2100 UT (Figure 4.8) showing a matching oscillation between the wind and temperature curves which resulted in a negative correlation between the wind and inverse temperature. The vertical wind varied between 29 ms^{-1} upwards and 35 ms^{-1} downwards over the interval. The temperature was greater than 350 K for most of the interval although it decreased briefly to a minimum value of 204 K. The positive correlation between the wind and temperature suggests that the largest upwards velocities are occurring at the higher altitudes and the downwards winds are occurring at lower altitudes.

In summary, there does not appear to be any systematic difference between the magnitude of the vertical winds measured during class I and class II intervals. However large upwards winds measured during class I intervals appear to be a direct response to strong auroral events. Such events are characterised by high intensities and low temperatures thus a positive correlation with the intensity and inverse temperature results. Large upwards winds measured during class II events, on the other hand, do not appear to be a direct response of the wind field to particular auroral events but rather appear to reveal a tendency for large upwards winds to be associated with higher temperatures and for smaller or downwards winds to be associated with lower temperatures. Further, since the ITBR does not hold for the case of class II events we cannot rule out the possibility that heating may have a significant effect on the measured

Doppler temperatures and may influence the observed correlation over the class II intervals,

4.7 COMPARISON WITH OTHER OBSERVATIONS OF VERTICAL WINDS

There have been a number of vertical wind measurements made in the upper thermosphere. However, there appears to be only one set of published results of vertical winds in the auroral zone lower thermosphere. Peteherych *et al.* (1985) have summarised their results as follows: "when the aurora is intense and its altitude is 'low', the velocity is upward and when the aurora is weak and its altitude is high, the velocity is downward" (Peteherych *et al.*, 1985). They found an upward wind of 22 ms^{-1} to be associated with the passage of an auroral arc. The observations made by Peteherych *et al.* used a time resolution of 10 min, compared with the time resolution of between 3 and 8 min used here. Peteherych *et al.* conclude that Joule heating provides the direct forcing of the upward winds, however they give no arguments for this conclusion.

Vertical winds in the F-region of the upper thermosphere have been determined from observations of the atomic oxygen λ630 nm emission. In this region the strongest vertical winds, which may exceed 150 ms^{-1}, are found to be a direct response to intense heating associated with brilliant aurorae (Herrero *et al.*, 1984; Rees *et al.*, 1984a and Wardill and Jacka, 1986). Wardill and Jacka found vertical winds of up to 50 ms^{-1} to be sustained for 30 min following a substorm, and then to be replaced by an oscillation of period 30 min. Rees *et al.* (1984a) measured upwards winds of 160 ms^{-1} during a bright and active aurora which were followed by downwards winds of 30 to 50 ms^{-1}. The intense upward winds lasted for 10 - 30 min which was comparable with the duration of the observations.

Models of the response of vertical winds in the lower thermosphere to auroral heat sources have considered much larger space and time averaged motions than those studied here. Such models estimate that vertical motions of up to a few ms^{-1} are produced by auroral heating (Bates, 1974b; Hays *et al.*, 1973). Recent model simulations have been more successful in

predicting large fluctuations in vertical speed in the upper thermosphere and have shown that intense upward winds may occur as a direct response to geomagnetic energy input. These models show upward winds of 200 ms^{-1} to be generated above localised regions of heating for periods of 10 to 30 min (Rees *et al.*, 1984a). Rees *et al.* estimate that the local vertical wind can absorb at least 30 % of the total substorm energy input.

The vertical wind velocities reported here are similar to the lower thermospheric vertical winds measured by Peteherych *et al.*. During low altitude aurorae upward winds with magnitudes of up to 32 and 22 ms^{-1} have been measured here and by Peteherych respectively. Vertical wind measurements in the F-region also show upward winds to be associated with intense auroral substorms (Rees *et al.*, 1984a and Wardill and Jacka, 1986) with magnitudes about five times greater than the lower thermospheric winds. However, Peteherych *et al.* show that the lower thermospheric vertical winds are larger, in terms of mass transport, by at least two orders of magnitude.

A further similarity between the upper and lower thermospheric winds is that an oscillating component in the vertical wind is sometimes measured following auroral events. An oscillating component of period 30 min was found on one night reported by Wardill and Jacka (1986) which may be compared with the oscillating components of period 60 min and 20 to 30 min measured here on days 285 and 278 respectively.

Vertical wind measurements have also been made in the upper mesosphere using various radar and rocket borne techniques. Measurements using the EISCAT UHF-radar show vertical winds of up to 2 ms^{-1} (upwards) and -6 ms^{-1} in the height range 80 to 85 km (Hoppe and Hansen, 1988). Foil cloud experiments show vertical winds of up to 10 ms^{-1} between 75 and 90 km (Widdel, 1987).

4.8 JOULE AND PARTICLE HEATING

The precipitating particles (usually electrons) which produce aurorae also lead to Joule and particle heating, which in turn lead to a general lifting of the thermosphere above the height of the heat input. "The principal consequence of atmospheric heating in the region extending from 100 to 300 km is an upward motion of gases..." (Hays *et al.*, 1973).

The Joule dissipation of ionospheric currents causes heating which is dependent on the Pedersen conductivity (Cole, 1962). Rocket data have shown that the altitude of maximum Pedersen conductivity can range between 120 km (no electrojet activity) to 136 km (-450 nT negative bay) suggesting that the height of maximum Joule heat input increases with increasing E-layer ionization (Thiele *et al.*, 1981). Observations with the Chatanika, Alaska, incoherent scatter radar show that Joule heating maximises around 125 to 130 km (Banks, 1977). Temperature profiles taken during both major and moderate geomagnetic storm conditions show significant heating between 110 and 150 km in the former case, as compared to the latter, with the difference being attributed to the effect of Joule heating (Figure 4.2) (Philbrick *et al.*, 1985).

The precipitation of particles causes heating mainly through the energy released during ionic recombination. About half the energy deposited by particle precipitation goes into atmospheric heating (Banks, 1977). Particle heating tends to maximise below the height of maximum Joule heating. Rocket soundings have shown the height of particle heating to vary between 92 and 124 km (Banks, 1977) and between 90 and 100 km (Torkar *et al.*, 1985). Measurements made by firing a rocket into an auroral arc showed particle heating to maximise at about 110 km and to be the result of the precipitation of electrons with energies between 15 and 35 KeV.

A direct comparison of Joule and particle heating rates has been made by Banks (1977). The measurements are spatially averaged over a horizontal distance of approximately 55 km at an altiude of 110 km. Two pairs of profiles have been selected which show how the relative magnitudes and heights of maximum Joule and particle heating may vary for different events (Figure 4.10). The event labelled A shows: the particle heating rate maximising at a height of

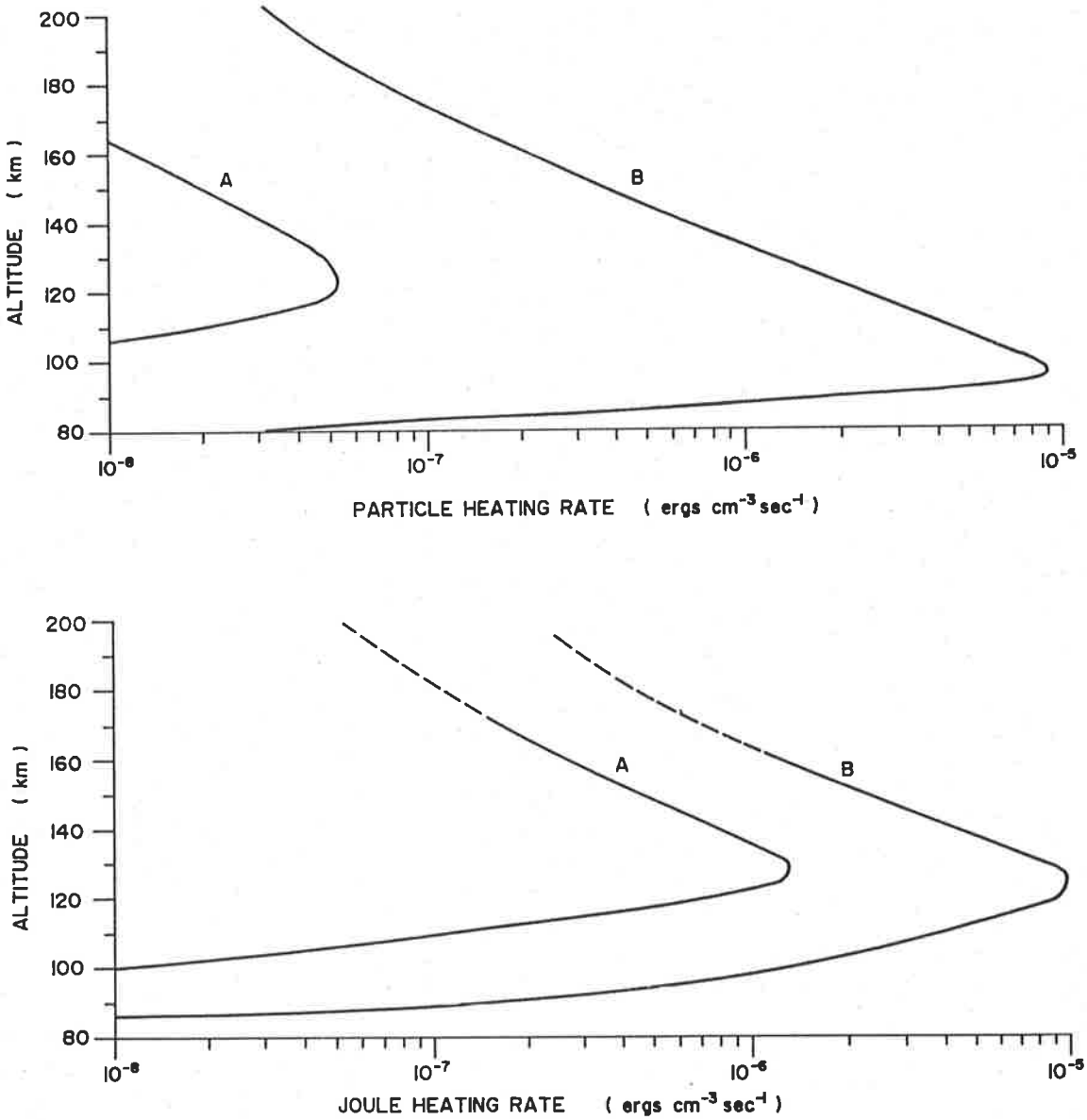

Figure 4.10: Altitude profiles of particle and Joule heating rates for two selected periods (marked A and B) on two different days (adapted from Banks, 1977). The event labelled A shows: the particle heating rate maximising at a height of 120 km, the Joule heating rate maximising at 125 km, the volume heating rate due to Joule heating being more than an order of magnitude greater than the volume heating rate due to particle heating. The event labelled B shows: the particle heating rate maximising at 100 km, the Joule heating rate maximising at approximately 130 km, the Joule and particle volume heating rates to be approximately equal.

120 km, the Joule heating rate maximising at 125 km, and the volume heating rate due to Joule heating being more than an order of magnitude greater than the volume heating rate due to particle heating. The event labelled B shows: the particle heating rate maximising at 100 km, the Joule heating rate maximising at approximately 130 km, and the Joule and particle volume heating rates to be approximately equal.

Joule heating will result in a greater energy input per neutral gas particle than particle heating of an equal volume heating rate due to the fact that Joule heating occurs at a relatively higher altitude. Also Joule heating has a much greater latitudinal extent than particle heating (Baumjohann *et al.*, 1985); the latter being restricted to regions of strong particle precipitation. Thus Joule heating is likely to have a much greater effect on the large scale dynamics of the thermosphere than does particle heating. However on a small scale and in regions of intense auroral arcs the effects of particle heating may be comparable to those of Joule heating. Rocket measurements by Evans *et al.* (1977) have shown that Joule dissipation associated with ionospheric current flow decreases abruptly from points just outside of to just within an auroral arc, although the total energy input to the neutral atmosphere does not. This suggests that particle heating within the arc is comparable to Joule heating outside of the arc.

In summary these results suggest that Joule heating tends to maximise in the height range 120 to 140 km whereas particle heating maximises in the range 90 to 124 km. Joule heating is associated with the dissipation of ionospheric currents and thus extends over a wide area. Particle heating on the other hand is a direct response to particle precipitation in the D and lower E-regions and may be highly localised, maximising within intense auroral arcs.

4.9 INTERPRETATION OF RESULTS

The class I and class II intervals show basic differences in terms of emission intensity, emission height, coincidence with both auroral events and enhanced D-region ionization as well as in the correlation of the vertical wind with temperature and intensity. It will be shown here that

these differences may be understood if the principal feature distinguishing the two categories is particle heating for the case of class I intervals and Joule heating for the case of class II intervals.

The Class I intervals appear to be a direct response of the wind field to intense auroral substorms. The observed positive correlation of the vertical wind with intensity and inverse temperature is then a result of the fact that these events are characterised by large emission intensities and low temperatures and that they produce large upward winds. The altitude of the peak emission is generally less than 110 km during such events; thus particle rather than Joule heating is the most likely cause of the upward winds. This conclusion is supported by the observation that enhanced ionization in the D-region was observed to accompany two out of the three events associated with class I intervals.

The response of the vertical wind to the heating events was almost instantaneous on one occasion when an upward wind of 28 ms^{-1} was measured at the onset of the most intense auroral substorm. On two other occasions the vertical wind was observed to increase steadily throughout the substorm, reaching a maximum of 32 and 27 ms^{-1} after about 2 h and 1 h respectively. If we assume that there is a certain minimum total heat input required for a significant vertical velocity to be produced, then this minimum is more likely to be reached in regions where the heating rate is large. In regions of smaller heat input there may be some time lag before an uplifting occurs. Thus it appears that particle heating associated with the most intense substorms is sufficient to produce sudden and large vertical winds at heights less than 110 km. However this was only observed on one occasion whereas on two other occasions there was some delay before the maximum velocity was attained. The magnitude of the maximum upward wind was approximately the same on all occasions.

The class II intervals do not appear to be a direct response to individual auroral events but they are associated with moderate to high levels of geomagnetic activity. They are typified by lower intensities and higher temperatures than the class I intervals, with temperatures greater

than 350 K and hence emission altitudes greater than 114 km for much of the time. The class II events may be due to a combination of Joule and particle heating, with the Joule heating dominating at the higher altitudes.

The observed negative correlation of the the vertical wind with intensity and inverse temperature during class II events may be interpreted in two ways:

1) the correlation may indicate that larger upward winds are associated with higher altitudes or

2) that higher temperatures are indicative of a higher level of heating producing larger upward winds.

The first possibility is reasonable considering that Joule heating tends to maximise towards the highest altitudes at which the peak in the λ558 nm emission occurs. It is also reasonable if we consider the effect upon the higher heights of heating at lower heights i.e. a vertical uplifting at one height will cause an upwards velocity at all greater heights after a time lag which is determined by the propagation time of the disturbance. The second possibility is also reasonable since it has been shown that the ITBR relation does not hold for the class II events. Although it does not necessarily follow from this that heating must be significant, this possibility cannot be ruled out. It is also possible that the observed correlation is a result of a combination of these two effects.

The history of preceding events on a particular night may influence the response of the vertical wind to further events later in the night. The auroral events which appeared to produce a direct response in the vertical wind all occurred near the beginning of geomagnetically disturbed periods. A large intensity peak measured at 2152 UT on day 286 (Figure 4.8b) following a number of hours of moderate auroral activity did not however produce any obvious response in the measured vertical wind. The largest vertical winds were only maintained for short periods (less than 10 min) and on two occasions large upwards winds were replaced by an oscillating component. It appears that other processes act to balance heat injection after some

time following which the effect of additional heat sources is reduced.

4.10 SUMMARY

The results and interpretation of the vertical wind observations are summarised below.

- Large upward winds of approximately 30 ms^{-1} magnitude have been measured and appear to be a direct response of the neutral atmosphere to intense auroral substorms which result in particle heating at altitudes less than 110 km. The observed upward winds are of slightly greater magnitude than those measured by Peteherych *et al.* (1985) under similar conditions.

- Large vertical winds of a similar magnitude are also measured at altitudes greater than 114 km during disturbed nights. These winds are not associated with individual events and appear to be produced by a combination of Joule and particle heating, with Joule heating dominating at the higher altitudes.

- The response of the vertical wind field to auroral activity in the lower thermosphere is similar to the response measured in the upper thermosphere by Wardill and Jacka, (1986) and modelled by Rees *et al.*(1984a). The magnitude of the vertical winds in the lower thermosphere is about five times less than that measured at F-region heights, although it is greater in terms of mass transport (Peteherych *et al.*, 1985).

Chapter 5.

TEST OF AN APPARENT CORRELATION BETWEEN THE HORIZONTAL WINDS AND GEOMAGNETIC ACTIVITY USING A RANDOMIZATION TECHNIQUE

5.1 INTRODUCTION

The dynamic structure of the upper thermosphere is strongly correlated with geomagnetic activity through the effects of direct heating and momentum transfer from the ions to the neutrals. In the mesosphere, the motions of the neutral atmosphere are dominated by upwardly propagating tides and gravity waves. The relation between geomagnetic disturbances and neutral air motions in the upper mesosphere/lower thermosphere are not well understood.

Correlations between geomagnetic activity and various components of the wind field have been discussed by Balsley *et al.* (1982), Manson and Meek (1986), Johnson and Luhmann (1985a,b), Johnson *et al.* (1987), and Phillips and Jacka (1987). Johnson and Luhmann (1985b) showed that anomalous correlations were obtained if preliminary analysis was not carried out to remove the tidal components. However the removal of the tides is complicated since the amplitude and phase of the tides, particularly the semidiurnal tide, can vary significantly over a period of a few days (Forbes, 1985). In this chapter a randomization technique is developed which allows anomalous correlations to be identified, allowing a correlation between the raw wind data and geomagnetic activity to be demonstrated.

Establishing whether a correlation exists between a pair of geophysical phenomena is difficult and determining whether a cause and effect relationship exists is even more so. One of the problems is that if two parameters are controlled by processes with similar but independent periodicities, then the two parameters may appear to be correlated if the matching periodicities are approximately in phase.

In this chapter a sample from the SAPR radar data set, covering the period from August to November, 1985, is used to demonstrate the randomization technique. In the following chapter

the data set is extended to cover a three year period. Daily variations in local geomagnetic activity, the data acquisition rate and the horizontal wind speed are discussed. Evidence for an apparent correlation between geomagnetic activity and the magnitude of the horizontal wind is presented and is tested using the randomization technique.

5.2 DAILY VARIATIONS

The local K-index is a three hourly index (defined in UT) which is used to indicate the level of geomagnetic activity at Mawson. It is dependent on the strength and variability of the auroral electrojet. In this work low, medium and high K values are defined as $K < 3$, $K = 3$ or 4, and $K > 4$ respectively. These groupings were chosen to give an even distribution of data points between the three K-index groups.

The distributions of high, medium and low K-indices throughout the day were calculated for the four month period under consideration (Figure 5.1). There is a clear tendency for low K-indices to be concentrated between 0900 and 1800 UT, and for high K indices to occur between 1800 and 2400 UT (2200 to 0200 LT). Magnetic midnight at Mawson occurs at around 2210 UT and thus the high K-indices tend to occur around magnetic midnight when the auroral electrojet is closest to Mawson.

The number of wind data points in each three hour period throughout the day is plotted for the four height ranges; 70-78 km, 80-88 km, 90-98 km and 100-108 km (Figure 5.2). In the 70 to 78 km height range there is a strong daily variation in the data acquisition rate, most data being obtained between 0600 and 1200 UT (1200 to 1800 LT). There is far less variation in the data acquisition rate above 80 km throughout the day.

The wind speed ($\sqrt{u^2 + v^2}$ where u and v are the zonal and meridional components of the wind) also shows a daily variation due to the presence of the diurnal and semidiurnal tides (assuming that the tides are not on average circularly polarised). The amplitude of the semidiurnal tide is large, typically 10 to 20 ms^{-1}, with a broad maximum around 85 to

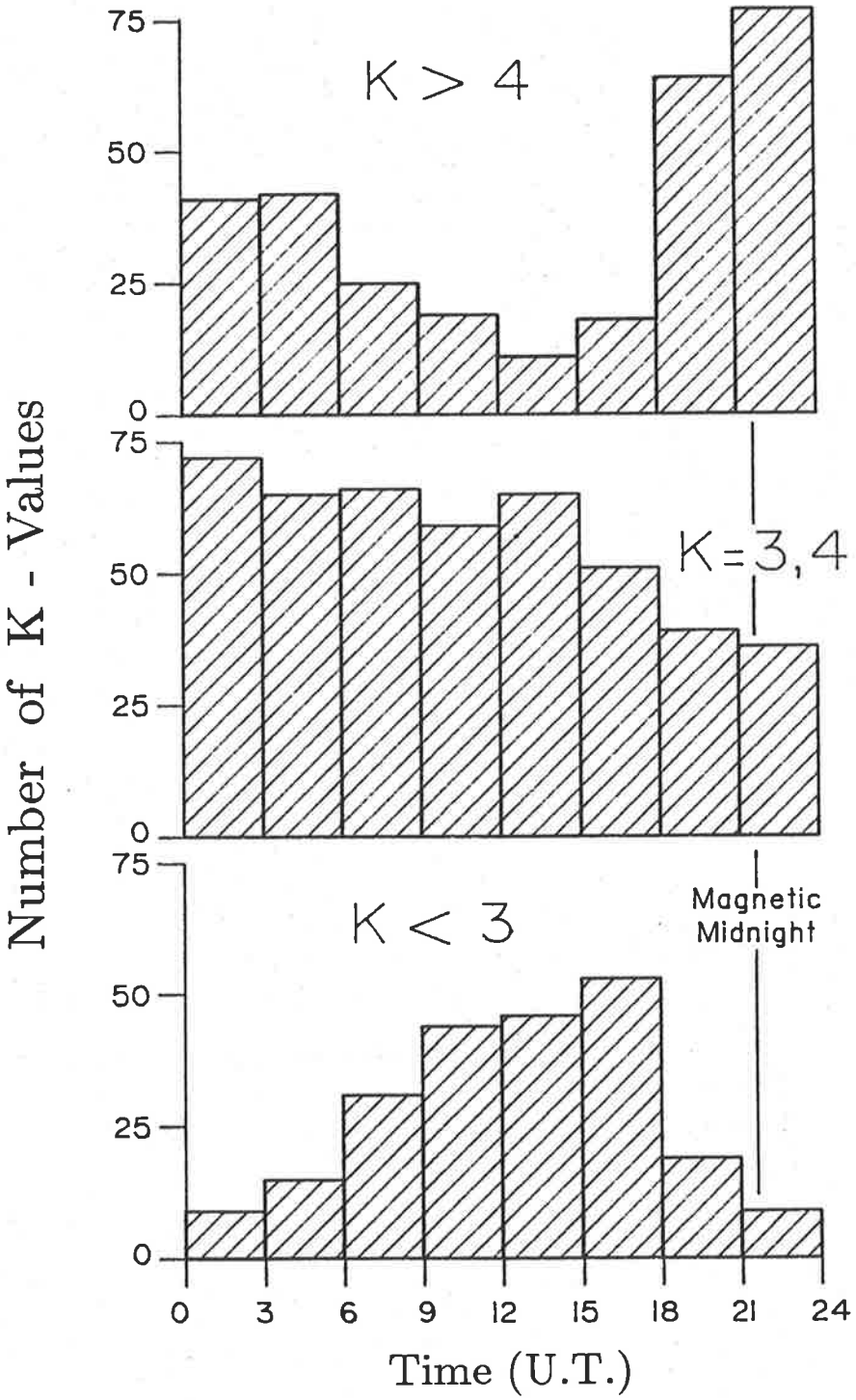

Figure 5.1: The distribution of high (K > 4), medium (K = 3, 4), and low (K < 3) K-indices throughout the day for the period August to November, 1985.

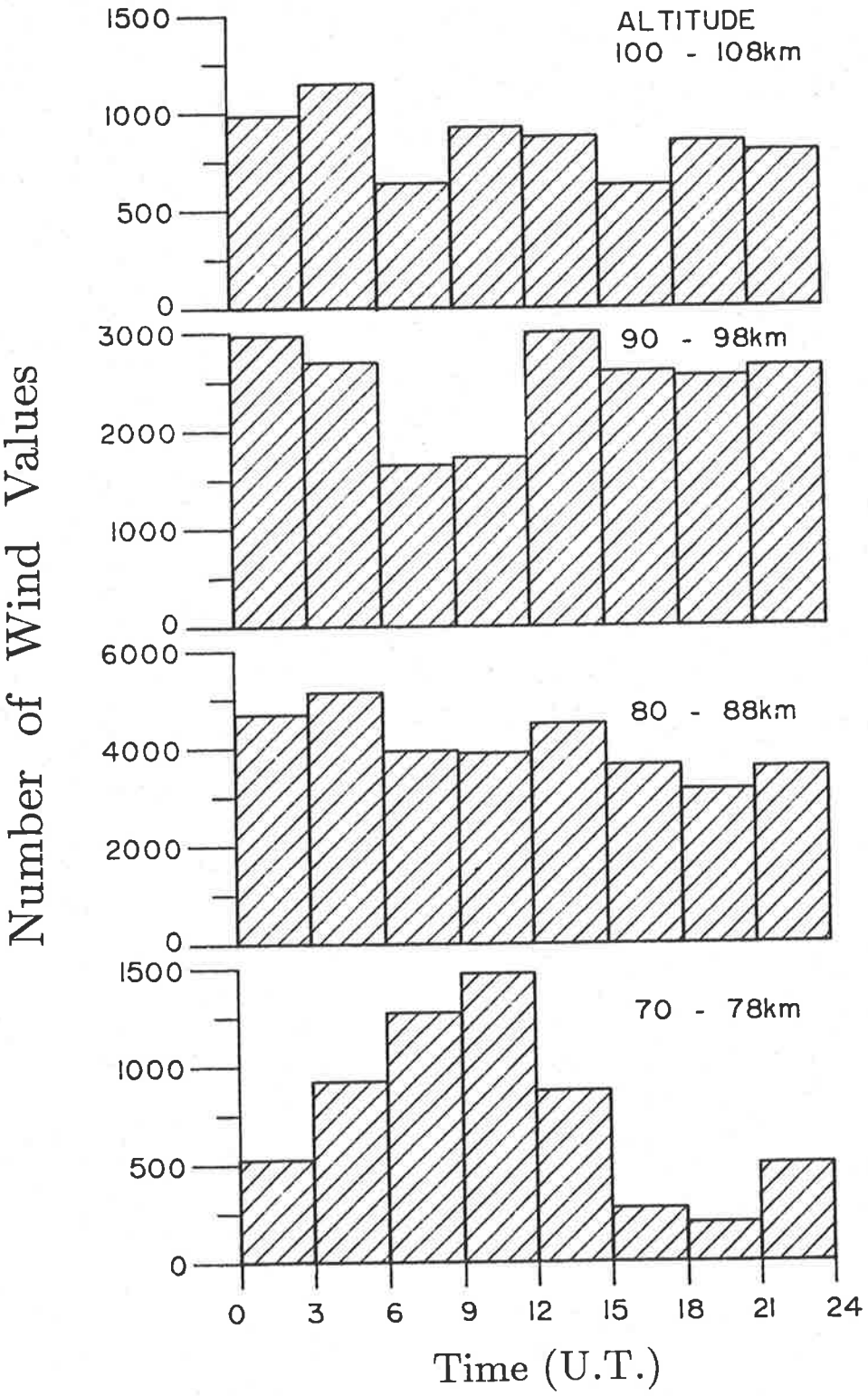

Figure 5.2: Histogram showing the number of wind values, obtained using the SAPR radar, versus time of day for the period August to November, 1985. The data points are divided into four altitude ranges; 70 - 78 km, 80 - 88 km, 90 - 98 km and 100 - 108 km.

95 km, while the diurnal tide is smaller, with an amplitude of 5 to 10 ms^{-1} (Phillips and Vincent, 1987). The semidiurnal tide at lower latitudes exhibits a large phase shift during spring (Tetenbaum *et al.*, 1986). A phase change of about 85 min was observed in the Mawson data over an eight day period in early October (Price *et al.*, 1987), (reproduced in Appendix 1).

In summary, a strong daily variation is seen in both the local K-index and the horizontal wind speed, where the strongest influence on the wind field is due to the semidiurnal tide. In addition the data acquisition rate varies strongly with the time of day at heights below 80 km. The data below 80 km were not used in this analysis for two reasons: firstly because a geomagnetic effect is least likely to be observed at the lower altitudes (section 1.4) and secondly, because of the large variability of the data acquisition rate with time of day.

5.3 AN APPARENT GEOMAGNETIC EFFECT

The measured wind values were divided according to the corresponding value of the local K-index into high, medium and low K groups. The wind speed distributions for the different K groups were then compared. Visual inspection of the speed distributions revealed no obvious difference between the three K index distributions at heights below 100 km. However, in the height range 100 to 108 km the peak of the high K-index distribution appears broader than that of the medium and low K distributions and there is a greater proportion of points in the high velocity wing of the distribution (Figure 5.3). The wind speed is clearly not normally distributed, particularly during periods of high geomagnetic activity, and therefore non-parametric statistics are appropriate in comparing the distributions.

The 50th and 75th percentiles of the high, medium and low K-index speed distributions were calculated for each 2 km height interval from 80 to 108 km. The 50th percentile is synonymous with the median of the distribution. The difference between the 75th and 50th percentiles gives a measure of the 'spread' of the distribution, and is here referred to as such. The median and spread of the high, medium and low K-index distributions are plotted as a function of height

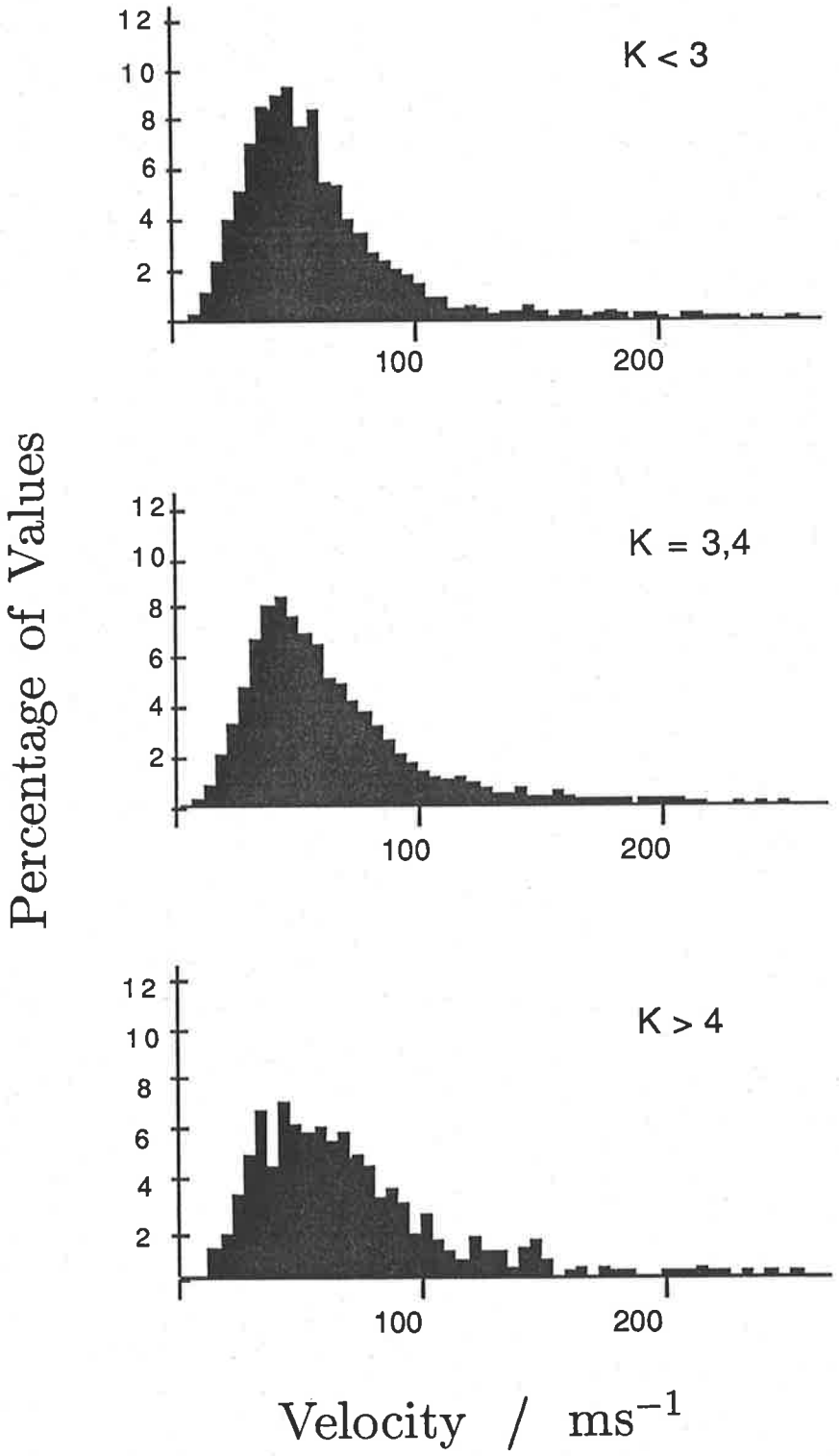

Figure 5.3: The distribution of horizontal wind speeds in the height range 100 to 108 km during periods of high (K > 4), medium (K = 3, 4) and low (K < 3) geomagnetic activity.

in Figures 5.4 a and b respectively.

The medians of the high K distributions are greater than those of both the medium and low K distributions at all altitudes above 90 km. At these altitudes there is in fact very little difference between the medians of the medium and low K distributions. Below 88 km the situation changes; the medians of the low K distributions are greater than the medians of the medium and high K distributions.

The spreads of the speed distributions show a similar height dependence to that of the medians. Above 88 km, there is a larger spread in the high K distributions than in the medium or low K distributions. However, unlike the medians, the spread becomes progressively larger from low to high K values at all altitudes above 100 km. Below 100 km there is little difference between the spread of the low and medium distributions.

The Mann-Whitney U test is used to investigate the difference between the medians of the high and low K distributions. (The test was confined to a comparison of the high and low K distributions only, as the percentile analysis had shown that values of the parameters describing the medium K-index distributions generally lay between those describing the high and low K-index distributions.) The hypothesis under test, H_o, is that the medians are the same and this is tested against two alternative hypotheses, namely

H_1: the median of the high K distribution is larger than the median of the low K distribution and

H_2: the median of the low K distribution is larger than the median of the high K distribution.

The test is nonparametric and involves ranking the combined distribution and, in this case, counting the number of times a speed from the low K distribution precedes a speed from the high K distribution. This determines the value of the test statistic 'U'. The probability of observing a given value of U, assuming the hypothesis H_o to be true, may then be determined (Siegel, 1956) from which the probabilities that either of the alternative hypotheses hold may

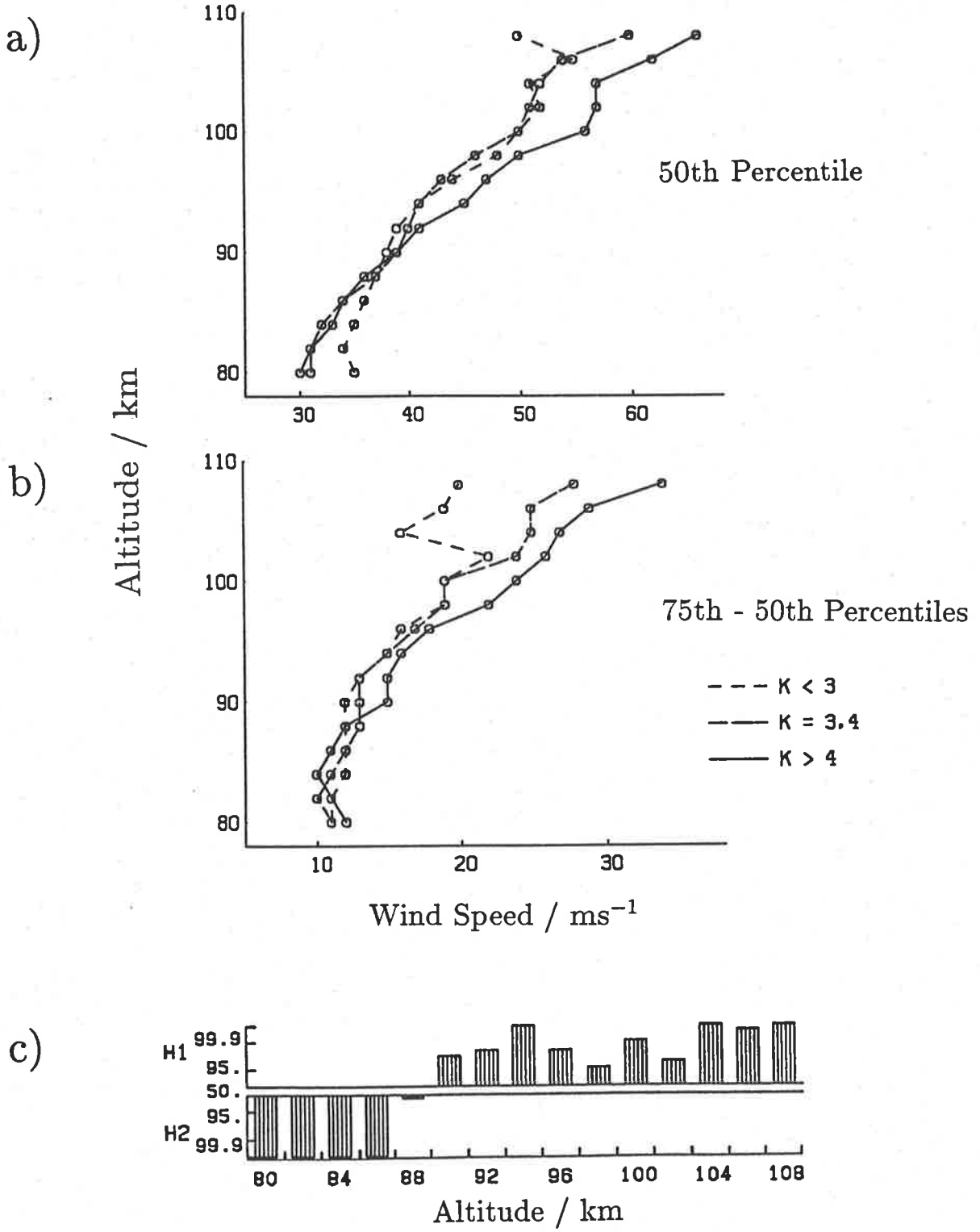

Figure 5.4: August to November, 1985 The height variation of a) the 50th percentile or median wind speed and b) the difference between the 75th and 50th percentiles or spread of wind speed during periods of high, (K > 4), medium (K = 3, 4) and low (K < 3) geomagnetic activity. c) The results of applying the Mann-Whitney U test to each 2 km height interval in the range 80 to 108 km; the top histogram gives the probability that the hypothesis H_1 is true, with the probability increasing up the page, and the bottom histogram gives the probability that the hypothesis H_2 is true, with the probability increasing down the page. Probabilities are plotted on a logarithmic scale.

be derived.

The Mann-Whitney U test was used to compare the low and high K distributions at each 2 km height interval. The results are plotted in the form of two histograms; the top histogram gives the probability that the hypothesis H_1 is true (with the probability increasing up the page), the bottom histogram gives the probability that the alternative hypothesis H_2 is true (with the probability increasing down the page). Probability is plotted on a logarithmic scale. Low probabilities suggest that neither of the alternative hypotheses are strongly favoured implying that the medians of the low and high K distributions are not significantly different.

5.4 APPLICATION OF A RANDOMIZATION TECHNIQUE

To test further the likelihood that the trends observed in the previous section were obtained by chance, the results could be compared with those obtained by grouping the wind data according to a set of randomly selected indices. However, a stronger test of the results would be attained if the wind data were grouped according to a randomly selected set of 'K like' indices i.e. a random distribution of numbers which have a similar auto-correlation function to the distribution of K-indices. In this way any correlation which resulted from periodicities in the wind values matching with periodicities in K would be preserved, and any correlation which occurred over and above this would be seen only in the correlation with the 'real' K-indices.

Although it would be possible to generate a set of random 'K-like' values a 'ready-made' source already exists in the past records of local K-indices from Mawson. Nineteen intervals, each of four months duration, were selected from records dating back to 1963 (Bureau of Mineral Resources, Geology and Geophysics, 1963-1986) (Table 5.1). Eight of these were chosen to cover different four month intervals throughout the year, and eleven sets were chosen to cover the same four month period (August to November) as the wind data. There were two sets (marked with an asterisk in Table 5.1) which covered the same months of the year and the same portion of the solar cycle as the wind data. A sequential number was assigned to each

Year	Months	Sequence Number
1985	AUG, SEPT, OCT, NOV	1 'REAL'
1985	MAR, APRIL, MAY, JUNE	2
1982	JAN, FEB, MAR, APRIL	3
1982	MAY, JUNE, JULY, AUG	4
1982	SEPT, OCT, NOV, DEC	5
1979	FEB, MAR, APRIL, MAY	6
1979	JULY, AUG, SEPT, OCT	7
1976	JUNE, JULY, AUG, SEPT	8
1973	JAN, FEB, MAR, APRIL	9
1973	AUG, SEPT, OCT, NOV	10
1986	AUG, SEPT, OCT, NOV	11
1984	AUG, SEPT, OCT, NOV	12
1983	AUG, SEPT, OCT, NOV	13
1982	AUG, SEPT, OCT, NOV	14
1981	AUG, SEPT, OCT, NOV	15
1980	AUG, SEPT, OCT, NOV	16
1979	AUG, SEPT, OCT, NOV	17
1975	AUG, SEPT, OCT, NOV	18
*1974	AUG, SEPT, OCT, NOV	19
*1963	AUG, SEPT, OCT, NOV	20

Table 5.1: The 19 sequences (numbers 2 to 20) of K-indices chosen to test the apparent correlation between the wind data and the 'real' K-indices (sequence 1). Sequences 2 to 9 cover different four month intervals throughout the year and sequences 10 to 20 cover the same four month period (August to November) as the wind data. Asterisks mark sequences covering the solar cycle in addition to the same months of the year as the wind data.

four month interval, where the 'real' set of K-indices (i.e. those appropriate to the wind data) are designated sequence 1. The other 19 sets of selected K-indices will be referred to as the 'unrelated' K-index sets.

The four months of wind data were grouped into three K-index groups (as defined in section 5.2) according to the K-indices contained in each of the nineteen sets of unrelated K-indices in sequences 2 to 20 in turn. The Mann-Whitney U test was applied to the low and high K distributions at each height for each of the nineteen different groupings of the wind data. The results are plotted in Figure 5.5 along with the results obtained in the previous section for sequence 1 (Figure 5.4c).

The results are best described by considering the height ranges above and below 96 km separately. Below 96 km, 9 out of twenty sequences showed the hypothesis H_1 to be supported within the 95 % level for at least three successive heights and five showed the hypothesis H_2 to be similarly supported. Large probabilities supporting either of the hypotheses H_1 or H_2 were generally obtained over a range of altitudes rather than being distributed randomly with height. For sequence 18 for example, probabilities supporting the hypothesis H_1 were greater than 99.9 % for 8 consecutive heights.

Large probabilities which extend over a range of heights appear to be a common occurrence at altitudes below 96 km suggesting that they represent anomalous correlations between geomagnetic activity and the wind. The most likely cause of such anomalous correlations is a matching of the daily variation of the wind due to tidal effects with the daily variation of the K-index. There are two trends in the results which support this hypothesis. Firstly, probabilities of greater than 99.9 % occurred most frequently in the height range 84 to 94 km which is the height range at which the semidiurnal tide maximises (Phillips and Vincent, 1987). Secondly, large probabilities tended to occur over a height range of typically 6 to 16 km. The diurnal tide at Mawson is evanescent, however the semidiurnal tide has a vertical wavelength of approximately 50 km during the spring (Phillips and Vincent, 1987). The height range over which

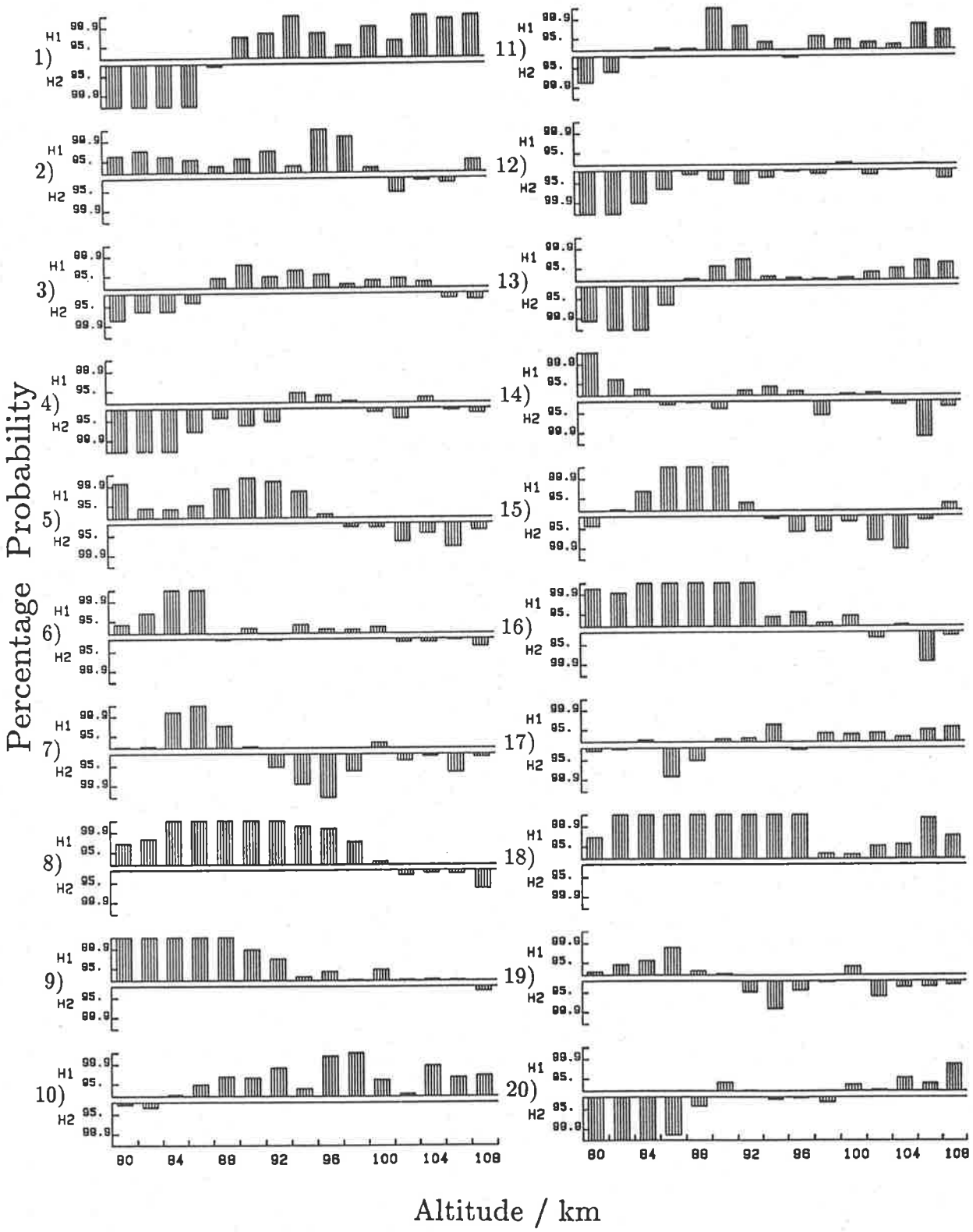

Figure 5.5: August to November, 1985 The results of the applying Mann-Whitney U test to each 2 km height interval in the range 80 to 108 km for the wind speeds grouped according to the K-indices in each of the sequences 1 to 20 as indicated. A pair of histograms describes the results associated with each set of K-indices where the top histogram gives the probability that the hypothesis H_1 is true, with the probability increasing up the page, and the bottom histogram gives the probability that the hypothesis H_2 is true, with the probability increasing down the page. Probabilities are plotted on a logarithmic scale.

large probabilities tend to occur is thus approximately a quarter of the vertical wavelength of the semidiurnal tide. Since we would expect the phase of the tide to be approximately constant over a quarter of a wavelength, this observation is also consistent with a tidal related cause for the apparent correlations.

At altitudes above 96 km there were only three sequences (1, 10, and 18) where the hypothesis H_1 was supported to within the 95 % level for at least three successive heights. Probabilities of H_1 being true were greater than 99.9 % for sequence 1 at altitudes above 102 km and greater than 95 % consistently at heights above 96 km. In the case of sequences 10 and 18, on the other hand, the probabilities were generally smaller and were not consistently high for more than three successive heights. There were no sequences for which the hypothesis H_2 was supported for more than two successive heights.

The question to be answered is whether the results obtained for sequence 1 are any more significant than those obtained for the other 19 sequences at altitudes above 96 km. The probabilities associated with sequence 1 were consistently large at all heights and showed a general tendency to increase with altitude. Sequence 1 was the only sequence showing either of the alternative hypotheses to be supported within the 99.9 % level for at least three successive heights in this height range. A geomagnetic effect on the wind field is most likely to be strongest at higher altitudes (section 1.4). We would also expect it to be fairly consistent over a number of altitudes rather than to 'single out' heights. These two conditions are better met in the results for sequence 1, than they are for any other sequence.

Sequence 10 ranks second in satisfying the conditions which a geomagnetic effect is expected to satisfy. It is interesting to note that this sequence of K-indices applies to the same months of the year and almost the same epoch of the solar cycle as the 'real' set. It is thus possible that the sequence of K-indices in this interval may in fact be very similar to the 'real' set. However there is no obvious tendency for the K-indices selected from the same time of the year as the 'real' values (sequences 10 to 20) to show more consistent results than those obtained from

other times of the year, thus seasonal effects do not appear to be important. It is also worth noting that had a synthetic set of 'K-like' indices been used in the randomization technique then the results may well have appeared more convincing, in the sense that the difference between the results obtained using the 'real' K-indices and those obtained using generated values would probably be greater than the difference observed between the results presented here.

5.5 CONCLUSION

The randomization test described in this chapter provides a means by which apparent correlations between geomagnetic activity and the wind can be tested. The test involves comparing results of correlating the wind and local K-index with the results of correlating the wind with 19 unrelated sets of K-indices. Evidence supporting the hypothesis that the median value of the wind speed is larger during high K-times than low K-times is strongest when the wind is correlated with the 'real' set of local K-indices for altitudes greater than 96 km. This conclusion is significant within the 95 % level since a total of 20 alternative ways of grouping the data were examined. The test shows that anomalous correlations between the raw wind speed and local K-index may be obtained at heights below 96 km.

Chapter 6.

THE EFFECT OF GEOMAGNETIC ACTIVITY ON THREE YEARS SAPR DATA

6.1 INTRODUCTION

In this chapter the randomization technique is applied to three years of SAPR data covering the period December, 1984 to November, 1987. The data have been divided into seasons and the randomization technique applied to each season of each year in turn. The geomagnetic effect is further investigated by calculating the hourly and half-hourly difference values, and applying the randomization technique to the resulting wind components, again for each season. An attempt is made to determine whether there is any difference in the direction of the wind between periods of high and low geomagnetic activity. Histograms of the distribution of wind direction are plotted for the raw wind and the filtered wind data.

The SAPR radar data can also be used to give some information about the nature of the scatterers. Three parameters viz: the pattern scale, elongation, and fading time are analysed using the randomization technique and a fourth parameter, the direction of elongation, is plotted out and compared for high and low K-times. These results show further the effect of geomagnetic activity on the upper mesosphere/lower thermosphere.

6.2 ANALYSIS

Each of the three years of SAPR data were divided into 4 seasons. The randomization technique described in the previous chapter was then applied to each season of each year in turn. This procedure was applied firstly to the raw wind data and then to two sets of filtered wind data derived as follows.

A difference filter was applied to both the zonal and meridional components of the wind by averaging the wind over a set time, τ, and then subtracting successive values. Two values of τ were used, τ=30 min and τ=60 min. The resultant filter function is dependent on τ (appendix 2); for τ=30 min frequencies in the range of approximately 1 to 3 h remain after

filtering and for τ=60 min frequencies in the range of approximately 2 to 6 h remain (see Appendix 2). Thus in both cases the diurnal and semidiurnal tidal components are removed. The terms 'high' and 'medium' frequency components of the wind are used here to describe these two frequency ranges respectively. The magnitudes of the high and medium frequency wind components were calculated by taking the square-root of the sum of the squares of the difference values of the meridional and zonal wind components.

The analysis involved studying the magnitude of the raw wind data and the high and medium frequency components of the wind over a total of 12 seasons. Applying the randomization technique to these data produces 36 sets of results, each set consisting of twenty plots. These results are summarised below.

6.3 CORRELATION BETWEEN GEOMAGNETIC ACTIVITY AND THE WIND

6.3.1 Raw Wind Values

The results of applying the randomization technique to each season separately for three years of SAPR data resulted in a significant correlation for most seasons. Exceptions were the data from the 1985 summer period which showed no correlation at any height and the 1987 spring which showed an apparent correlation only at heights below 100 km.

Apparent correlations at heights below about 100 km are probably anomalous and a result of daily variations in the wind due to the tides matching with daily variations in the local K-index (as discussed in Chapter 5). Such apparent correlations are often preserved when the wind data are grouped according to the unrelated K-values as well as with the 'real' K-values (since the unrelated K-indices, in being selected from the historical records, preserve any local time variations). Apparent correlations at heights below 100 km were strongest during the spring of each year and during the summer of 1987. They did not appear to occur at heights above 100 km. During the autumns of 1985 and 1987 apparent correlations mainly supported the hypothesis H_2 (i.e. that the medians of the low K distributions are larger than the medians

of the high K distributions), suggesting that at this time of year the tidal components tend to be out of phase with daily variations in the local K-value.

6.3.2 Filtered Data

The results of applying the randomization technique to the filtered wind data showed that in general the geomagnetic effect is present, and in some cases appears to be stronger, at higher frequencies. The results for the raw data and medium and high frequency components of the wind for the 1986 **spring** are shown in Figures 6.1 a to c respectively. Correlations which are considered anomalous are seen in the results corresponding to several of the sets of unrelated K-indices in the case of the raw data. Such correlations are not apparent in the filtered data. The results for the filtered data show that the large probabilities supporting the hypothesis H_1 (i.e. that the median of the high K distributions are larger than the medians of the low distributions), which are obtained above 88 km when the wind is grouped according to the 'real' K-indices, are not found when the wind is grouped according to any of the unrelated K-index sets. This therefore represents very strong evidence for the presence of a geomagnetic effect on the medium and high frequency components of the wind.

The data from the 1985 summer period, which showed no evidence of a correlation in the raw data, showed the same result in the filtered data. Data from the 1987 spring which also showed no correlation in the raw data did however show evidence of a geomagnetic effect in the filtered data with the strongest effect seen in the high frequency component. During the 1986 summer period a geomagnetic effect was seen at heights above 94 km in the raw data and above 88 km in the medium and high frequency components (Figure 6.2a). During the 1985 spring the geomagnetic effect was more marked and appeared to extend down to lower heights for the higher frequency components of the wind (Figure 6.2b). The high frequency component showed a significant effect down to a height of 86 km.

The results of applying the Mann-Whitney U test to the medium and high frequency wind

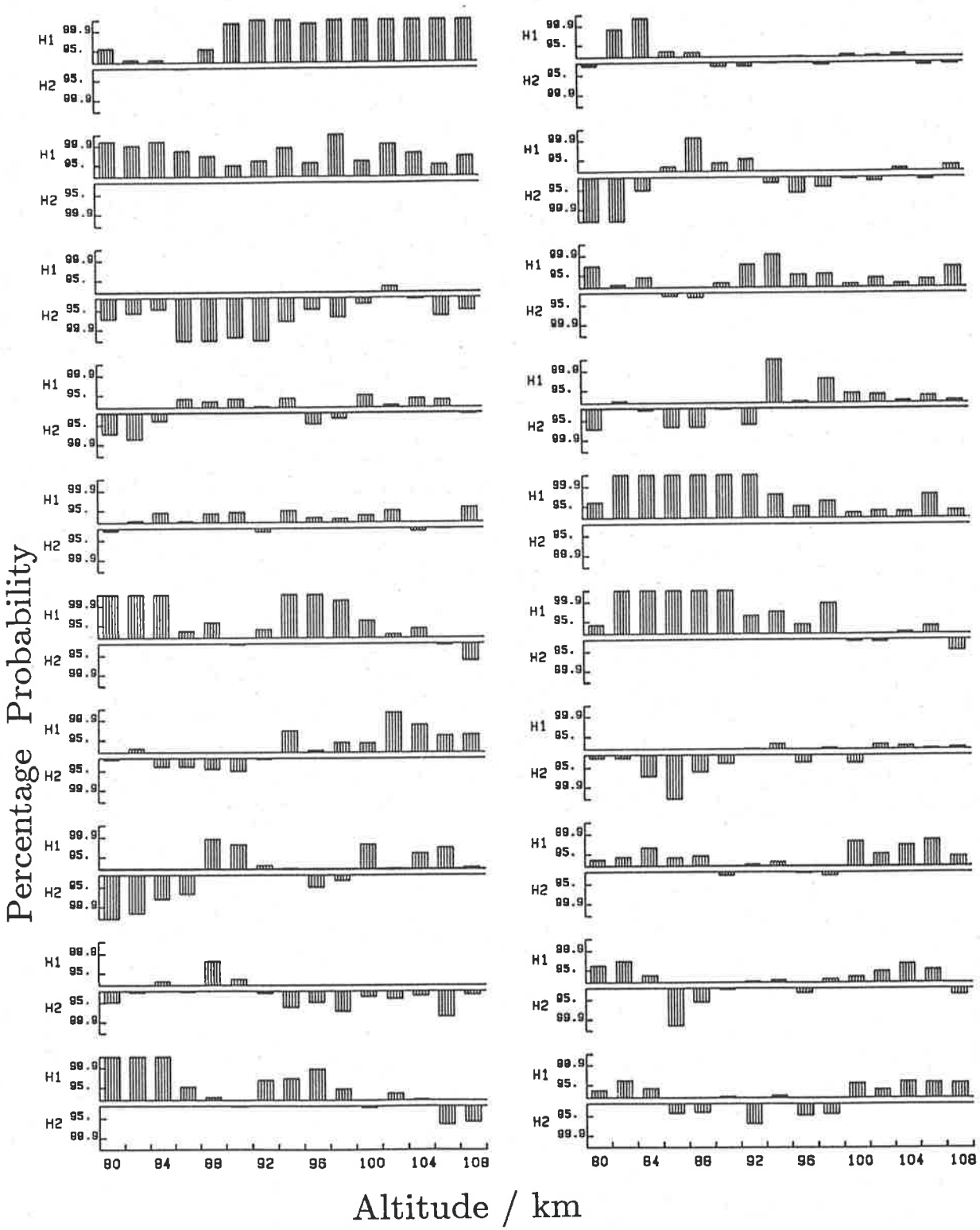

Figure 6.1: (a) Spring 1986 - Raw wind data. The results of the applying Mann-Whitney U test to each 2 km height interval in the range 80 to 108 km for the wind speeds grouped according to the K-indices in each of the sequences 1 to 20 as indicated. A pair of histograms describes the results associated with each set of K-indices where the top histogram gives the probability that the hypothesis H_1 is true, with the probability increasing up the page, and the bottom histogram gives the probability that the hypothesis H_2 is true, with the probability increasing down the page. Probabilities are plotted on a logarithmic scale.

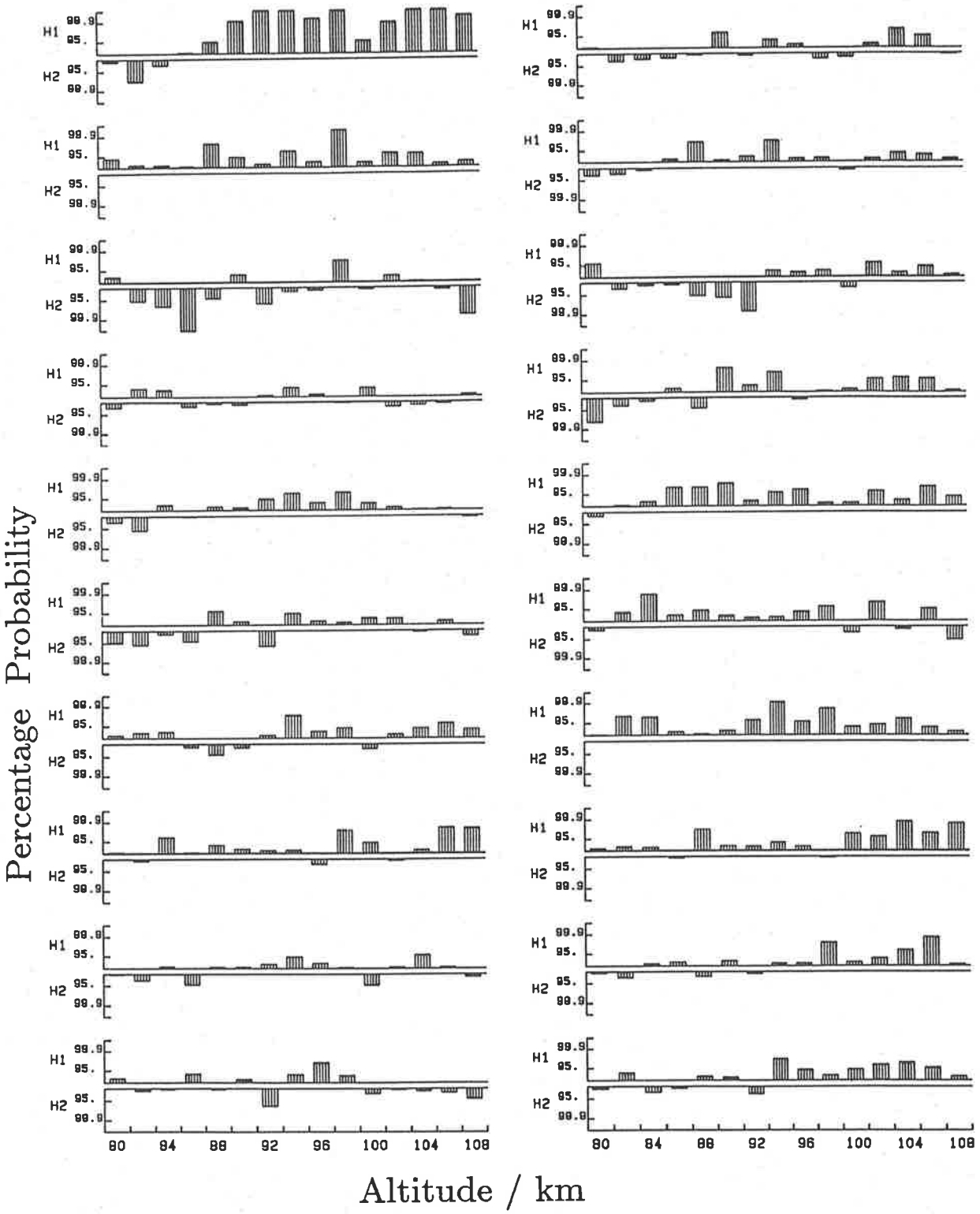

Figure 6.1: (b) Spring 1986 - medium frequency component. As for Figure 6.1(a).

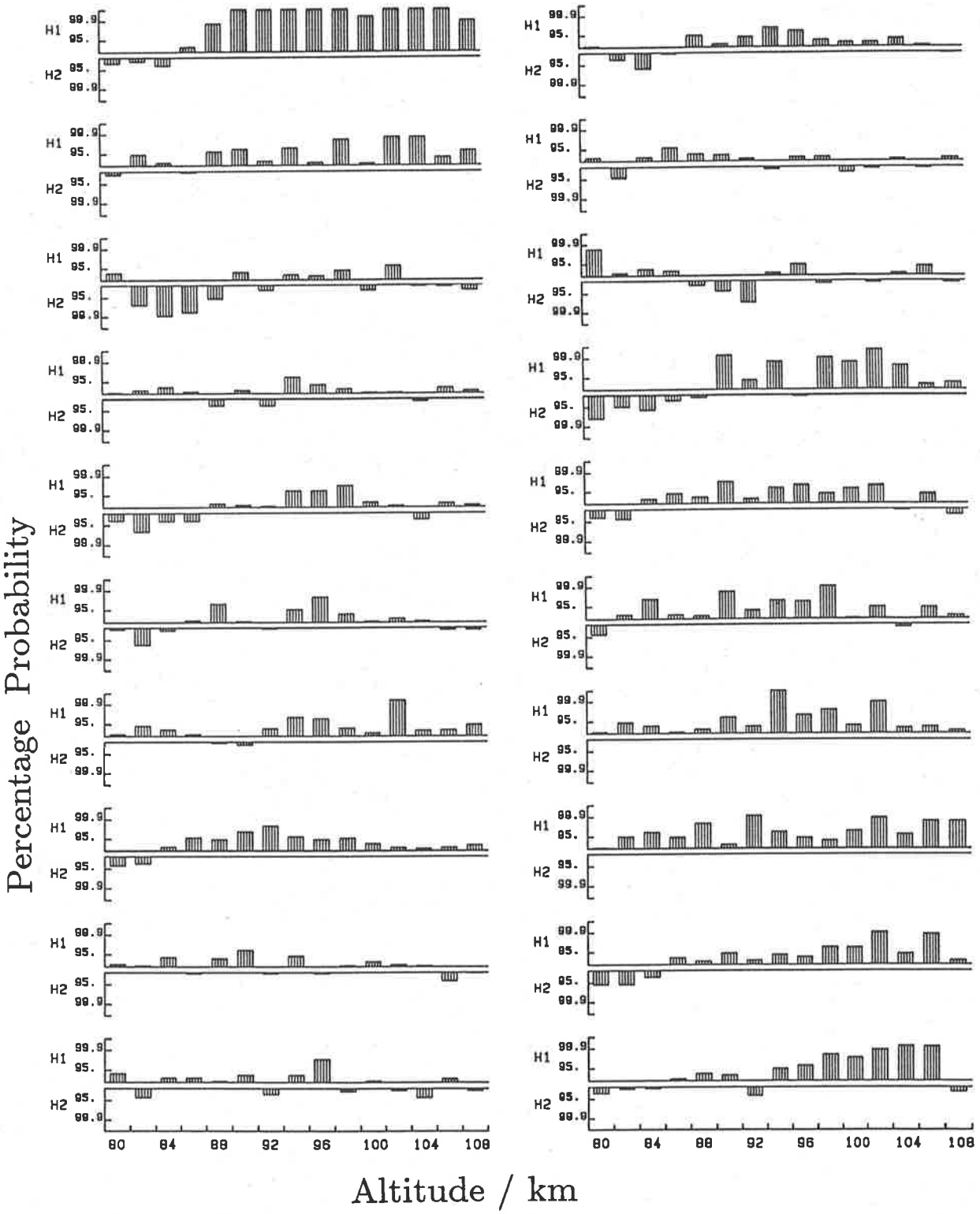

Figure 6.1: (c) Spring 1986 - high frequency component. As for Figure 6.1(a).

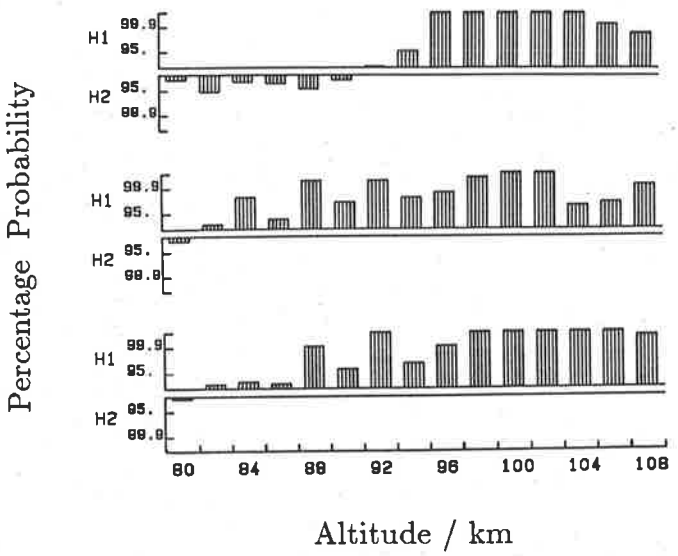

Figure 6.2: (a) Summer 1986 The results of applying the Mann-Whitney U test to the raw wind data (*top*), and to the medium (*middle*) and high (*bottom*) frequency components of the wind when grouped according to the 'real' set of K-indices. The axis are as for Figure 6.1.

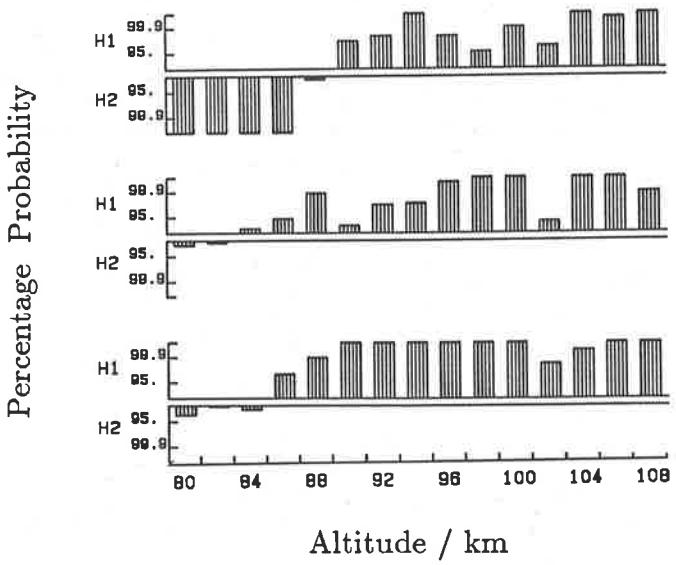

Figure6.2: (b) Spring 1985 As for Figure 6.2(a).

components, when binned according to the 'real' set of K-indices, is shown in Figure 6.3. The component of the wind which resulted in the strongest evidence for a geomagnetic effect is plotted. The geomagnetic effect shows a seasonal dependence, being stronger during spring and summer when it is evident down to heights around 86 km, and weaker in autumn and winter. Exceptions are the summer of 1985 which showed no correlation and the autumn of 1987 which showed strong evidence for a correlation. The effect appears to be strongest in the filtered data and to extend to lower heights for the high as compared to the medium frequency components. The effect is distinguishable in the raw data only at heights above 100 km as anomalous correlations are produced at heights below this.

6.4 DIRECTION

In order to determine whether there was any preferred direction for the enhanced winds during periods of high geomagnetic activity, the distribution of the wind vector directions was plotted for each season. This was done for the high and medium frequency components, and for the raw data it was carried out separately for different times of the day. Each day was divided into eight lots of three-hour periods corresponding to the periods over which the local K-values are calculated. In this way the effect of the diurnal tide, and to a lesser extent the semidiurnal tide, on the raw wind directions could be considered to be fairly constant in direction over each time-of-day interval. The distributions of wind direction were plotted for 3 different height ranges, viz: 80 - 88 km, 90 - 98 km and, 100 - 108 km. All directions are in geographic coordinates unless stated otherwise.

6.4.1 Direction of the Raw Wind

The distribution of K-values with time of day shows a large variation (Figure 5.1) and thus the ratio of the number of wind data points occurring at high and low K-times varies dramatically with the time of day. Around magnetic mid-day there is at least an order of magnitude more data points obtained during low K-times than high K-times and around magnetic midnight the

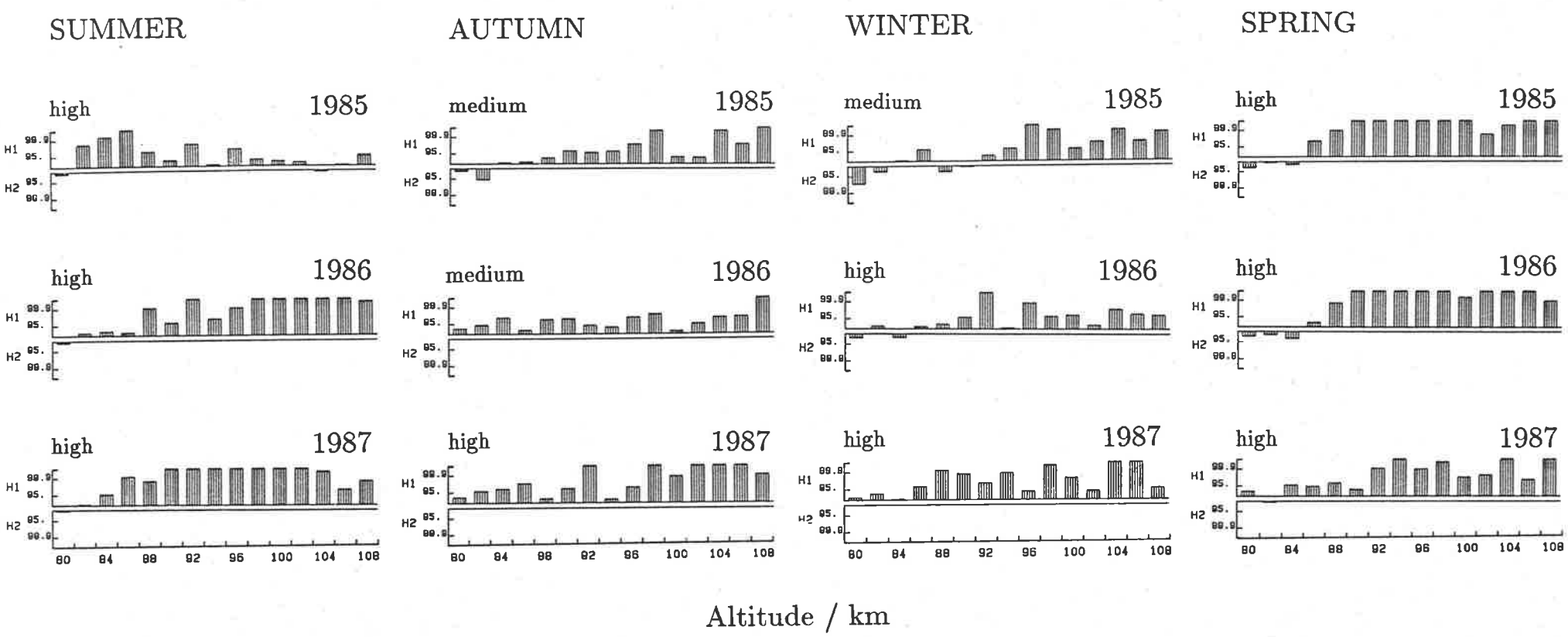

Figure 6.3: The results of applying the Mann-Whitney U test to the filtered wind data, when grouped according to the 'real' set of K-indices, for each season over three years. The component of the wind which resulted in the strongest evidence for a geomagnetic effect is plotted for each season over the three year observing period. The axis are as for Figure 6.1. Each plot is labelled 'high' or 'medium' indicating the frequency component which gave the most significant results.

reverse is true. It was therefore not possible to make meaningful comparisons of the wind directions during high and low K-times at all times of the day. Comparisons were only considered to be worthwhile when there was a similar number of data points contributing to the distributions for both of the K-value groups. This generally limited the comparisons to times between 0400 and 0700 LT and between 2200 and 0100 LT.

The distributions of wind direction for high and low K-times are very similar between 2200 and 0100 LT but show some differences for the time interval 0400 to 0700 LT, for all seasons. It should be noted that magnetic midnight at Mawson is at 0215 LT ±15 min thus the first time interval is just prior to magnetic midnight and the latter some hours after. The distribution of wind direction for the three height ranges 80 to 88 km, 90 to 98 km, and 100 to 108 km, which corresponded to low and high K-times for the time interval 0400 to 0700 LT, are shown in Figure 6.4 for all seasons. A general tendency is seen for wind directions to be in the NW to NE quadrant during high K-times. The effect is most obvious in the spring and summer at heights below 100 km and least apparent in the autumn, where for heights below 90 km the reverse appears to be true. During the summer this trend is also evident in the time interval 0700 to 1000 LT, below 100 km.

6.4.2 Direction of the Medium and High Frequency Components

Distributions of the directions of the filtered wind data were plotted; these distributions were fairly uniform with angle. A significant 'polarization' effect became apparent, however, if the wind speeds of small magnitude were removed and the resulting distribution plotted. Removing small magnitude winds had the effect of removing the noise component and for the high and medium frequency wind components this left the large amplitude wave motions. The effects of removing winds of speed less than 30 ms^{-1} and also winds with speed less than 50 ms^{-1} were studied and the polarization effect was found to be stronger in the latter case.

The results are very similar for the medium and high frequency components and the results

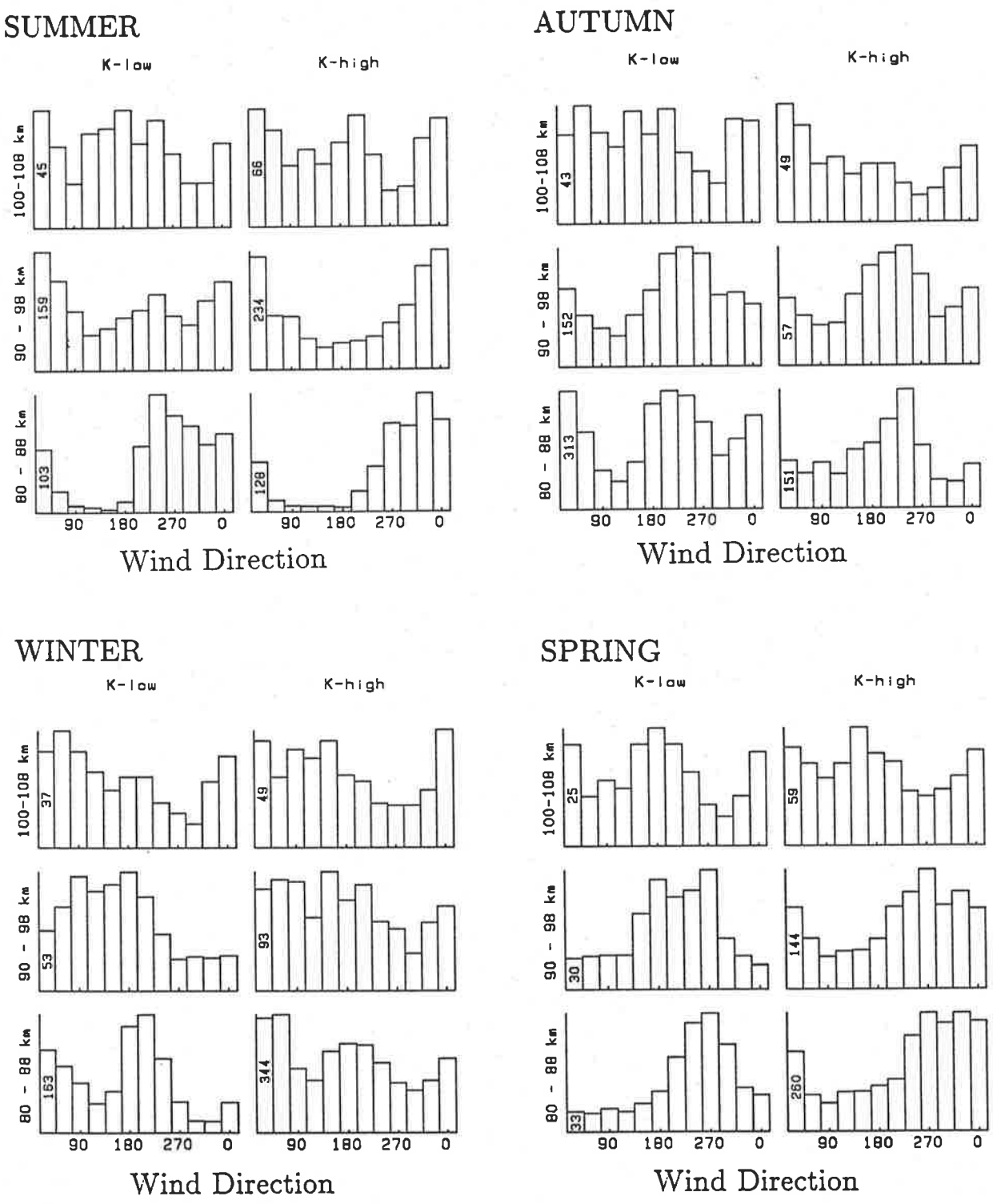

Figure 6.4: Distributions of wind direction for the raw data between the times 0400 and 0700 LT and averaged over three years for summer, autumn, winter, and spring. Histograms are plotted for high and low K-times as shown and the data are divided into three height ranges: 80 to 88 km, 90 to 98 km, and 100 to 108 km. Wind direction is in degrees clockwise from geographic north. The number of points in the first column of each histogram is shown.

of the medium frequencies, where wind of speeds less than 30 ms^{-1} have been removed, are shown in Figure 6.5. The most obvious feature of the results is that the direction of polarization, when present, is always in the geographic meridional direction. The degree of polarization is greatest in the 80 - 88 km height range. There was a slight tendency for the perturbation velocities to be more polarized at low rather than high K-times, however the difference was not considered to be very significant.

6.5 THE EFFECT OF GEOMAGNETIC ACTIVITY ON THE FCA ANALYSIS PARAMETERS

The scale, elongation, and orientation of the characteristic ellipse (see section 2.4) describing the ground diffraction pattern of the backscattered radar signal are determined by applying the full correlation analysis (FCA) to the received signals (see section 2.4). The 'fading period' or time taken for the observed auto-correlation function to fall to 0.5 is also recorded. The randomization technique was used to determine if the first three of these parameters showed any significant variation with geomagnetic activity. A procedure similar to that used to analyse the wind was adopted giving results for each season of the 3 years. The technique was only applied to heights above 80 km, as was the case for the wind data. The directions of pattern elongation were compared for high and low K-times.

6.5.1 Pattern Scale

The results of applying the randomization technique show that a significant correlation between geomagnetic activity and pattern scale is evident on eight of the 12 seasons over the three year period; the scale being larger when the K-index is large. The results of applying the Mann-Whitney U test to the pattern scale data obtained during high and low K-value times (using the 'real' set of K-values) are shown in Figure 6.6. The results are designated: 'significant', 'questionable', or 'not significant' which describes how significant the observed results of the Mann-Whitney U test were when the data were grouped according to the 'real' set of K-indices

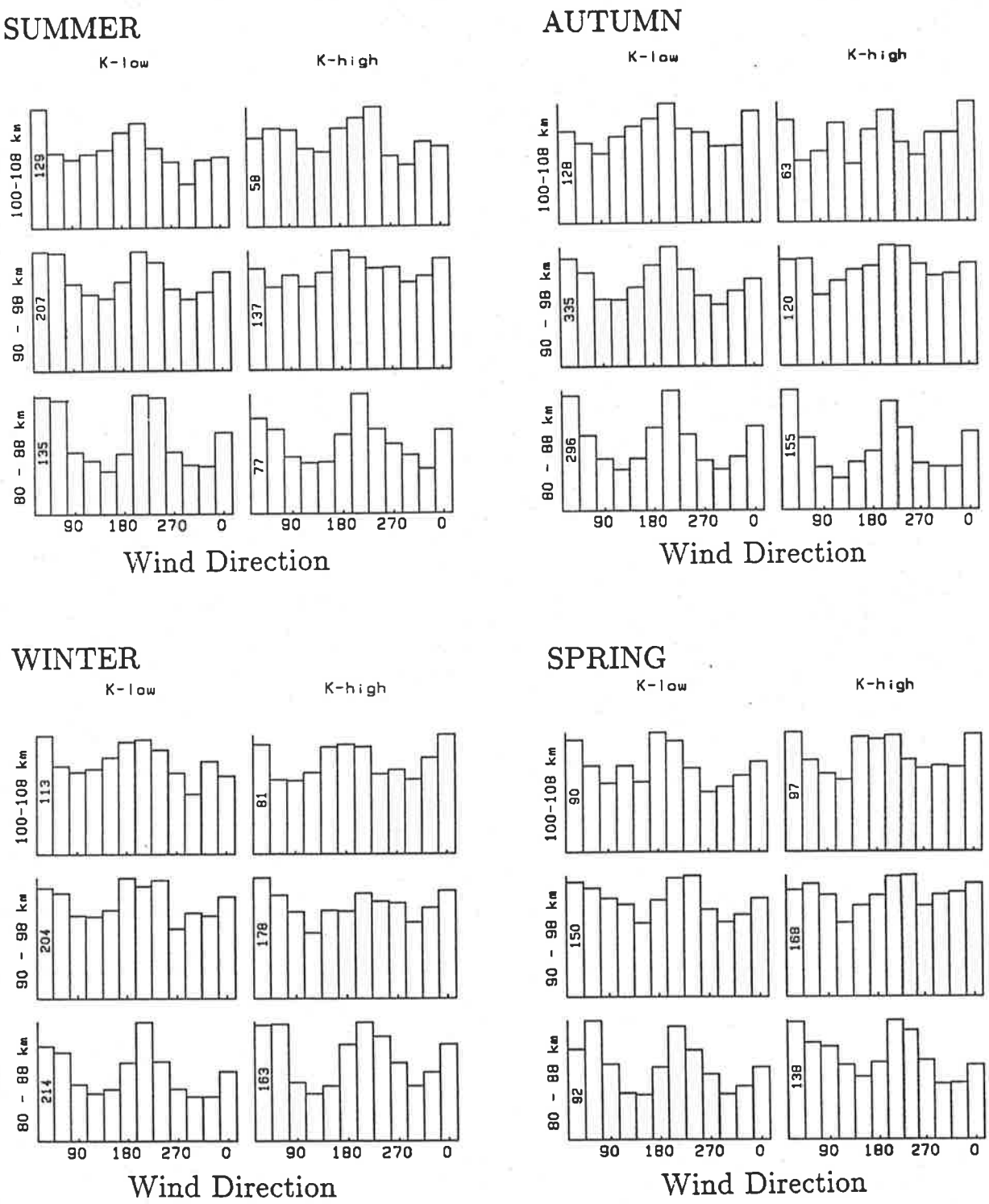

Figure 6.5: Distributions of wind direction for the medium frequency (2 to 6 h) component of the wind averaged over three years and shown for summer, autumn, winter, and spring. Wind speeds of magnitude less than 30 ms^{-1} have been removed. Histograms are plotted for high and low K-times as shown and the data are divided into three height ranges: 80 to 88 km, 90 to 98 km, and 100 to 108 km.

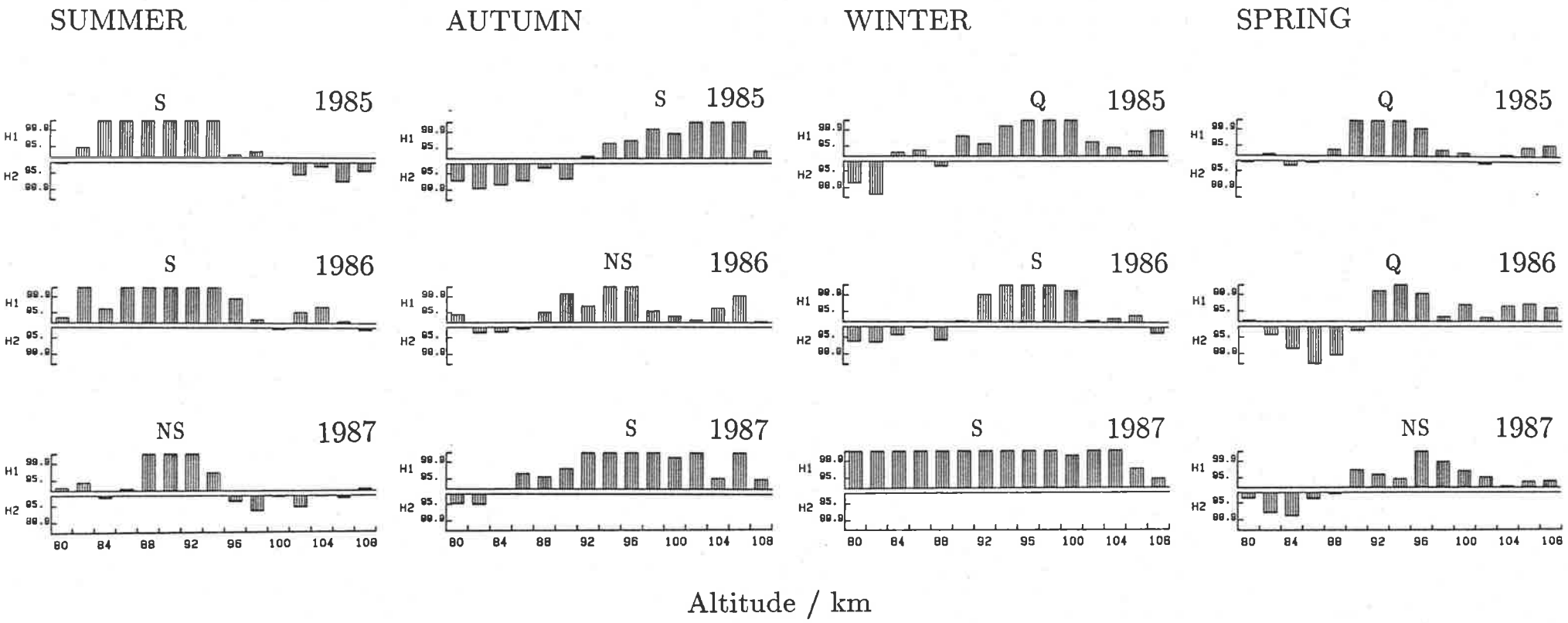

Figure 6.6: The results of applying the Mann-Whitney U test to values of the pattern scale when grouped according to the 'real' set of K-indices for each season over three years. The results are designated significant 'S', questionable 'Q', and not significant 'NS' which describes how significance of the results of grouping the data according to the 'real' K values is as compared to the results obtained when the data are grouped according to the unrelated sets of K-values. The axis are as for Figure 6.1.

compared with the results obtained by grouping the data according to 20 sets of unrelated K-indices.

The correlation between pattern scale and geomagnetic activity was designated as significant for two of the three winter periods studied and as questionable for the third. The correlation extended over the largest height range for the 1987 winter period when the Mann-Whitney U test showed the hypothesis H_1 (that the median of the high K distribution is larger than the median of the low K distribution) being supported within the 99.9 % level at all heights between 80 and 104 km. Significant correlations were measured on two of the three autumn periods with probabilities greater than 99.9 % measured between 98 and 106 km in the autumn of 1985 and between 92 and 102 km in the autumn of 1987. During the summer, apparent correlations were found to be significant at heights between 84 and 94 km in 1985 and between 86 and 96 km in 1986. The observed correlation appears to be weakest in the spring with questionable correlations measured for two of the three spring periods and no correlation measured on the third.

The variation of the mean pattern scale with height is shown for each season in Figure 6.7. Mean values are calculated for the data corresponding to high, medium, and low geomagnetic times respectively. The mean values suggest that a geomagnetic effect is evident in all seasons. However, consideration must be given to the nature of the distribution of pattern scales and of the effect of daily variations in this parameter as discussed in chapter 5. These factors are taken into account by applying the randomization technique and the height ranges where the apparent difference between the high and low K curves is found to be significant, for at least two of the three contributing seasons, are shaded. (Note that the randomization technique was not applied to data from heights below 80 km). The effect of geomagnetic activity on pattern scale is significant at lower heights in summer than in autumn or winter and the apparent correlation observed in spring is not found to be significant.

The pattern scale ($\sqrt{ab}$ where a and b are the distances along the minor and major axes

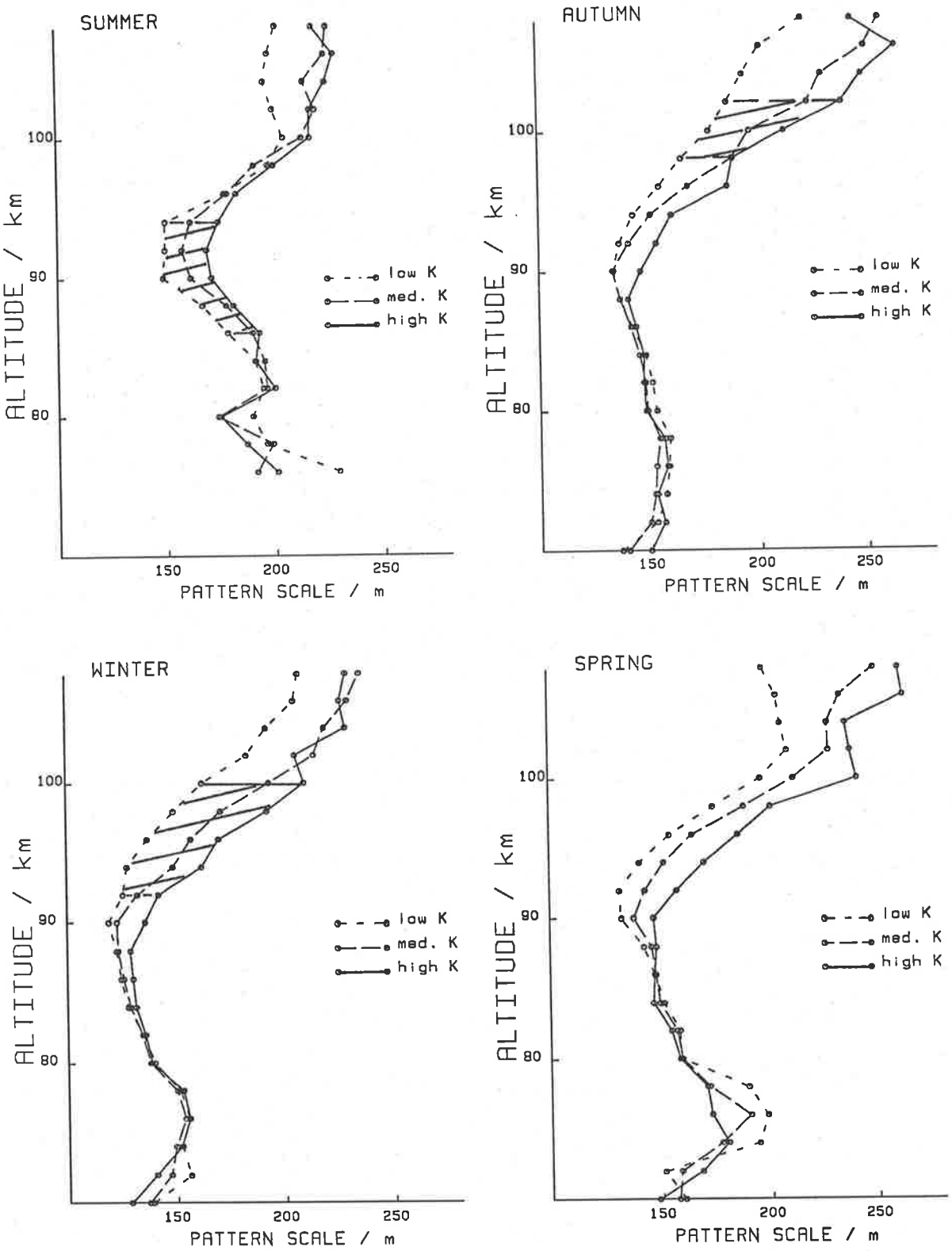

Figure 6.7: The variation of the mean pattern scale with height as averaged over three years for each season. Mean values are calculated for the data corresponding to high, medium, and low K-times. The height ranges where the apparent difference between the high and low K curves is found to be significant, from application of the randomization technique, for at least two of the three contributing seasons are shaded.

of the characteristic ellipse respectively) is an arbitrarily defined parameter, here defined from the width of the modulus of the spatial auto-correlation function. It is related to the angular spread of the echoes; the larger the angular spread the smaller the pattern scale and vice versa. Although it is possible to determine the mean angular spread of the echoes if certain assumptions are made regarding the nature of the scatterers (Briggs and Vincent, 1973), these assumptions do not hold over the full range of heights observed by the SAPR and thus a qualitative discussion of the results is considered more appropriate.

The pattern scale shows a local maximum below 80 km in winter, spring, and summer although there is little data obtained from this region in summer; the local maximum is less evident in autumn. This suggests that the reflecting irregularities are more specular below 80 km. The pattern scale decreases with altitude above this height, reaching a minimum between 90 and 94 km for all seasons of the year. This suggests that the scattering irregularities are more isotropic above 80 km which is consistent with observations reported at lower latitudes and discussed in section 2.5.3. The pattern scale then increases with increasing height due firstly to the increase in electron concentration which causes the scatterers to become more specular and secondly due to the fact that viscosity tends to dampen out small scale motions which generally cause the scatterers to become more isotropic. Finally, total reflection of the radio waves occurs at the base of the E-region. The mean pattern scales tend to be larger at heights below 90 km in summer, which is consistent with there being a larger electron concentration in this season due to the presence of increased ionization by solar radiation.

The mean pattern scale is seen to increase during periods of high geomagnetic activity implying that the angular spread of the return echoes decreases. Increased ionization due to the effects of precipitating particles accompanies geomagnetic disturbances which may effect the returned echoes in either or both of the following ways: firstly, it may cause the reflecting irregularities to become quasi-specular or, secondly, it may lead to increased absorption which will have a greater effect on the off-zenith reflections which must traverse a larger distance

through the absorbing medium. During winter, when the geomagnetic effect on the pattern scale appears to be strongest, the magnitude of the effect is of the order of the variation in pattern scale generally observed between echoes observed below and above 80 km.

6.5.2 Fading Period

The results of applying the randomization technique show that the hypothesis H_2 (i.e. that the medians of the low K distributions are larger than the medians of the high K distributions) is strongly supported but only during the spring. This implies that the fading period is negatively correlated with K-index. Significant negative correlations were measured over each spring of the three years studied. The results of applying the Mann-Whitney U test to the fading period data obtained during high and low K-value times (using the 'real' set of K-values) are shown (Figure 6.8). Large probabilities supporting H_2 were observed throughout most of the height range 82 to 108 km for two of the spring periods and over the range 92 to 108 km for the third. Less significant correlations were measured for the 1985 summer and the 1987 autumn, however no significant correlations were measured during these seasons in the other years. No correlation was seen during the winter of any years.

The corrected fading period, which is denoted $T_{0.5}$ and is the fading period which would be measured by an observer moving with the ground diffraction pattern, may be used to estimate the random velocity of the scatterers within the scattering volume (Briggs, 1980). The velocity components of the scattering irregularities selected by the radar are assumed to have a Gaussian distribution along any chosen direction. The line of sight RMS velocity, v_o, of the component velocities is then given by

$$v_o = \frac{\lambda\sqrt{2ln2}}{4\pi T_{0.5}} \tag{6.1}$$

where, λ is the radar wavelength. For approximately isotropic or volume scatter v_o gives an indication of the degree of turbulent motion within the scattering irregularities. Strictly the equation does not hold when quasi-specular reflections are apparent, however we can physically

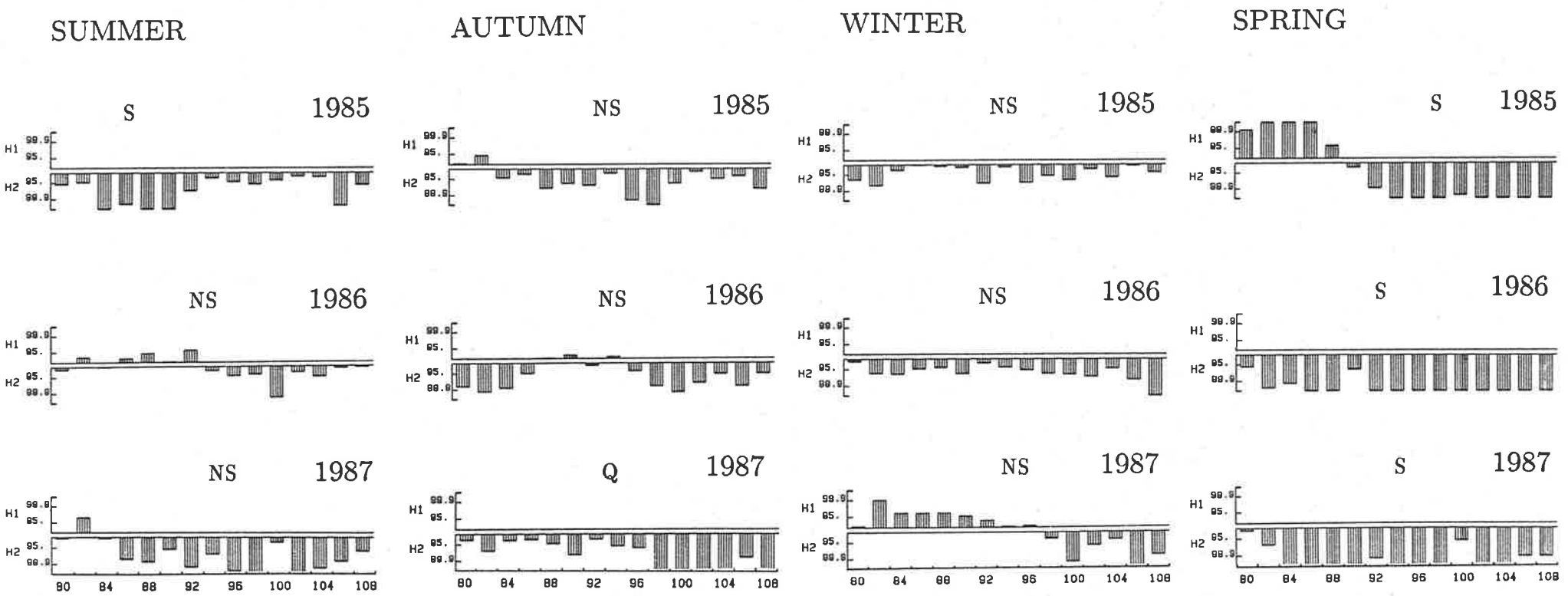

Figure 6.8: The results of applying the Mann-Whitney U test to values of the fading period when grouped according to the 'real' set of K-indices for each season over three years. The results are designated significant 'S', questionable 'Q', and not significant 'NS' which describes the significance of the results of grouping the data according to the 'real' K values as compared to the results obtained when the data are grouped according to the random sets of K-values. The axis are as for Figure 6.1.

interpret v_o as giving an indication of the degree of turbulent motion at the surface of the reflecting layer (like the turbulent motion at the surface of a boiling liquid).

The variation of the mean value of v_o with height is shown for each season in Figure 6.9. As in the case of the pattern scale, the mean values are calculated separately for the data corresponding to high, medium, and low K-times separately. Once again shaded areas indicate the height ranges where the apparent difference between the high and low K curves is found to be significant, using the randomization technique, for at least two of the three contributing seasons.

The vertical profiles of the mean RMS velocity are very similar for each season, the most obvious feature being a tendency for v_o to increase with altitude. The mean RMS velocity tends to increase during geomagnetically active times suggesting that the small scale or turbulent motions of the atmosphere are greater during such times, but this effect is found to be statistically significant in the spring only.

6.5.3 Pattern Elongation and Orientation

Results of applying the randomization technique to the ratio of the major to the minor axis of the characteristic ellipse, which describes the elongation of the ground diffraction pattern, failed to show any evidence of a geomagnetic effect on this parameter. Evidence of a geomagnetic effect on the orientation of the major axis was investigated by comparing the distribution of measured angles during high and low geomagnetic times as it is not appropriate to apply the Mann-Whitney U test to this parameter. Histograms of the distribution of the angle of orientation were plotted for each season and over five height intervals between 80 and 108 km. There was no obvious difference between the histograms corresponding to high and low K-times over any height range for any season and it was therefore concluded that this parameter is not affected by geomagnetic activity.

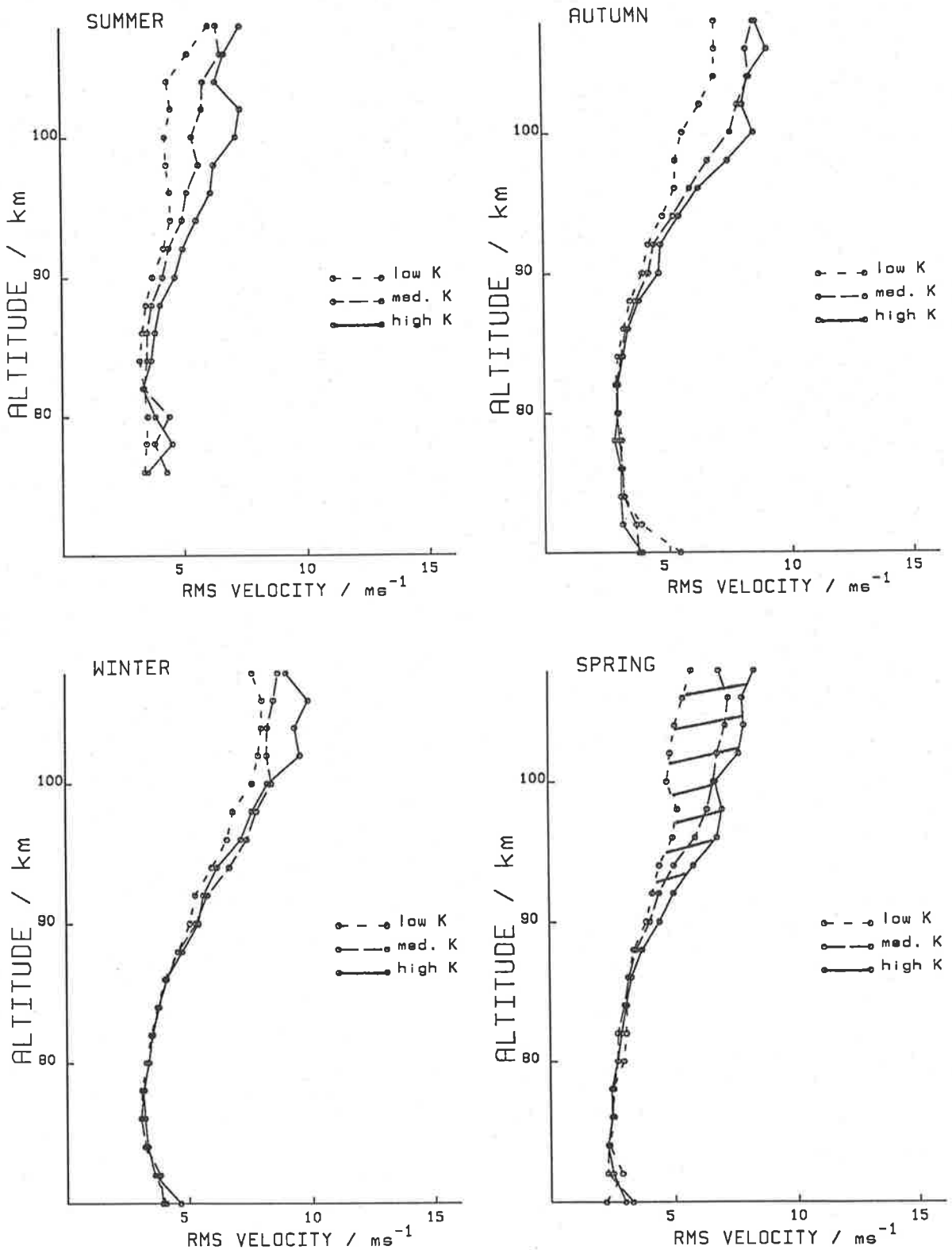

Figure 6.9: The variation of the line of sight RMS velocity with height as averaged over three years for each season. Mean values are calculated for the data corresponding to high, medium, and low K-times. The height ranges where the apparent difference between the high and low K curves is found to be significant, from application of the randomization technique, for at least two of the three contributing seasons are shaded.

6.6 COMPARISON WITH OTHER OBSERVATIONS

A summary of wind observations that are reported to be associated with variations in geomagnetic activity or which have been correlated with various parameters describing geomagnetic conditions is given in Table 6.1. Emphasis is placed on altitudes below 100 km where the most data is obtained by the SAPR radar. Incoherent scatter radars and Fabry Perot spectrometers which have provided evidence for a geomagnetic effect on the neutral wind at heights above 100 km have not been included. These results are generally inconclusive and most involve observations for periods of less than 20 days. The results reported by Johnson and Luhmann (1985a) and Manson and Meek (1986) describe data sets covering longer time periods; however these results are inconsistent, particularly with regard to the effect of geomagnetic activity on the diurnal tide.

Enhanced winds in the equatorward direction between local midnight and dawn have been reported by Hook (1970), Prikryl *et al.* (1986) and Phillips and Jacka (1987). These observations are consistent with results found here which show that the unfiltered wind vectors shift towards the geographic northward direction between 0400 and 0700 LT.

6.7 SUMMARY AND DISCUSSION

The results from this chapter may be summarised as follows:

- A significant correlation between the raw wind data and geomagnetic activity was seen for nearly all seasons over the three years. The correlation was also present in the medium (2 - 6 h) and high (1 - 3 h) frequency components where it was seen to be significant down to heights of 86 km.

- The effect of geomagnetic activity on the magnitude of the high and medium frequency components of the wind appears to show a seasonal dependence; the correlation is strongest during summer and spring, with the exception of the summer of 1984/85 when there was no significant correlation measured.

Author (year)	method and length of observations	parameters correlated	height of comparison	direction enhanced winds	general comments
Hook (1970)	meteor radar 19 disturbed days		height average - most data 80 to 100 km	geomagnetically southward after local midnight	variation in wind direction greatest during early mornig hours and greater in spring than winter
Balsley *et al.* (1982)	MST radar 19 days in summer	mean zonal wind fluctuations with electrojet int.	88 km	westward	diurnal and semi-diurnal tides reduced
Ogawa (1986)	meteor radar 16 days in summer		85 to 95 km		winds greater than 100m/s only observed during high Kp
Johnson and Luhmann (1985a) (1985b)	MST radar 3 yr, summer only 4 days following PCA event	wind fluctuations with masgnetic H fluctuations	86 km	mean zonal wind twice as strong to the west	auroral electrojet appeared to act both destructively and constructively on low frequencies components. 24 hour zonal amplitude enhanced 12 hour zonal amplitude decreased
Manson and Meek (1986)	MF radar 2 and 5 years	mean wind, E0 24 and 12hr tide, with Ap	91 to 108km	mean winds more northward(summer)	GW amplitudes positively correlated with AP and amplitude tidal components negatively correlated E0 maximum on disturbed days
Prikryl*et al.* (1986)	Meteor/auroral and PR radars 5 days		90 to 100km	equatorward around local midnight	enhanced winds observed in meteor trails and not PR radar
Phillips and Jacka (1987)	SAPR radar 1 year	meridional 24hr amplitude and Kp	80 to 108km	equatorward near dawn	the correlation is strongest above 95km and increases with altitude.
Price (present work)	SAPR radar 3 yr	raw wind, 2-6 h, 1-4 h, RMS vel with local-K index	86 to 108km	equatorward early morning hours	the correlation is strongest in summer and spring and generally strongest in the high frequency RMS vel is enhanced only in Spring

Table 6.1: Directions of winds reported to be correlated with geomagnetic activity at heights below 108 km

- A general tendency for the raw wind values to be in the geographic NW to NE quadrant during high K-times for the time interval 0400-0700 LT in all seasons was measured. The effect was seen at heights down to 80 km and was most obvious in the spring and summer at heights below 100 km. There was no difference in wind direction between high and low K-times for the time interval 2200-0100 LT.

- The high and medium frequency components of the wind were found to be polarized in the geographic meridional direction during all seasons of the year once the small magnitude wind values had been removed. The degree of polarization was greatest in the 80 to 88 km height range.

- The scale of the ground diffraction pattern, formed by the backscattered radar signals, was found to increase and hence the angular spread of the return echoes to decrease, during high K-times. An apparent correlation seen during most seasons was tested using the randomization technique and found to be most significant in winter.

- The mean RMS velocity of the scatterers was found to increase during geomagnetically active times. The application of the randomization technique showed this effect to be significant only in spring.

It is difficult to draw any simple conclusion from these results except that understanding the influence of geomagnetic activity on the wind field is far from straight forward. Various physical processes which may be taking place are discussed and the predicted effects compared with the observed results. The apparent seasonal dependence of the geomagnetic effect is hard to explain. It is possible that this variation may be anomalous if other processes, such as the deposition of momentum by breaking gravity waves, are taking place which affect the wind in similar ways but which show a strong seasonal dependence. Gravity wave activity in the mesosphere is greatest during the winter as the mean winds at lower heights favour the upward propagation of a large portion of the gravity wave spectrum from the lower atmosphere. This

may cause a geomagnetic effect to be less distinguishable in winter which is consistent with the observations.

Three processes which may be contributing to the observed enhancement of the wind in the geographic northward direction after magnetic midnight are: ion drag, the effect of enhanced electric fields, and heating. However, it is not possible to determine which, if any, of these processes are dominant. The polarization of the high frequency components is discussed in terms of biases which may be inherent in the gravity wave generation mechanisms.

The process of ion drag, or the transfer of momentum from the ions to the neutrals, results in the driving of the neutrals towards a direction between the $\mathbf{E} \times \mathbf{B}$ and $\mathbf{E}$ directions in the lower thermosphere. This direction is roughly calculated from the two cell plasma drift model shown in Figure 1.8 and it is found to lie between the magnetic E and NW directions between 0200 and 0500 LT. At Mawson magnetic north is $\sim 60°$ W of geographic north; thus ion drag would act between the geographic NE and W. This is consistent with the observed enhancement toward the geographic NE to NW found here at heights down to 80 km.

The effect of ion drag on the wind field at 120 km has been modelled by Fuller-Rowell and Rees (1980, 1984). Results of this model have been successfully used to describe horizontal neutral winds measured from observations of the λ558 nm emission in the height range 100 to 130 km (Jones and Jacka, 1987). It is possible that ion drag is effective below 100 km although it is unlikely that it it is effective at heights in the vicinity of 80 km as the collision frequency becomes greater than the electron gyro-frequency at this height.

Joule and particle heating in the vicinity of the electrojet are likely to lead to the formation of meridional circulation cells (section 1.4). Heating leads to expansion upwards and away from the heated region with a return flow at lower altitudes. During geomagnetically active times the auroral electrojet is generally situated to the magnetic north of Mawson (i.e. geographically NW) during the night; thus the observed winds are consistent with the return flow associated with a meridional circulation cell situated on the poleward side of the electrojet.

Large electric fields present during geomagnetically active times may cause ionized irregularities which produce radar scatter to become decoupled from the neutral wind. Reid (1983) has estimated that for a typical electric field, with the magnetic meridional component greater than the zonal component, the largest drifts are produced in the magnetic meridional direction. For a northward component in the electric field, as observed here during the times under discussion, this drift is in the magnetic northward (geographic NW) direction. Thus a decoupling of the ionised irregularities from the neutral wind is also consistent with the observations.

The observed polarization of the medium and high frequency components of the wind may be interpreted as evidence of polarization of the perturbation velocities of gravity waves. The fact that the direction of polarization does not show a seasonal dependence suggests that the bias is introduced in the gravity wave generation process rather than by the effect of filtering of the waves by the background wind. It is interesting that similar biases have been measured using different techniques at mid-latitude sites (Vincent and Fritts, 1987; Eckermann and Vincent, 1989).

One possible lower atmosphere source of gravity waves in the Antarctic is that of wind shear at the top of the katabatic flow. The katabatic wind flows off the polar cap in an approximate geographic meridional direction and it is possible gravity waves generated by shear excitation may have perturbation velocities which are polarized in the meridional direction.

The auroral electrojet also provides a source for the generation of gravity waves. A rich spectrum of gravity waves is present in the source region causing the wave perturbation velocities to appear impulsive rather than oscillatory in nature. Velocity fluctuations produced by the auroral electrojet in the near field have been modelled by Luhmann (1980). Both Joule heating and the Lorentz force produce velocity perturbations approximately perpendicular to the direction of the electrojet with magnitudes of 100 ms^{-1} at 100 km and 40 ms^{-1} at 80 km. The perturbation velocities produced by this source are therefore likely to be in the magnetic meridional direction whereas the observed waves are polarized in the geographic meridional

direction.

The general tendency for winds to be enhanced during high K-times could be due to any of the processes described above, however distinguishing between these processes is difficult. This point is discussed further in the concluding chapter. The observation that the geomagnetic effect extends down to heights of 80 km suggests that a complex coupling between electrodynamic forcing and neutral air motions is likely to be taking place. A similar study of the effect of geomagnetic activity on the tidal components may lead to a better understanding of this coupling.

Chapter 7.

CONCLUSIONS AND SUGGESTIONS FOR FURTHER WORK

The effect of auroral and geomagnetic activity on the vertical and horizontal winds in the auroral zone have been discussed. Vertical winds as determined from FPS observations of the λ558 nm emission are found to have magnitudes up to 30 ms^{-1}. Large upward winds at altitudes below 110 km appear to be associated with intense auroral substorms and it is suggested that these are primarily a result of particle heating. During periods of more moderate auroral activity both particle and joule heating are likely to affect vertical wind motions.

The horizontal wind, as measured using an SAPR radar, is found to be generally enhanced during geomagnetically active times. A randomization technique was developed which showed that correlations of both the raw and filtered data with the local K-index are significant. The raw winds tend to increase in the geographic NW to NE quadrant at high K-times during the interval 0400-0700 LT (after magnetic midnight). This is consistent with the expected response of the neutral wind to either ion drag or heating in the vicinity of the auroral electrojet. It is also consistent with the direction of drift expected if the ionized irregularities become decoupled from the neutral wind in the presence of strong electric fields. Correlations between the medium (2 - 6 h) and high (1 - 3 h) frequency components of the wind and the local K-index are seen at heights down to 86 km. The correlation shows a seasonal dependence.

These results, or specifically the magnitude of the observed vertical winds and the height down to which geomagnetic activity appears to influence the horizontal wind, suggest that geomagnetic activity has a significant influence on wind motions in the upper mesosphere/lower thermosphere. Continued investigation is required to further substantiate these results and suggestions for further work are given below.

There have been very few measurements of vertical winds in the auroral zone lower thermosphere as there are few techniques capable of probing this region. FPS observations of the λ558 nm emission, while allowing neutral wind motions to be determined, have the drawback

that the emission height and hence height of observation is very variable. In many cases, and particularly during strong auroral events, the emission temperature is shown to be primarily dependent on the emission height. The emission temperature may be used to determine this height if a temperature profile can be assumed. Rocket flights carried out in the auroral zones, during various geomagnetic conditions, currently provide useful temperature profiles. Further measurements would be valuable.

Further measurements of the vertical wind during various auroral conditions are required. The FPS at Mawson is well suited to such observations as, with the feature of a fast scan time ($\sim$6 sec), large variations in the emission intensity can be tolerated. A number of sources of bias and error in the vertical wind measurements have been investigated and as a result the following recommendations are made.

(i) The instrument should be operated in either the semi-automatic or preferably manual mode of operation so that the profile acquire times may be varied according to the level of auroral activity.

(ii) Calibrations should be made after about six profiles have been acquired, but not between profiles as is the case when the instrument is operated in automatic mode.

(iii) In order to avoid large day-to-day variations in the 'zero wind' velocity care should be taken to accurately reset the central-scan voltage to the centre of the operating range at the start of each night.

Estimating the instrument drift curve is considered to be one of the major sources of error in the vertical wind determinations. Investigations into the causes of instrument drift would be worthwhile by, for example, carrying out a long series of observations of the λ546 nm calibration source while attempting to 'disturb' the instrument. Currently several alternative calibration sources are being investigated which include Europium λ557.7 nm and krypton λ557.0 nm. Although these emissions are likely to be weaker than the mercury λ546 nm emission, they have the advantage that they are close to the observation wavelength. Calibration could therefore

be carried out without changing the broad band filter, and thus reducing the possibility of disturbing the instrument. Modifications to the instrument to allow continuous calibration, by use of an off-axis calibration source together with a second off-axis detection system, would allow the instrument drift to be accurately monitored. An additional advantage would be that such modifications would allow calibration to be carried out without making mechanical changes to the system.

Further work comparing the SAPR data acquisition heights with the vertical wind measurements from the FPS are considered worthwhile. The SAPR radar is sensitive to variations in electron concentration at heights below 100 km. It is in fact more sensitive than the ionosonde which is routinely operated at Mawson by the Ionospheric Prediction Service (IPS). There are plans to install new riometers at Mawson and hopefully these records will provide additional information on the level of particle precipitation. This will assist in the identification of events which are likely to produce significant levels of particle heating. Further investigation of the 'pattern scale', determined by applying the full correlation analysis to the SAPR received signals, may also provide additional information on the 'state' of the upper mesosphere during particular auroral events.

The question of what velocity is being measured by the SAPR radar remains one of the greatest sources of uncertainty in the 'wind' measurements determined using this technique. The direction of the enhanced winds during high K-times cannot be used to rule out the possibility that the ionized irregularities become decoupled from the neutral winds during such times. In fact the direction of the enhanced winds is consistent with the predicted effects of ion drag, enhanced electric fields, and heating. The first two effects will cause the measured 'winds' to be enhanced in the same direction and thus these two effects cannot be distinguished on this basis. One way in which they can be distinguished, however, is by comparison with wind motions measured using a FPS for which there is no question that it is the velocity of the neutral atmosphere which is being measured.

The sodium emission maximises at a height of between 85 and 92 km and is not part of the emission spectrum induced by auroral activity. As such, determinations of wind velocity from FPS observations of the sodium emission lend themselves well to comparison with wind measurements determined using the SAPR radar. Such comparisons have been made at the mid-latitude site of Adelaide, Australia (Greet, 1988) and plans are underway for a similar study to be carried out at Mawson during 1989. The results of this work will be invaluable in determining how effective the SAPR radar is at measuring neutral wind motions, particularly in the presence of large electric fields present during geomagnetically disturbed times.

The observed polarization of the medium and high frequency components of the wind in the approximate geographic meridional direction, at all times of the year and during various geomagnetic conditions, is perhaps unexpected. Such findings may have important implications on the momentum budget. A comprehensive study of gravity wave parameters including the horizontal momentum flux would be worthwhile both at Mawson and at other sites. In addition, carrying out a similar study at Australia's Casey station, where local magnetic north is approximately 90° W of geographic north, would allow biases introduced by geographic factors to be more readily distinguished from those associated with the auroral electrojet.

The effect of geomagnetic activity on the raw wind values, and on the medium and high frequency components of the wind, has been carried out. A similar study of the effect of geomagnetic activity on the low frequency and tidal components would be worthwhile. Such a study may lead to a better understanding of the complex coupling of electrodynamic forcing with neutral air motions which appears to occur in the auroral zone upper mesosphere/lower thermosphere.

APPENDIX 1

The following paper appeared in ANARE (Antarctic National Antarctic Research Expeditions) Research Notes 48, edited by G. B. Burns and M. Craven, Antarctic Division, Department of Science, 1987.

Price, G., Vincent, R. A. & Jacka, F. (1987). Winds and temperatures in the mesosphere and lower thermosphere at Mawson, Antarctica. *ANARE Research Notes 48,* 148-159.

APPENDIX 2

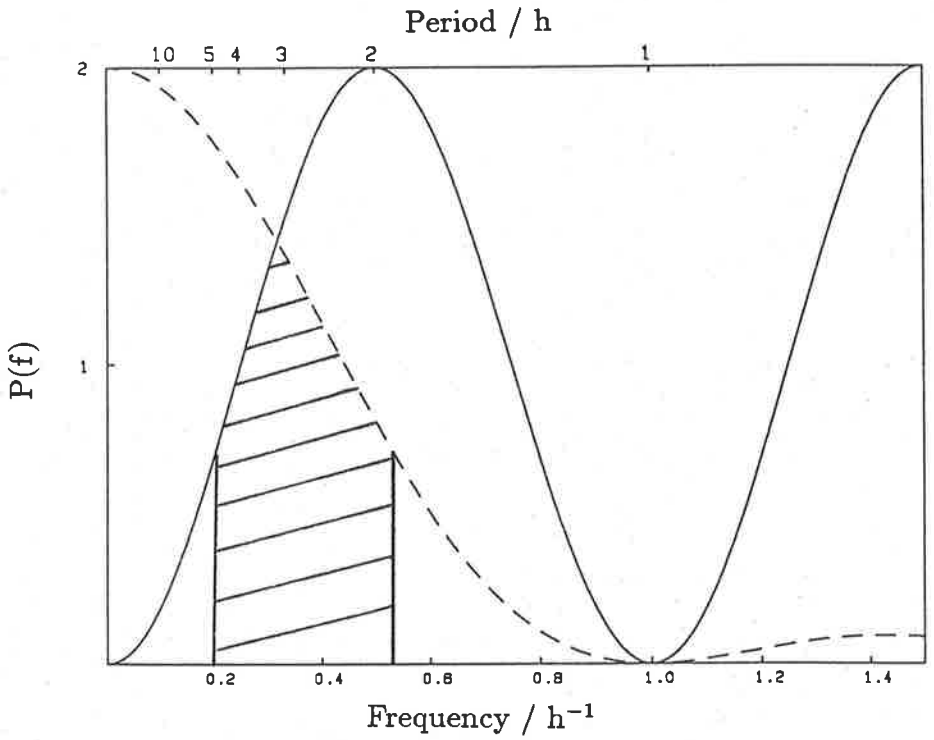

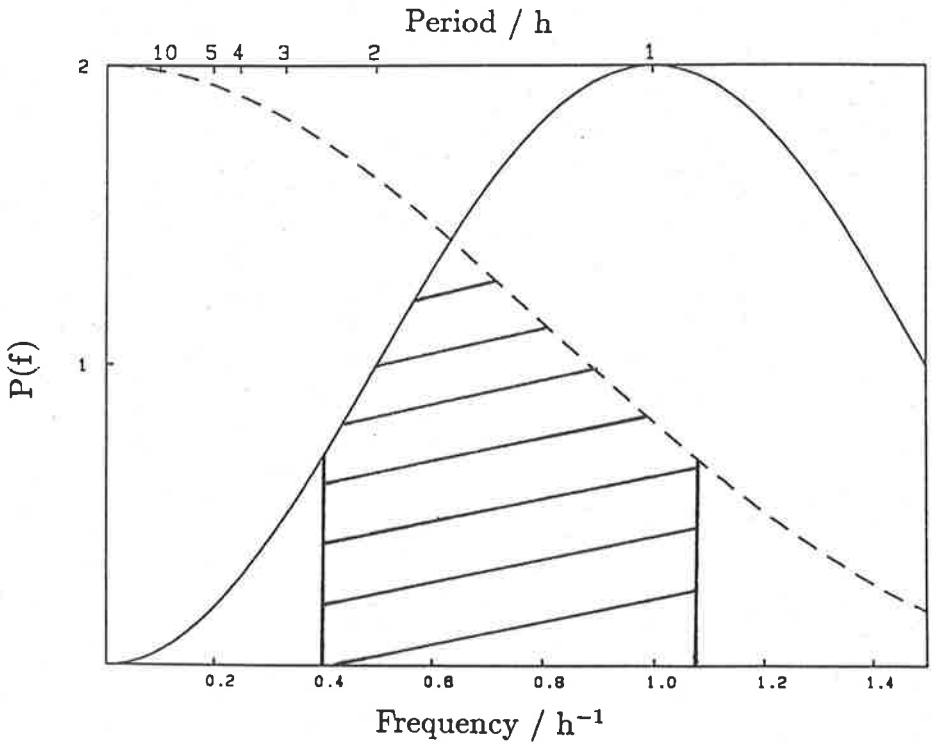

Form of the filter functions resulting from averaging the wind over the time interval τ and then subtracting successive values. A block filter given by $P(f) = (\frac{sin(\pi f \tau)}{\pi f \tau})^2$ (dashed curves) is produced by averaging the data and a function of the form $P(f) = 1 - cos(2\pi f \tau)$ (continuous curve) results from subtracting successive values (Meek *et al.*, 1985b). The combined effect is represented by the area under the two curves which has been shaded down to the half-power points. Two values of τ were used in the analysis: τ=60 min (*top diagram*) which filtered out frequencies in the range 2 - 6 h and τ=30 min (*bottom diagram*) which filtered out frequencies in the 1 - 3 h range.

REFERENCES

Armstrong, E.B. (1956). "The airglow and the aurora: The observation of line profiles in the airglow and aurora with a photoelectric Fabry-Perot interferometer", Pergamon Press, New York.

Armstrong, E.B. (1969). "Doppler shifts in the wavelength of the OI λ 6300 $\mathring{A}$ line in night airglow", Planet. Space Sci., **17**:957-974.

Armstrong, E.B. (1982). "The association of visible airglow features with a gravity wave", J. Atmos. Terres. Phys., **44**:325-336.

Balsley, B.B., Carter, D.A. and Ecklund, W.L. (1982). "On the relationships between electrojet intensity fluctuations and the wind field near the mesopause", Geophys. Res. Lett., **9**:219-222.

Balsley, B.B, Ecklund, W.L., and Fritts, D.C. (1983). "VHF echoes from high-latitude mesosphere and lower thermosphere: observations and interpretations", J. Atmos. Sci., **40**:2451-2466.

Banks, P.M. (1977). "Observations of joule and particle heating in the auroral zone", J. Atmos. Terres. Phys., **39**:179-199.

Banks, P.M. and Kockarts, G. (1973). "Aeronomy Part A", Academic Press, New York and London.

Bates, H.F. (1974b). "Thermospheric changes shortly after the onset of daytime joule heating", Planet Space Sci., **22**:1625-1636.

Bates, D.R. (1981). "The green light of the night sky", Planet. Space Sci., **29**:1061-1067.

Baumjohann, W., Gustafsson, G., Nielsen, E., Ranta, H., and Evans, D.S. (1985). "Latitude-integrated Joule and particle heating rates during the Energy Budget Campaign", J. Atmos. Terres. Phys., **47**:27-39.

Belrose, J.S., Burke, M.J., Coyne, N.R., and Reed, J.E. (1972). "D-region measurements with the differential-absorption, differential-phase partial-reflection experiments", J. Geophys. Res., **77**:4829-4838.

Bevington, P.R. (1969). "Data reduction and error analysis for the physical sciences", McGraw-Hill Book Company.

Blanc, W., and Richmond, A.D. (1980). "The ionospheric disturbance dynamo", J. Geophys. Res., **85**:1669-1686.

Bolgiano Jr, R. (1968). "The general theory of turbulence in the atmosphere. Winds and turbulence in stratosphere, mesosphere and ionosphere", North-Holland Publishing Company-Amsterdam, ed. K. Rawer, p.371-400

Booker J.R., and Bretherton, F.P. (1967). "The critical layer for internal gravity waves in a shear flow", J. Fluid Mech., **27**:513-539.

Bretherton, F.P. (1966). "The propagation of groups of internal gravity waves in a shear flow", Quart. J. Roy. Met. Soc., **92**:466.

Briggs, B.H. (1977). "Ionospheric drifts", J. Atmos. Terres. Phys., **39**:1023-1033.

Briggs, B.H. (1980). "Radar observations of atmospheric winds and turbulence: a comparison of techniques", J. Atmos. Terres. Phys., **42**:823.

Briggs, B.H. (1984). "The analysis of spaced sensor records by correlation techniques", Handbook for MAP, **13**:166-186.

Briggs, B.H. and Vincent, R.A. (1973). "Some theoretical considerations on remote probing of weakly scattering irregularities", Aust. J. Phys., **26**:805-814.

Bureau of Mineral Resources, Geology and Geophysics (1963-1987). "Geophysical observatory reports", **7-35**.

Chimonas, G. and Hines, C.O. (1970). "Atmospheric gravity waves launched by auroral currents", Planet. Space Sci., **18**:565-582.

Cocks, T.D., Creighton, D.F., and Jacka, F. (1980). "Application of a dual Fabry-Perot spectrometer for daytime studies", J. Atmos. Terres. Phys., **42**,499-511.

Cole, K.D. (1962). "Joule heating of the upper atmosphere", Aust. J. Phys., **15**:223-235.

Cole, K.D. (1987). "The role of the Antarctic in international upper atmosphere programs", ANARE Research Notes, **48**:206-214.

Czechowsky, P., Ruster, R., and Schmidt, G. (1979). "Variations of mesospheric structures in different seasons", Geophys. Res. Lett., **6**:459-462.

Devlin, T., Hargreaves, J.K., Collis, P.N. (1986). "EISCAT observations of the ionospheric D-region during auroral radio events", J. Atmos. Terres. Phys., **48**:795-805.

Eckermann, S.D. and Vincent, R.A. (in press). "Falling sphere observations of anisotropic gravity wave motions in the upper stratosphere over Australia", J. Pure Appl. Geophys., March, 1989.

Evans, D.S., Maynard, N.C., Trom, J., Jacobsen, T., and Egeland, A. (1977). "Auroral vector electric field and particle comparisons 2. Electrodynamics of an arc", J. Geophys. Res., **82**:2235-2249.

Einaudi, F. and Hines, C.O. (1970). "WKB approximation in application to acoustic-gravity waves", Can. J. Phys., **48**:1458-1471.

Forbes, J.M. (1985). "Atmospheric Tides between 80 and 120 km", Handbook for MAP, **16**:278-289.

Francis, S.H. (1975). "Global propagation of atmospheric gravity waves: A review", J. Atmos. Terres. Phys., **37**:1011-1054.

Fraser, G.J. (1965). "The measurement of atmospheric winds at altitudes of 64-120 km using ground based radio equipment", J. Atmos. Sci., **22**: 217-218.

Fraser, G.J. (1968). "Seasonal variation of southern hemisphere mid-latitude winds at altitudes of 70-100 km", J. Atmos. Terres. Phys., **30**:707-719.

Fraser,G.J. (1984). "Summer circulation in the Antarctic middle atmosphere", J. Atmos. Terres. Phys., **46**:143-146.

Fraser, G.J. and Kochanski, A. (1970). "Ionospheric drifts from 64-108 km altitudes at Birdlings Flat", Ann. Geophys., **26**:675-687.

Freund, J.T. and Jacka, F. (1979). "Structure in the λ557.7 nm [0I] airglow", J. Atmos. Terres. Phys., **41**:25-31.

Fritts, D.C. (1984). "Gravity wave saturation in the middle atmosphere: A review of theory and observations", Rev. Geophys. Space Phys., **22**:275-308.

Fritts, D.C. (1985). "A numerical study of gravity wave saturation: nonlinear and multiple wave effects", J. Atmos. Sci., **42**:2043-2058

Fritts, D.C., Geller, M.A., Balsley, B.B., Chanin, M.L., Hirota, I., Holton, J.R., Kato, S., Lindzen, R.S., Shoeberl, M.R., Vincent, R.A., and Woodman, R.F. (1984). "Research status and recommendations from the Alaska workshop on gravity waves and turbulence in the middle atmosphere Fairbanks, Alaska, 18-22 July 1983", Bulletin of the American Meteorological Society, **65**:149-159.

Fritts, D.C. and Vincent, R.A. (1987). "Mesospheric momentum flux studies at Adelaide, Australia: observations and a gravity wave-tidal interaction model", J. Atmos. Sci., **44**:605-619.

Fuller-Rowell, T.J. and Rees, D. (1980) "A three-dimensional time-dependent global model of the thermosphere", J. Atmos. Sci., **37**:2545-2567.

Fuller-Rowell, T.J. and Rees, D. (1984) "Interpretation of an anticipated long-lived vortex in the lower thermosphere following simulation of an isolated substorm", Planet. Space Sci., **32**:69-85

Gardner, F.F. and Pawsey, J.L. (1953). "Study of the ionospheric D-region using partial reflections", J. Atmos. Terres. Phys., **3**:321-344.

Gavrilov, N.M., and Shved, G.M. (1982). "Study of internal gravity waves in the lower thermosphere from observations of the nocturnal sky Airglow [0I] 5577$\AA$ in Ashkhabad", Ann. Geophys., **38**:789-803.

Georges, T.M. (1968). "HF Doppler studies of travelling ionospheric disturbances", J. Geophys. Res., **78**:3841.

Gerdjikova, M.G. and Shepherd, G.G. (1987). "Evaluation of Auroral 5577-$\AA$ excitation processes using Intercosmos Bulgaria 1300 satellite measurements", J. Geophys. Res., **92**:3367-3374.

Golley, M.G. and Rossiter, D.E. (1970). "Some tests of methods of analysis of ionospheric drift records using an array of 89 aerials", J. Atmos. Terres. Phys., **32**:1215-1233.

Greet, P.A. (1988). "Observations on the sodium layer", Ph.D. Thesis, University of Adelaide.

Gregory, J.B. and Rees, D.T. (1971). "Wind profiles to 100km near 53 N during 1969", J. Atmos. Sci., **20**:1079-1082.

Gregory, J.B., Meek, C.E., and Manson, A.H. (1982). "An assessment of winds data (60-110 km) obtained in real-time from a medium frequency radar using the radio wave drifts technique", J. Atmos. Terres. Phys., **44**:649-655.

Guha, D. and Geller, M.A, (1973). "Computer simulation studies of a spaced-receiver drift experiment", J. Atmos. Terres. Phys., **35**:1853-1867.

Hargreaves, J.K. (1980). "D-region electron densities observed by incoherent-scatter radar during auroral-absorption spike events", J. Atmos. Terres. Phys., **42**:783-789.

Haurwitz, B. and Fogle, B. (1969). "Wave forms in noctilucent clouds", Deep-Sea Research., **16**:85-95.

Hays, P.B. and Roble, R.G. , (1971). "Direct observations of the thermospheric winds during geomagnetic storms", J. Geophys. Res., **76**:5316-5321.

Hays, P.B., Jones, R.A., and Rees, M.H. (1973). "Auroral heating and the composition of the neutral atmosphere", Planet. Space Sci., **21**:559-573.

Heelis, R.A., Lowell, J.K., and Spiro, R.W. (1982). "A model of the high-latitude ionospheric convection pattern", J. Geophys. Res., **87**:6339-6345.

Heisler, L.H. (1958). "Anomalies in ionosonde records due to travelling ionospheric disturbances", Australian J. Phys., **11**:79-90.

Henriksen, K., Egeland, A. (1988). "The interpretation of the auroral green line", EOS, **69**:721.

Hernandez, G. (1976). "Lower-thermosphere temperatures determined from the line profiles of the OI 17,924-K (5577 $\AA$) emission in the nights sky 1. Long term behaviour", J. Geophys. Res., **81**:5165-5172.

Hernandez, G. (1982). "Vertical motions of the neutral thermosphere at midlatitude", Geophys. Res. Lett., **9**:555-557.

Hernandez, G. and Roble, R.G. , (1976). "Direct measurements of night-time thermospheric winds and temperatures. 1. Seasonal variations during geomagnetic quiet periods", J. Geophys. Res., **81**:2065-2074.

Herrero, F.A., Hans, G.M., Harris, I., and Varosi, F. (1984). "Thermospheric gravity waves near the source: Comparison of variations in neutral temperature and vertical velocity at Sondre Stromfjord", Geophys. Res. Lett., **1**:939-942.

Hilliard, R.L., Shepherd, G.G. (1966). "Upper atmospheric temperatures from Doppler line widths - IV. A detailed study using the OI 5577 $\AA$ auroral and nightglow emission", Planet. Space Sci., **14**:383-406.

Hines, C.O. (1960). "Internal gravity waves in ionospheric heights", Can. J. Phys., **38**:1441.

Hines, C.O. (1968). "Some consequences of gravity-wave critical layers in the upper atmosphere", J. Atmos. Terres. Phys., **30**:837-843.

Hocking, W.K. (1979). "Angular and temporal characteristics of partial reflections from the D-region of the ionosphere", J. Geophys. Res., **84**:845-851.

Hocking, W.K. (1981). "Investigation of the movement and structure of D-region ionospheric irregularities", Ph.D Thesis, University of Adelaide.

Hocking, W.K. (1985). "Measurement of turbulent energy dissipation rates in the middle atmosphere by radar techniques: A review", Radio Sci., **20**:1403-1422.

Hocking, W.K. and Vincent, R.A. (1982a). "A comparison between HF partial reflection profiles from the D-region and simultaneous Langmuir probe electron density measurements", J. Atmos. Terres. Phys., 44:843-854.

Hocking, W.K. and Vincent, R.A. (1982b). "Comparative observations of D-region HF partial reflections at 2 and 6 MHz", J. Geophys. Res., **87**:7615-7624.

Hodges, R.R. (1969). "Eddy diffusion coefficients due to instabilities in internal gravity waves", J. Geophys. Res., **74**:4087.

Hook, J.L. (1970). "Winds at the 75-110 km level at College, Alaska", Planet. Space Sci., **18**:1623-1638.

Hoppe, U.P. and Hansen, T. (1988). "Studies of vertical motions in the upper mesosphere using the EISCAT UHF radar", Ann. Geophys., **6**:181-186.

Hunsucker, R.D. (1982). "Atmospheric gravity waves generated in the high-latitude ionosphere: A review", Rev. Geophys. Space Phys., **20**:293-315.

International Union of Geodesy and Geophysics (1963). "International Auroral Atlas", Edinburgh University Press, Great Britain.

Jacka, F. (1984). "Application of Fabry-Perot spectrometers for measurement of upper atmosphere temperatures and winds", Handbook for MAP, **13**:19-40.

Jacka, F., Bower, A.R.D., Creighton, D.F., and Wilksch, P.A. (1980). "A large-aperture high-resolution Fabry-Perot spectrometer for airglow studies", J. Phys. E: Sci. Instrum., **13**:562-568.

Johnson, R.M. and Luhmann, J.G. (1985a). "Neutral wind spectra at the auroral zone mesopause: Geomagnetic effect?", J. Geophys. Res., **90**:1735-1743.

Johnson, R.M. and Luhmann, J.G. (1985b). "High-latitude mesopause neutral winds and geomagnetic activity: A cross-correlation analysis", J. Geophys. Res., **90**:8501-8506.

Johnson, R.M., Wickwar, V.B., Roble, R.G., and Luhmann, J.G. (1987). "Lower-thermospheric winds at high latitude: Chatanika radar observations", Ann. Geophys., **5A**:383-404.

Jones, N. P. and Jacka, F. (1985). "Winds in the lower thermosphere over Mawson, Antarctica," Handbook for MAP, **18**:477-481.

Jones, N. P. and Jacka, F. (1987). "Dynamics of the thermosphere over Mawson, Antarctica: The lower thermosphere", ANARE Research Notes., **48**:138-147.

Kalchenko, B.V., Kashcheyev, B.T., and Oleynikov, A.N. (1985). "Radiometeor studies of the vertical structure of internal gravity waves and irregular motion", Atmospheric and Oceanic Physics., **21**:93-98.

Kellogg, W.W. and Schilling, G.F. (1951). "A proposed model of the circulation in the upper stratosphere", J. of Met., **8**:222-230.

Kent, G.S. and Wright, R.W.H. (1968). "Movements of ionospheric irregularities and atmospheric winds", J. Atmos. Terres. Phys., **30**:657-691.

Killeen, T.L. and Hays, P.B. (1983). "O(^{1}S) from dissociative recombination of O_2^+: non-thermal line profile measurements from dynamics explorer", J.Geophys. Res., **88**:10163-10169

Kochanski, A. (1964). "Atmospheric motions from sodium cloud drifts", J. Geophys. Res., **69**:3651.

Koop, C.G. (1981). "A preliminary investigation of internal gravity waves with a steady shearing motion", J. Fluid Mech., **113**:347-386.

Korobeynikova, M.P. and Nasirov, G.A. (1976). "Influences of the internal gravity waves on the behaviour of the nightglow emission 557.7 nm", Ann. Geophys., **32**:39-41.

Krassovsky, V.I., Potapov, A.I., Semenov, A.I., Shagaev, M.V., Shefov, N.N., Sobolev, V.G., and Toroshelidze, T.I. (1977). "Internal gravity waves near the mesopause and the hydroxyl emission", Ann. Geophys., **33**:347-356.

Liller, W. and Whipple, F.L. (1954). "High-altitude winds by meteor-train photography", in Rocket Exploration of the Upper Atmosphere, special supplement to J. Atmos. Terres. Phys., **1**:112.

Lindner, B.C. (1975). "The nature of D-region scattering of vertical incidence radio waves. II. Experimental observations using spaced antenna reception", Aust. J. Phys., **28**:171-184.

Leovy, C.B. (1964). "Simple models of thermally driven mesospheric circulation", J. Atmos. Sci., **21**:327-341.

Lindzen, R.S. (1981). "Turbulence and stress due to gravity wave and tidal breakdown", J. Geophys. Res., **86**:9707.

Luhmann, J.G. (1980). "Atmospheric pressure and velocity fluctuations near the auroral electrojet", J. Geophys. Res., **85**:1749-1756.

McDade, I.C. and Llewewllyn, E.J. (1986). "The excitation of $O(^1S)$ and O_2 bands in the nightglow: a brief review and preview", Can. J. Phys., **64**:1626-1630.

MacLeod, R.I. (1986). "Dynamics of the Antarctic mesosphere", Ph.D. Thesis, University of Adelaide.

MacLeod, R. and Vincent, R.A. (1985). "Observations of winds in the Antarctic summer mesosphere using the spaced antenna technique", J. Atmos. Terres. Phys., **47**:567-574.

Maekawa, Y., Fukao, S., and Kato, S. (1987). "Vertical propagation characteristics of internal gravity waves around the mesopause observed by the Arecibo UHF radar", J. Atmos. Terres. Phys., **49**:73-80.

Manson, A.H., Gregory, J.B., and Stephenson, D.G. (1973). "Winds and wave motions (70-100 km) as measured by a partial reflection radiowave system", J. Atmos. Terres. Phys., **35**:2055-2067.

Manson, A.H., Gregory, J.B., and Stephenson, D.G. (1976). "Gravity waves in the lower atmosphere", J. Atmos. Terres. Phys., **38**:143-148.

Manson, A.H. and Meek, C.E. (1984). "Partial reflection D-region electron densities", Handbook for MAP, **13**:113-123.

Manson, A.H. and Meek, C.E. (1986). "Comparisons between neutral winds near 100 km at Saskatoon (52°N, 107°W, L = 4.4) and variations in the geomagnetic field (1979-1983)", Ann. Geophys., **4**:281-286.

Manson, A.H. and Meek, C.E. (1988). "Gravity wave propagation characteristics (60 - 120 km) as determined by the Saskatoon MF radar (Gravnet) system: 1983 - 1985 at 52°N, 107°W", J. Atmos. Sci., **45**:932-946.

Manson, A.H., Meek, C.E., and Gregory, J.B. (1981). "Winds and waves (10 min-30 days) in the mesosphere and lower thermosphere at Saskatoon (52°N, 107°W, L = 4.3)during the year, October 1979 to July 1980", J. Geophys. Res., **86**:9615-9625.

May P.T. (1988). "Statistical errors in the determination of wind velocities by the spaced antenna technique", J. Atmos. Terres. Phys., **50**:21-32.

Mayr, H.G., Harris, I., Varosi, F., and Herrero, F.A. (1984a). "Global excitation of wave phenomena in a dissipative multiconstituent medium - transfer function of the earth's thermosphere", J. Geophys. Res., **89**:10929-10959.

Mayr, H.G., Harris, I., Varosi, F., and Herrero, F.A. (1984b). "Global excitation of wave phenomena in a dissipative multiconstituent medium - impulsive perturbations in the earth's thermosphere", J. Geophys. Res., **89**:10961-10986.

Mazaudier, C., and Bernard, R. (1985). "Saint-Santin radar observations of lower thermospheric storms", J. Geophys. Res., **90**:2885-2895.

Meek, C.E., Reid, I.M., and Manson, A.H. (1985a). "Observations of mesospheric wind velocities. 1. Gravity wave horizontal scales and phase velocities determined from spaced wind observations", Radio Sci., **20**:1363-1382.

Meek, C.E., Reid, I.M., and Manson, A.H. (1985b). "Observations of mesospheric wind velocities. 2. Cross sections of power spectral density for 48-8 hours, 8-1 hours, and 1 hour to 10 min. over 60-110 km for 1981", Radio Sci., **20**:1383-1402.

Murgatroyd, R.J. and Goody, R.M. (1958). "Sources and sinks of radiative energy from 30 to 90 km", Quart. J. Roy. Met. Soc., **84**:225-234.

Murgatroyd, R.J. and Singleton, F. (1961). "Possible meridional circulation in the stratosphere and mesosphere", Quart. J. Roy. Met. Soc., **87**:125-135.

Munro, G.H. (1950). "Travelling disturbances in the ionosphere", Proc. Roy. Soc., **202**:208-209.

Munro, G.H. (1953). "Reflexions from irregularities in the ionosphere", Proc. Roy. Soc., **219**:447.

Munro, G.H. (1958). "Travelling ionospheric disturbances in the F region", Aust. J. Phys., **11**:91-112.

Ogawa, T., Igarashi, K., and Kuratani Y. (1986). "Some initial results of 50 Mhz meteor radar observations at Syowa station", (private communication).

Orlanski, I. and Bryan, K. (1969). "Formation of the thermocline step structure by large-amplitude internal gravity waves", J. Geophys. Res., **74**:6975-6983.

Pekeris, C.L. (1939). "The propagation of a pulse in the atmosphere, Part I", Proc. Roy. Soc. Lond., **A171**:434-443.

Pekeris, C.L. (1948). "The propagation of a pulse in the atmosphere, Part II", Phys. Rev., **73**:145-154.

Peteherych, S. and Shepherd, G.G. (1971). "Interferometric measurements of daytime aurora and airglow", EOS, **52**, 309.

Peteherych, S., Shepherd, G.G., and Walker, J.K. (1985). "Observations of vertical E-region neutral winds in two intense auroral arcs", Planet. Space Sci., **33**:869-873.

Philbrick, C.R., Schmidlin, F.J., Grossmann, G., Lange G., Offermann, D., Baker K.D., Krankowsky, D., and von Zahn, U. (1985). "Density and temperature structure over northern Europe", J. Atmos. Terres. Phys., **47**:159-171.

Phillips, A. and Jacka, F. (1987). "Winds in the middle atmosphere at Mawson, Antarctica: Geomagnetic and 'meteorological' effects", ANARE Research Notes, **48**:107-113.

Phillips, A. and Vincent, R.A. (1987). "Winds in the middle atmosphere at Mawson, Antarctica: II Tides" , ANARE Research Notes, **48**:93-106.

Price, G.D., Vincent, R.A., and Jacka, F. (1987). "Winds and temperatures in the mesosphere and lower thermosphere at Mawson, Antarctica", ANARE Research Notes, **48**:148-159.

Prikryl, P., Koehler, J.A. and Sofko, G.J. (1986). "Simultaneous CW radio measurements of meteor and auroral drifts", Radio Sci., **21**:271-282.

Ramsay, J.V. (1962). "A rapid-scanning Fabry-Perot interferometer with automatic parallelism control", Appl. Opt., **1**:411-413.

Rastogi, P.K., Brekke, A., Holt, O., and Hansen, T. (1982). "Variability of D-region electron densities at Tromso", J. Atmos. Terres. Phys., **44**:313-323.

Ratcliffe, J.A. (1972). "An introduction to the ionosphere and magnetosphere", Cambridge University Press, London.

Rees, M.H. (1963). "Auroral ionization and excitation by incident energetic electrons", Planet Space Sci., **11**:1209-1218.

Rees, D., Smith, R.W., Charleton,P.J., McCormac, F.G., Lloyd, N., and Steen, A. (1984a). "The generation of vertical thermospheric winds and gravity waves at auroral latitudes - observations of vertical winds", Planet. Space Sci., **32**:667-684.

Rees, D., Smith, M.F., and Gordon, R. (1984b). "The generation of vertical thermospheric winds and gravity waves at auroral latitudes - theory and numerical modelling of vertical winds", Planet. Space Sci., **32**:685-705.

Reid, G.C. (1983). "The influence of electric fields on radar measurements of winds in the upper mesosphere", Radio Sci., **18**:1028-1034.

Reid, I.M. (1986). "Gravity wave motions in the upper middle atmosphere (60-110 km)", J. Atmos. Terres. Phys., **48**:1057-1072.

Reid, I.M. and Vincent, R.A. (1987). "Measurements of mesospheric gravity wave momentum fluxes and mean flow accelerations at Adelaide, Australia", J. Atmos. Terres. Phys., **49**:443-460.

Richmond, A.D. (1978). "Gravity wave generation, propagation, and dissipation in the atmosphere", J. Geophys. Res., **83**:4131-4144.

Richmond, A.D. and Matsushita, S. (1975). "Thermospheric response to a magnetic substorm", J. Geophys. Res., **80**:2839-2850.

Romick, F.J . (ed.) (1987). The Cedar Post, **5**, No. 4.

Rosenberg, N.W. and Edwards, H.D. (1964). "Observations of ionospheric wind patterns through the night", J. Geophys. Res., **69**:2819.

Rottger, J., Rastogi, P.K., and Woodman, R.F. (1979). "High-resolution VHF radar observations of turbulence structures in the mesosphere", Geophys. Res. Lett., **6**:617-620.

Royrvik, O. (1983). "Morphology of the scattering targets: fresnel and turbulent mechanisms", Handbook for MAP, **14**:80.

Royrvik, O. (1985). "Radar comparison of 2.66-MHz and 40.92-MHz signals scattered from the mesosphere", Radio Sci., **20**:1423-1434.

Royrvik, O., Gibbs, K.P., and Bowhill, S.A. (1982). "VHF power scattered from the mesosphere at mid-latitudes", J. Geophys. Res., **87**:2501-2508.

Sharp, W.E., Rees, M.H., Stewart, A.I. (1979). "Coordinated rocket and satellite measurements of an auroral event. 2. The rocket observations and analysis", J. Geophys. Res., **84**:1977-1985.

Schoeberl, M.R. and Strobel, D.F. (1978). "The zonally averaged circulation of the middle atmosphere", J. Atmos. Sci., **35**:577

Siegel, S. (1956). "Nonparametric Statistics for the behavioural sciences", McGraw-Hill Kogakusha, Ltd.

Smith, S.A., Fritts, D.C., Balsley, B.B., and Philbrick, C.R. (1986). "Simultaneous rocket and MST radar observation of an internal gravity wave breaking in the mesosphere", Handbook for MAP., **20**:136-146

Stubbs, T.J. (1973). "The measurement of winds in the D-region of the ionosphere by the use of partially reflected radio waves", J. Atmos. Terres. Phys., **35**:909-919.

Stubbs, T.J. and Vincent, R.A. (1973). "Studies of D-region drifts during the winters of 1970 - 72", Aust. J. Phys., **26**, 645-660.

Testud, J. (1970). "Gravity waves generated during magnetic substorms", J. Atmos. Terres. Phys., **32**:1793-1805.

Tetenbaum, D., Avery, S.K., and Riddle, A.C. (1986). "Observations of mean winds and tides in the upper mesosphere during 1980 - 1984, using the Poker Flat, Alaska, MST radar as a meteor radar", J. Geophys. Res., **91**:14539-14555.

Theon, J.S., Nordberg, W., Katchen, C.B., and Horvath, J.J. (1967). "Some observations on the thermal behavior of the mesosphere", J. Atmos. Sci., **24**:428.

Thiele, B., Bostrom, R. , Dumbs, A., Grossmann, K.U., Krankowsky, D., Lammerzahl, P., Marklund, G., Neske, E., Schmidtke, G., and Wilhelm, K. (1981). "In situ measurements of heating parameters in the auroral ionosphere", Planet. Space Sci., 4:455-468.

Thomas, R.J., and Barth, C.A. (1984). "Seasonal variations of ozone in the upper mesosphere and gravity waves", Geophys. Res. Lett., **11**:673-676.

Thomas, R.J. and Donahue, T.M. (1972). "Analysis of Ogo-6 observations of the OI 5577$\AA$ tropical nightglow", J. Geophys. Res., **77**:3557-3565.

Thrane, E.V., Grandal, B., Fla, T., Brekke, A. (1981). "Fine structure in the ionospheric D-region", Nature, **292**:221-223.

Thrane, E.V., Blix, T.A., Hall, C., Hansen, T.L., von Zahn, U., Meyer, W., Czechowsky, P., Schmidt, G. and Widdel, H.U. (1987). "Small scale structure and turbulence in the mesosphere and lower thermosphere at high latitudes in winter", J. Atmos. Terres. Phys., **49**:751-762.

Torkar, K.M., Urban, A., Bjordal, J., Lundblad, J.A., Soraas, F., Smith, L.G., Dumbs, A., Grandal, B., Ulwick, J.C., and Vancour, R.P. (1985). "Energy deposition rates by charged particles", J. Atmos. Terres. Phys., **47**:61-71.

Tuan, T.F., Hedinger, R., Silverman, S.M., and Okuda, M. (1979). "On gravity wave induced Brunt-Vaisala oscillations", J. Geophys. Res., **84**:393.

Turgeon, E.C. and Shepherd, G.G. (1962). "Upper atmospheric temperatures from Doppler line widths - II", Planet. Space Sci., **9**:295-304.

Vallance Jones, A.J . (1974). "Aurora", D. Reidel Publishing Company, Dordrecht, Holland.

Van Zandt, T.E and Fritts, D.C. (in press). "A theory of enhanced saturation of the atmospheric gravity wave spectrum due to changes in stability", J. Pure Appl. Geophys., March, 1989.

Vincent, R.A. (1972). "Ionospheric irregularities in the E-region", J. Atmos. Terres. Phys., **34**:1881.

Vincent, R.A. (1984a). "Gravity-wave motions in the mesosphere", J. Atmos. Terres. Phys., **46**:119-128.

Vincent, R.A. (1984b). "MF/HF radar measurements of the dynamics of the mesopause region-A review", J. Atmos. Terres. Phys., **46**:961-974.

Vincent, R.A. and Ball, S. (1977). "Tides and gravity waves in the mesosphere at mid and low-latitudes", J. Atmos. Terres. Phys., **39**:965-970.

Vincent, R.A. and Ball, S. (1981). "Mesospheric winds at low and mid-latitudes in the southern hemisphere", J. Geophys. Res., **86**:9159-9169.

Vincent, R.A. and Belrose, J.S. (1978). "The angular distribution of radio waves partially reflected from the lower ionosphere", J. Atmos, Terres. Phys., **40**:35-47.

Vincent, R.A. and Fritts, D.C. (1987). "A climatology of gravity wave motions in the mesosphere at Adelaide, Australia", J. Atmos. Sci., **44**:748-760.

Vincent, R.A. and Reid, I.M. (1983). "HF doppler measurements of mesospheric gravity wave momentum fluxes", J. Atmos. Sci., **40**:1321-1333.

Vincent, R.A. and Stubbs, T.J. (1977). "A study of motions in the winter mesosphere using the partial reflection drift technique", Planet. Space Sci., **25**:441-455.

Vincent, R.A., Stubbs, T.J., Pearson, P.H.O., Lloyd, K.H., and Low, C.H. (1977). "A comparison of partial reflection drifts with winds determined by rocket techniques-1", J. Atmos. Terres. Phys., **39**:813-821.

Walterscheid, R.L. and Boucher, D.J. (1984). "A simple model of the transient response of the thermosphere to impulsive forcing", J. Atmos. Sci., **41**:1062-1072.

Wardill, P. and Jacka, F.J. (1986). "Vertical motions in the thermosphere over Mawson, Antarctica", J. Atmos. Terres. Phys., **48**:289-292.

Widdel, H.U. (1987). "Vertical movements of the middle atmosphere derived from foil cloud experiments", J. Atmos. Terres. Phys., **49**:723-741.

Wilksch, P.A. (1975). "Measurement of thermospheric temperatures and winds using a Fabry-Perot spectrometer", Ph.D Thesis, University of Adelaide.

Witt, G. (1962). "Height, structure, and displacements of noctilucent clouds", Tellus, **14**:1.

Zwick, H.H. and Shepherd, G.G. (1973). "Upper atmospheric temperatures from Doppler line widths - V. Auroral electron energy spectra and fluxes deduced from the 5577 and 6300 $\AA$ atomic oxygen emissions", Planet. Space Sci, **42**:783-789.